BOUNDARY EFFECTS ON FLOW PAST BLUFF BODIES

Pai Mow Lee

A THESIS

in the

Faculty of Engineering

Presented in partial fulfilment of the requirements for
the Degree of Doctor of Engineering at
Sir George Williams University
Montreal, Canada

August, 1973

TABLE OF CONTENTS

PAGE

LIST OF FIGURES

FIGURE		PAGE
23	C_p, Prism (θ = 0), Gap = 0	58
24	C_p, Prism (θ = 60°), Gap = 0	59
25	C_p, Cylinder, Gap = 0	60
26	S, S_1, S_j, vs b/B, Multiple Prisms (θ = 0°) .	61
27	S, S_1 vs b/B, Multiple Prisms (θ = 60°) . .	62
28	S, S_1 vs d/B, Multiple Cylinders.	63

LIST OF TABLES

BOUNDARY EFFECT ON FLOW PAST BLUFF BODIES

ABSTRACT

The effects of boundary interference on the drag force and vortex shedding frequency for equilateral prisms and cylinders are reported. Test bodies were of single and multiple-body (single row) configurations. For the former, the models were mounted in the test section with and without eccentricity. For each case, the empirical constant k $(=u_s/u)$ was determined to get an estimate of the separation velocity u_s. The latter is nearly equal to the contracted jet velocity u_j. Using u_j as the reference velocity, it was possible to obtain the drag coefficient C_{Dj} which was independent of blockage for all the bluff shapes tested. For centrally mounted cylinders (subcritical) and prisms at 60° the drag coefficient C_{D_1} based upon the gap velocity u_1 was almost constant. Since both C_{Dj} and C_{D_1} are constant, it can be deduced that the contraction coefficient C_c must remain invariant for these shapes over the ranges of blockage tested.

The forebody pressure distributions for bluff shapes indicate that the earlier concept of interpreting blockage as an increase in stream velocity is not valid in spite of the fact that the values of C_{Dj} are nearly constant for all the shapes tested, when they are centrally mounted.

For multiple-body configurations, the Strouhal number S_1 and S_j were determined using u_1 and u_j as the reference

velocities. S_1 was found to be nearly constant for prisms at 60° and cylinders (subcritical) up to a blockage of 0.5. For prisms at 0°, S_j was constant up to 0.3. Interference effects on the drag force and vortex shedding frequency caused by the side walls of a single-body configuration were similar to interference effects caused by neighbouring bodies on other members of a multiple-body (single row) configuration.

ACKNOWLEDGEMENT

The author wishes to express his appreciation to Dr. A.S. Ramamurthy for his guidance in the course of the investigation.

Thanks are also due to Dr. S. Lin for many helpful discussions.

Part of the equipment was procured under NRC Grant No. E3474 and A7608.

NOTATIONS

b	Width of triangular prisms, (Fig. 1)
B	Width of test section, or distance between center lines of adjacent bodies for multiple bodies, (Fig. 1)
b/B, d/B	Blockage or constraint (two-dimensional flows)
C_c	Contraction coefficient
C_D	Drag coefficient normalized by u, (=Steady Drag/($\frac{1}{2}\rho u^2 bL$))
C_{D_1}	Drag coefficient normalized by u_1, (=Steady Drag/($\frac{1}{2}\rho u_1^2 bL$))
C_{Dj}	Drag coefficient normalized by u_j, (=Steady Drag/($\frac{1}{2}\rho u_j^2 bL$))
C_{Da}	Drag coefficient of aftbody
C_{Df}	Drag coefficient of forebody
C_{Dt}	Theoretical drag coefficient
C_p	Pressure coefficient based upon u
C_{pb}	Back pressure coefficient
C_{ps}	Pressure coefficient at the separation point
D	Drag force acting on unit height of test body
d	Diameter of circular cylinders, (Fig. 1)
e	Distance between the center line of the test body and that of the wind tunnel; (Fig. 1)
e/b, d/d	Eccentricity
f	Vortex shedding frequency
G	Distance between the test body and the side wall of the wind tunnel (narrow side), (Fig. 1c)

$G/b, G/d$	Gap width
k	An empirical constant $(=u_s/u)$
L	Span of the body
p_b	Base pressure
p_s	Pressure at the separation point
p_w	Wake pressure
p	Pressure of the undisturbed flow
R	Reynolds number based upon b or d, $(=ub/\nu$, or $ud/\nu)$
S	Strouhal number normalized by u, $(=fb/u$, or $fd/u)$
S_1	Strouhal number normalized by u_1, $(=fb/u_1$, or $fd/u_1)$
S_j	Strouhal number normalized by u_j, $(=fb/u_j$, or $fd/u_j)$
s	Separation point, (Fig. 1)
u	Mean undisturbed velocity, (Fig. 1)
u_1	Mean gap velocity, (Fig. 1)
u_j	Contracted jet velocity, (Fig. 1)
u_s	Velocity along the separation streamline, (Fig. 1)
ρ	Density of fluid
ν	Kinematic viscosity of fluid
θ	Angle of orientation of prism, (Fig. 2)

INTERRELATIONS

$k^2 = 1 - C_{ps}$ $\qquad C_c = 1/(1-b/B)k$ $\qquad u_j = u_s = ku$

$u_1 = u/(1-b/B)$ $\qquad C_{D_1} = (u/u_1)^2 C_D$ $\qquad C_{Dj} = C_c^2 C_{D_1}$

$S_1 = (u/u_1)S$ $\qquad S_j = S/k$ $\qquad S_j = C_c S_1$

$C_c = \frac{u_1}{U} k = \frac{u_1}{U}\frac{u}{u_j} = \frac{u_1}{u_j}$ $\qquad \times \qquad C_c = \frac{B}{B-b}\frac{u}{u_j}$ $\qquad (B-b)C_c = B\frac{u}{u_j}$

CHAPTER 1

INTRODUCTION

Earlier building codes provided guide-lines for selecting wind loads on buildings, as though they were single structures. Only recently, these codes have been revised to include the interference effects of neighbouring structures, while evaluating wind loads. Interference effects may lead to major modifications of the load pattern on an existing building due to the erection of a neighbouring building. Leuthesser [1] has conducted model studies for flow past a building complex to show that very large negative pressures could develop due to the interference effects. This type of loading would be detrimental to the large glass panels of the prototype structure. McLaren [2] considered interference effects of twin rectangular structures. His test data determined the critical spacing between the structures to avoid interference wind loading over a range of turbulence intensities. Klenhofer [3] observes that the suction loading experienced by the roof tops of buildings caused by interference effects is a function of both the spacing and relative heights of the buildings. Recently, considerable interest has also been given to the pattern of air flow around buildings. This forms a significant design factor for the architect concerned with architectural aerodynamics.

Interference effects are also important from a different viewpoint. Although laboratory models are exposed to air flow which is subject to lateral constraint, prototype structures are acted upon by wind which has no such constraint. One of the immediate effects of this interference due to the tunnel walls of a test facility is to increase the velocity of the flow past a model (Fig. 1). This effect may become very severe if over-sized models are used during tests. Often, one adopts an over-sized model to incorporate details of the field structure. Under such circumstances the nature of interference loading associated with the test program should be known.

It is not uncommon to find a relatively large object such as a pillar of a building passing through an air duct system in a large building complex. In such cases, power requirements for maintaining the air flow in the duct can be computed if the total drag experienced by the obstacle including interference effects is known.

CHAPTER 2

REVIEW OF PREVIOUS INVESTIGATIONS

2.1 DRAG CORRECTION FOR WEAKLY CONSTRAINED FLOW

In the ensuing discussion, blockage or constraint causing boundary effects for flow past bluff bodies is defined as the ratio of model area to the area of the test section (Fig. 1a). When multiple body configurations (two-dimensional) are considered, the area of the test section is replaced by the area between the centre lines of adjacent bodies (Fig. 1b).

To account for the interference effects due to the side walls of the test facility, Glauert [4] proposed a constant increment to the flow velocity. This increment is supposed to take care of the increase in the velocity past the model. He provided a good appraisal of the nature of interference effects associated with constrained flows and used the method of image to arrive at the induced interference velocities on wing sections. Lock [5] also adopted the method of images to study the interference effects on symmetric objects. According to him, the increment in the velocity to account for the interference effects is proportional to the square of the blockage.

Besides increasing the velocity in the vicinity of the body, the side walls increase the velocity of the flow just outside the wake. This reduces the wake pressure and hence the body experiences a higher drag force. Lastly, the existence of the side walls in a test facility is associated with a longitudinal pressure gradient, when the side walls are parallel. Glauert [4] observes that this is of little consequence in evaluating bluff body drag. Maskell [6] used the experimental results of Fail et al [7] to advance a formula for the drag coefficient C_D, which included interference effects. He assumed that the flows in constrained and unconstrained situations were dynamically similar and that the wake pressure p_w was close to the base pressure p_b. In general, this is not true [8,9]. In arriving at the above formula, Maskell used the momentum relations. Modified versions of his formula have been used successfully by different authors [10,11,12]. The data used by Maskell to substantiate his theory was associated with very limited blockage [7]. Denoting the velocity at the separation point as u_s (Fig. 1a) the velocity of the undisturbed stream as u and the ratio u_s/u as k, Maskell showed that the value of C_D/k^2 was constant for a given shape over a low range of blockages. This is a necessary condition for dynamic similarity. Nevertheless, the invariance of C_D/k^2 does not ensure dynamic similarity as implied in his theory. In fact, pressure measurements taken during the course of the present investigation and also those presented by Shaw [13] demonstrate this fact for flow past bluff shapes subject to interference effects.

2.2 DRAG CORRECTION FOR STRONGLY CONSTRAINED FLOW

Shaw [13] has provided a detailed analysis of the flow past a normal plate subject to side wall constraint. Further, his test results [13,14] cover a broad range of blockage and provide supporting evidence to the method proposed by him to include interference effects. According to him, the velocity u_j at the contracted jet section is close to the separation velocity u_s. As such, in the case of flow past bluff objects subject to interference effects, the contraction coefficient C_c is a significant parameter. In fact, in a related study [15], it was possible to successfully adopt Shaw's theoretical values of C_c to provide the proper reference velocity to normalize the drag coefficients of bluff objects. In a slightly different context, Sarpakya [16] obtained the expressions for the contraction coefficients of flow past inclined plates which denoted butterfly valves.

Modi [10] obtained a better correlation to his data related to flow past a circular cylinder subject to a relatively strong lateral constraint by including higher order terms in Maskell's analysis. Interference effects as applied to axisymmetric bodies have been reported by Lin [17,18].

2.3 BLUFF BODY ATTACHED TO WALL

In the limit, an eccentrically mounted model becomes a model attached to one of the walls (Fig. 1c). Field applications of such configurations include pipelines crossing the beds of waterways and pillars crossing air ducts. The flow past a bluff body attached to a wall is characterized by flow separation upstream of the body and the absence of free oscillations of the wake in the rear of the body. Arie [19] observed that the floor boundary layer upstream of the body was a secondary factor to contend with, in analyzing the characteristics. However, Good [20] has shown that the characteristics of the upstream boundary layer flow is a primary factor that determines the nature of flow past a wall-mounted normal plate. Although its importance was recognized, no attempt was made during the present test program to simulate the upstream boundary layer. The models attached to the side wall were viewed as the extreme case of mounting the bodies eccentrically in the test section. The boundary layer at the test section was very thin relative to the model size for the clear tunnel case.

2.4 INTERFERENCE DRAG FOR GROUP CONFIGURATIONS

Besides studies on building groups [2], the interference effects on the drag force experienced by an individual member of a group of bodies has application in the area of pile groups [21] and pier rows [22]. A brief discussion related to interference drag for flow past single rows of circular cylinders and streamlined struts is provided by Biermann [23].

2.5 VORTEX SHEDDING FREQUENCY CORRECTION FOR CONSTRAINED FLOW

Abernathy [24] extended Roshko's notched hodograph theory [25] to include flow past inclined plates subject to side wall interference and provided experimental data to support his theoretical model. Like Roshko [26], he too, proposed a universal Strouhal number based on the velocity along the separation streamline, the distance between the free streamlines and the frequency of vortex shedding. This Strouhal number was found to be nearly constant for a wide range of blockage and plate inclinations. Chen [27] conducted tests on a 90° wedge which was subject to varying degrees of blockage. According to him, Roshko's proposition related to the universal Strouhal number [26] was only applicable in a very narrow range of blockage for the 90° wedge. Tozkas [28] conducted tests on circular cylinders and normal plates set in a narrow channel and found that the so-called universal Strouhal number concept was not applicable when blockage effects are present.

Toebes [29] has reported the values of Strouhal number for flow past circular cylinders and triangular prisms subject to a maximum blockage of 0.445. In particular, for the prisms at $\theta = 60^o$ (Fig. 2) and circular cylinders (subcritical flow), he used the gap velocity u_1 $(=u_j\ C_c)$ to normalize the vortex shedding frequency. The choice of u_1 in place of u_j as the reference velocity is appropriate (see Notations-Interrelations), if C_c does not vary with blockage. For both the prism at 60^o and the circular cylinder, the results of Von Mises [30] and Toch [31] provided indirect evidence that C_c does not vary with blockage. The data compiled in the present investigation provides evidence to support this fact. However, for the triangular prism at $\theta = 0^o$, Toebes used the contracted jet velocity u_j as the scaling factor to obtain the Strouhal Number S_j. To compute u_j, the values of C_c were obtained on the basis of Shaw's analysis [13] related to constrained flow past a normal plate. For this prism, S_j remained constant for low blockages ($b/B < 0.3$) and increased gradually for higher blockages. These results have been further confirmed in a recent investigation [15]. Toebes [9] also investigated the near wake characteristics of the triangular prism ($\theta = 0^o$) and concluded that the actual wake bubble geometry was quite different from the theoretical quasi-steady wake bubble [6].

Shaw [32] has studied the vortex shedding frequency of bluff bodies placed in eccentric locations between two side walls. For this purpose, he towed two-dimensional bluff shapes in a water tank and obtained the vortex shedding frequencies from visual observations.

2.6 VORTEX SHEDDING FREQUENCY OF GROUP CONFIGURATIONS

Vibration of tube banks is a serious problem in the design of heat exchangers and a number of investigators [33, 34,35] have studied the vortex shedding frequency of multiple body configurations. In this context, some current research trends are reviewed by Mair [36]. Recently, Borges [37] provided useful data related to the vortex shedding frequency of single and multiple rows of circular tubes. He observed that the flow downstream of a single row of cylinders becomes unstable when the spacing between adjacent cylinders was reduced to twice the diameters of the cylinders. According to him, up to a blockage of 0.5, the mean velocity u_1 in the gap between the cylinders was the controlling velocity for forming the Strouhal number S_1 which was found to be nearly constant.

The vortex shedding frequency of twin rigid cylinders spaced at various spacing ratios were determined by Spivak [38]. He found that the cylinders ceased to shed individual vortices when the gap between the cylinders was less than their diameters. For such a situation, the vortices were shed by the composite body formed by the two cylinders. Livesey [39] investigated the flow induced forces on a pair of cylinders which were free to vibrate. When the gap between the cylinders was of the order of their diameters or more, they vibrated independently confirming Spivak's observation that individual vortices are shed from the twin cylinders at these spacings. For smaller gaps Livesy's data indicated "in phase vibration" of the cylinder pair which further confirms the "composite body" effect observed by Spivak for comparable gaps between the twin cylinders.

2.7 SCOPE OF THE PRESENT INVESTIGATION

The present investigation was undertaken to study the boundary effects on the drag force experienced by circular and equilateral triangular bodies (Fig. 2). Aerodynamically, they provide a sharp contrast from the point of view of flow separation. Drag forces obtained either by direct measurement with the aid of a force gage or by integrating the pressures taken around a body. To study the interference effects, the models were mounted both in the central and eccentric locations. For the central case, single and multiple body configurations were included. The modification in the vortex shedding frequency of these shapes subject to interference effects is also reported. For the eccentric case, only single body configuration was studied. To predict the drag coefficient, a theoretical formula has been derived based upon the momentum balance.

CHAPTER 3

EXPERIMENTAL SET-UP AND PROCEDURES

3.1 FORCE GAGE MODELS

Tests were conducted in a wind tunnel whose test section was 14 $\frac{3}{16}$" x 10". The Styrofoam models were 10" long and the model surfaces were sanded to a smooth finish. Circular cylinders and equilateral prisms formed the basic shapes (Fig. 2). The models were attached to a force gauge in which a displacement transducer was housed (Fig. 3). For the design of the force gage, see Appendix 3.

The steady forces on the models were obtained from direct static calibration results. The vortex shedding frequency was determined from the record on a paper chart or through spectral analysis. For the latter, a B & K analyser (Fig. 4) was used. At higher vortex shedding frequencies, the model was held rigid and the vortex shedding frequency was obtained from hot wire surveys in the wake of the bluff body.

3.2 PRESSURE TAP MODELS

For surface pressure measurements, machined metal models were used. They were rigidly fixed at the ends in the test section. The surface pressures on the models were measured with the help of an inclined manometer. Integration of pressure gave the steady forces acting on the models. Hot wire wake surveys yielded the information about the vortex shedding frequency for the models. The pressure coefficient C_{ps} at the separation points for all the shapes was determined experimentally for a large range of blockages and gaps (Fig. 1). This enabled the estimation of k's which were needed for a few models that do not have pressure holes.

However, the tests dealing with the drag force of multiple configurations (Fig. 1b) could not be extended to the lower range of blockages, as the small size of the cylinders did not allow sufficient numbers of holes to be drilled around their peripheries. A wide range of blockage was covered for determining the vortex shedding frequency of multiple bodies.

3.3 OTHER EXPERIMENTAL PROCEDURES

The velocity at the entrance to the test section was obtained with the help of a pitot tube-micro manometer combination. This, in turn, was correlated to the mean undisturbed velocity u at the test section. The intensity of turbulence in the test section was estimated to be of the order of 1%. For the calibration of the wind tunnel, see Appendix 2. In conducting the tests on the bluff body attached to the wall, the side walls of the test section were replaced with two adjustable plates.

CHAPTER 4

ANALYSIS OF RESULTS

4.1 THE EFFECTIVE VELOCITY

In the foregoing discussions, the contracted jet velocity u_j (Fig. 1) is considered to be the proper reference velocity to normalize the drag force and the vortex shedding frequency of bluff bodies subject to boundary interference. In the free streamline model the velocity is assumed to be invariant along the free streamline (sw in Fig. 1). This implies that the separation velocity u_s is equal to the contracted jet velocity u_j. For flow past a normal plate set in a narrow channel, u_j is close to u_s and is uniform all across the contracted section for flows which are at least moderately constricted [13]. The estimation of u_s can be obtained either through the determination of the pressure coefficient C_{ps} near the separation point or from the estimates of the contraction coefficient C_c.

By applying the energy relation along the free streamline, it can be shown that

$$k^2 = 1 - C_{ps} \qquad (4.1)$$

where

$$k = u_s/u \tag{4.2}$$

$$C_{ps} = (p_s - p)/\tfrac{1}{2}\rho u^2) \tag{4.3}$$

When blockage is increased for flow past a bluff body, the contribution of the downstream suction becomes disproportionately large compared to the upstream thrust and when the blockage is high, the pressure distribution in the rear of the bluff body is generally uniform. Under these circumstances, the drag coefficient C_D and the pressure coefficient C_{ps} have a strong correlation. The empirical coefficient k is directly connected to C_{ps}. Consequently, the ratio C_D/k^2 remains almost constant especially when the blockage is high.

4.2 THE EMPIRICAL CONSTANT, k

The theoretical relationship between k and the blockage b/B for the normal plate [13] is sketched in Fig. 5. The present experimental values of k for the prism at $\theta = 0^{\circ}$ are also plotted in the same figure. These estimates were obtained through the determination of the pressure coefficient C_{ps} near the separation point. The values of k for the prism at $\theta = 0^{\circ}$ deviate a little bit from the corresponding theoretical values of k for the normal plate when the blockage is small. Part of this discrepancy can be traced to the arbitrariness associated with the estimation of the undisturbed pressure p while determining C_{ps}. However, the discrepancy becomes negligible when the blockage increases as errors in the estimate of p become less significant. The estimate of k and C_{ps} are not influenced significantly by the after body of this prism (central mounting).

In Fig. 5, the experimental values of k for prisms set at $\theta = 60^{\circ}$, circular cylinders, and 90° wedges [27] are included. The fact that the 90° wedge and the prism set at 60° seem to have a common curve for the variation of k with blockage is again traced to the minor errors that are built into the definition of the reference pressure p. In the present tests, it was determined by estimating the static pressure at a section 15 inches ahead of the model center. The value of k for $b/B \rightarrow 0$ denotes the case where boundary interference is absent.

4.3 SIMILARITY OF PRESSURE DISTRIBUTION

Although it is reported that the pressure distribution in the rear of the flat plate is uniform [13], the pressure distribution in the rear of the prism ($\theta = 0^{\circ}$) is non-uniform (Fig. 6). This may be due, in part, to the presence of the prism's after body. Compare Fig. 7, C_p for prism, $\theta = 60^{\circ}$. However, as stated earlier, the value of C_{ps} for the prism ($\theta = 0^{\circ}$) yielded k values which approached the theoretical value of k for the flat plate. The non-dimensional form of the pressure distribution $C_p/\bar{C}_{ps}$ in the rear of the prism ($\theta = 0^o$) set at several blockages resulted in a single distribution, (Fig. 8). Since $C_{pb}/C_{ps} = (p_b-p)/(p_s-p)$, the pattern of pressure differential (p_b-p) at any point in the rear of the prism is determined by the pressure differential p_s-p at the separation point. In other words, there is a similarity in the distribution of the pressure differential in the rear of the prism when these differences are normalized by the pressure differential at the separation point. Not even this type of similarity is present in the wetted portion of the prism (forebody), because the stagnation pressure coefficient is always unity (point 7, Fig. 6) for all blockages (central case) while C_{ps} in the vicinity of the separation point (points 1 and 13 in Fig. 6) attain different (lower) values at higher blockages. This indicates that in general, it is not possible to represent the pressure distribution around the bluff body by choosing a scaling factor. Published pressure distributions for flow past a normal plate set in a narrow channel [13] also defy any attempt to group the upstream pressure distribution for different blockages. Briefly stated, Maskell's [6] "Interpretation of constraint as an effective increase in the stream velocity" is not appropriate, especially when the constraint is severe.

4.4 DRAG COEFFICIENTS OF BLUFF MODELS IN CENTRAL LOCATION

The drag force on the three shapes (Fig. 2) have been normalized by the velocities u, u_1, and u_j. The mean gap velocity u_1 (Fig. 1) is readily obtained from the continuity equation. In each case, C_{ps} was determined. This, in turn, yielded an estimate of k (Fig. 5). These experimental values of k were used to evaluate $u_j (=ku)$.

For the prism ($\theta = 0^{o}$), the drag coefficient $C_{Dj} (=C_D/k^2)$ was obtained by adopting u_j as the reference velocity. The nearly constant values of C_{Dj} shown in Fig. 9 (see also Appendix 1) confirms earlier predictions [15] related to the invariance of C_{Dj} for this prism. However, it should be noted that in the previous investigation, the values of k were obtained from reference [33]. In the same graph, (Fig. 9), the points denoting $b/B = 0.371$ and 0.486 belong to the multiple body configurations (single row) and these points seem to fit well with the general trend for C_D, C_{D_1} and C_{Dj} for single body configurations.

The drag coefficients C_D, C_{D_1} and C_{Dj} for the prism ($\theta = 60^{o}$) and the circular cylinder (subcritical) are shown in Figs. 10, 11 and 12. (See also Tables 1 and 2). The values of C_{D_1} remains constant for the prism ($\theta = 60^{o}$). Since C_{Dj} and C_{D_1} are both constant (Fig. 10) and $C_{Dj} = (C_{D_1}) C_c^2$ (see Notations, Interrelations), the value of the contraction coefficient C_c should also be nearly constant for this prism in the range of blockages considered. A similar conclusion can be drawn for circular cylinders (subcritical) by observing the nearly constant values of C_{D_1} and C_{Dj} in Figs. 11 and 12. Indeed, the assumption that C_c is constant for the prism ($\theta = 60^o$) and the circular cylinder (subcritical) was taken for granted in the analysis of data in some of the earlier investigations [15,20]. In Fig. 10, the point denoting b/B = .647 belongs to the multiple body configurations (single row) and this point seems to fit well with the general trend for C_D, C_{D_1} and C_{Dj} for single body configurations.

The drag force data for circular cylinders has been plotted in Figs. 11 and 12 (See also Table 2). The single cylinder's drag data can be grouped together to yield a constant value for C_{D_1}. In so doing, only the data corresponding to the subcritical Reynolds numbers were chosen. This was done by restricting the selection of data to a range where C_D did not vary appreciably with Reynolds number (Fig. 11). The cylinder drag force was again normalized using u_j to yield C_{Dj}. Fig. 12 indicates that C_{D_1} and C_{Dj} are both nearly constant for the single circular cylinder (subcritical), when the blockage is at least moderate. As mentioned in an earlier section, this leads to the conclusion that C_c is constant for flow past single cylinders in the range of blockages tested.

In Fig. 11, the data for the multiple cylinders is also presented. Although the value of C_{D_1} for the multiple cylinder (critical flow) falls short of the mean C_{D_I} for the single cylinder (subcritical flow), the values of C_{Dj} for both the single and multiple configuration are nearly the same. For the multiple body configuration, the pressure distribution (Fig. 13) around the cylinder surface indicates that the flow is approaching the critical range, especially for the three larger values of the Reynolds numbers. At these Reynolds numbers, the point of separation appears to have moved downstream (Fig. 13). This lowers the value of C_{ps} and hence k. The value of C_D also decreases with the increase of the Reynolds number. (See Table 2, Runno 28-32). Hence, C_{Dj} has nearly the same value for multiple cylinders over the range of Reynolds numbers considered.

Fig. 14 indicates the drag contribution of the pressure acting on the upstream and downstream portions of the central prisms. For the prism ($\theta = 0^o$), the acceleration of the flow in the forebody leads to suction pressures which amount to a large forward thrust, when blockage is severe. However, even larger suction pressures develop in the rear of the prism (Fig. 6) and the final result is an increase in the net drag force.

4.5 DRAG COEFFICIENTS OF BLUFF MODELS IN ECCENTRIC LOCATIONS

The experimental drag force on all the three shapes for the case of eccentric mounting has been normalized, using u', u_1 and u_j as the reference velocities. For the two prisms, C_D, C_{D_1} and C_{Dj} are plotted in Figs. 15 and 16 (See also Table 3). The interference effect of the side wall appears to be negligible when the gap G/b is more than one. This seems to be the case for all blockages tested. The values of C_{Dj} seem to be constant for both the prisms for a large range of blockages and gap widths. However, the value of C_{D_1} displayed a much wider spread at low gaps G/b.

The pressure distribution around eccentrically mounted cylindrical models indicate that the value of C_p at the stagnation point is much lower than unity (Fig. 17). Further, the stagnation point on the cylinder surface gets shifted towards the narrow gap side by a small angle. Comparison of the pressure data for the cylinder mounted with and without eccentricity indicates that the flow meets the cylinder at an oblique angle when the mounting is eccentric. In fact, by giving a constant angular increment to all the pressure tap locations, the symmetry of the pressure coefficient graph (Fig. 17) can be improved. Some visual observations were made in a smoke tunnel to establish the fact that the flow approaches the circular cylinder at an oblique angle when it is eccentrically mounted (Fig. 1e).

Fig. 18 depicts C_D, C_{D_1} and C_{Dj} for different gaps, G/d, over a range of Reynolds number from 2 x 10^4 to 3 x 10^5. (See also Table 2 and 3). Fig. 19 was produced by choosing from the above figure the data in the subcritical region. From Fig. 19, it can be seen that C_{D_1} and C_{Dj} remain nearly constant. However, C_D shows some erratic trends as the gap G/d is reduced. This is traced in part, to the deflection of the oncoming flow induced by the eccentrically mounted cylinders. This deflection of the flow generally resulted in a downstream shift of the separation point on the narrow gap side (Fig. 17). The location of the separation point on the wide gap side did not display any clear trend. It is felt that its specific location was dependent on the distribution of the deflected flow in the two gaps. Biermann [23] who conducted drag tests on twin cylinders in a very wide wind tunnel observed that the flow characteristics change rapidly when the spacing is nearly 1.75 diameters. These changes are rapid and can result in a positive or negative increment to the drag forces at this critical spacing ratio. He also comments on the possibility of flow changes even when the spacing is held constant.

The forebody pressure distribution around the eccentrically mounted prism set at 60^o displayed a peculiar form (Fig. 20). The flow separates on the wide gap side and re-attaches to the model surface at a downstream location. For a fixed eccentricity (e = 3.5" in Fig. 20), the re-attachment point seemed to move downstream with increased blockage. Fig. 1d shows the smoke tunnel photograph of the instantaneous streamlines for the deflected flow past an eccentrically mounted prism set at 60^{o}.

When the prism ($\theta = 0^{o}$) was mounted in the test section with a large eccentricity, the values of the pressure coefficient C_{ps} at the two separation points were not always equal, Fig.21. At lower blockages, the values of C_{ps} differed slightly. However, this difference became almost negligible when the blockage increases. Further, the pressure distribution, in the rear of the body was nearly uniform at higher blockages. On the other hand, for eccentrically mounted circular cylinders and prisms set at $\theta = 60^{o}$ the values of C_{ps} at the two separation points did not differ from each other for all the blockages tested (Figs. 17 and 20). Part of this behaviour may be traced to the fact that the after body beyond the points of separation in these two shapes is either too short or non-existent.

4.6 GEOMETRICALLY SIMILAR MODEL

4.6.1 Contracted Coefficients for Eccentrically Located Prisms ($\theta = 0^{o}$)

As mentioned in the previous section, for eccentric prisms ($\theta = 0^{o}$), the values of C_{ps} (and hence k) at the two separation points are almost equal, especially when the blockage is high. Thus, for either branch of the divided flow, the blockage must be nearly equal, since blockage uniquely determines k, (Fig. 5). Consequently, C_c for either side must be nearly equal. With reference to the sketch (p.25), it can be seen that $b_1/B_1 = b_2/B_2$ or $b_1/b_2 = B_1/B_2$. Hence, the stagnation streamline pq which divides the flow between the two branches will assume such a position as to yield almost equal contraction coefficients. However, Fig. 21 indicates that the location of the stagnation point was closer to the wide gap than that indicated by this model. Part of this situation can be traced to the fact that the streamlines in the actual flow get deflected toward the wide gap. (Fig. 22a).

4.6.2 Evaluation of C_D for Eccentric Prisms ($\theta = 0^\circ$) by Using the Expression for Central Normal Plate

For eccentric prisms ($\theta = 0^\circ$), C_D can be predicted by using an equation which was primarily derived for a central normal plate. When the prism is eccentrically mounted, the stagnation streamline will divide it into two parts, each of which can be considered as a gate protruding from the wall with approximately equal blockage. Define $m = \frac{b_1}{b}$. Clearly, the position of the stagnation streamline will be completely determined once the value of m is found. It can be seen that m is given by

$$m = \frac{B_1}{B-b}$$

The following expression is adopted to obtain C_D for each portion of the body

$$C_D = \frac{1}{2A^2(\frac{B-D}{B})}\left[(A^2+1)(A-1)^{-2} - \frac{2}{\pi}(A^2-1)^{2}\tan^{-1}\left(\frac{A^2-1}{2A}\right)\right] + $$

$$+ (A^2-1) \quad (4.4)$$

where, using notations of [13]

$A = k_j\ B/D'$ and

k_j = an empirical constant to relate the separation and jet velocity.

Consequently, the total drag force acting on the body can be computed. This, in turn, yields the drag coefficient C_D for the eccentric prism.

The results are shown in Table 4. From this, it can be seen that for blockage greater than .30, the agreement between the predicted and experimental values is reasonable with the exception of those corresponding to low m values. For blockages smaller than .30, referring to Eqn.(4.4).the values of k_j have to be determined with some difficulty [13](Fig. 11). Further, due to machining limitation, the corner along the length edges of the body can hardly be made as sharp as implied in the theoretical model. This limitation is particularly true for bodies made of styrofoam. As a result, at large eccentricities, i.e., small m's, the narrower divided portion of the body will make a smaller contribution to the total C_D than predicted by Eqn. (4.4). These may be the reasons for the discrepancy between the theoretical and experimental values of C_D for $b/B < .30$, and at low m's for $b/B > .30$.

4.6.3 Momentum Balance Model

The drag force acting on a prism that is mounted eccentrically, can also be predicted by using the momentum balance. For this purpose, a control volume HGNM is taken, as shown in the accompanying sketch.

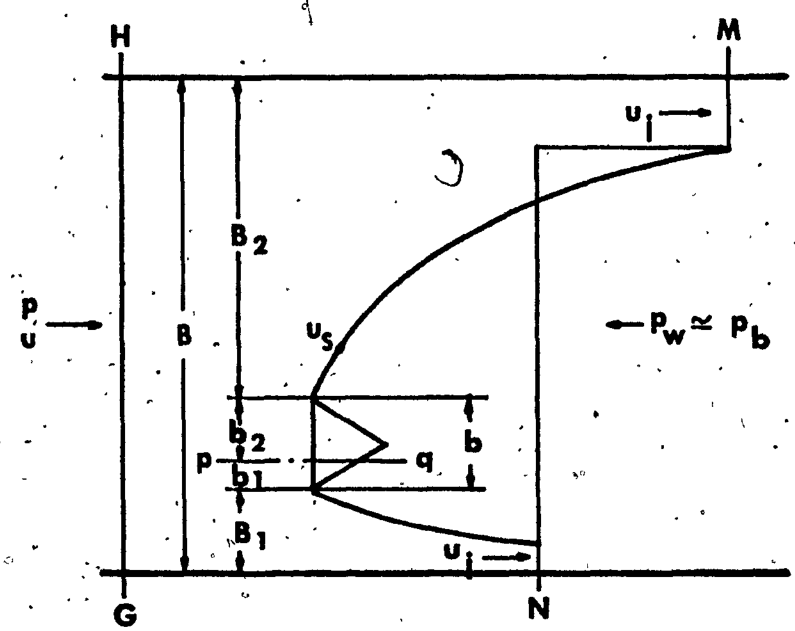

SKETCH MOMENTUM BALANCE MODEL

With reference to Section 4.1, let p_w be equal to p_b. With this assumption, one notes that the pressure is nearly uniform all across the control surface MN. The momentum relation yields

$$D = (p-p_b)B - \rho u_j^2(B-b)C_c + \rho u^2 B \qquad (4.5)$$

From continuity

$$(B-b)C_c = \frac{u}{u_j}B = \frac{B}{k}$$

and using Eqn. (4.1)

$$C_{ps} = (p_b-p)/\tfrac{1}{2}\rho u^2 = -(k^2-1)$$

Hence

$$D = \tfrac{1}{2}\rho u^2 B(k-1)^2$$

and the theoretical drag coefficient

$$C_{Dt} = \frac{D}{\tfrac{1}{2}\rho u^2 b} = \frac{1}{(\frac{b}{B})}(k-1)^2 \qquad (4.6)$$

The values of theoretical and experimental drag coefficients are compared in Table 3. From this, it can be seen that for blockage greater than .30, the agreement is quite close. However, for $b/B < .30$, C_{Dt} is larger than C_D. This may be explained as follows. When blockage is low, the pressure is less uniformly distributed across the contracted jet section (see Section 4.1) and there is a negative pressure gradient from the free streamline toward the wall. Hence, the mean pressure is smaller than the assumed pressure p_b. Accordingly, the mean contracted jet velocity is greater than u_j. Rewrite Eqn. (4.5) as

$$
\begin{aligned}
D &= pB + \rho u^2 B - p_b (B-b) C_c - p_w \left[B-(B-b)C_c\right] - \rho u_j^2 (B-b) C_c \\
&= pB + \rho u^2 B - (p_b + \tfrac{1}{2}\rho u_j^2)(B-b) C_c - p_w \left[B-(B-b)C_c\right] \\
&\quad - \tfrac{1}{2}\rho u_j^2 (B-b) C_c \qquad (4.7)
\end{aligned}
$$

In Eqn. (4.7), it can be readily seen that the third term yields a fixed value for a certain flow condition, and the fourth term provides a correct estimate. However, in the last term, using u_j in place of the mean contracted jet velocity will result in an overestimation of the drag force. Therefore, for blockage smaller than .30, the theoretical is greater than the experimental drag coefficients.

4.7 BLUFF BODY ATTACHED TO WALL

For a bluff body attached to the wall, the upstream standing eddy makes the forebody pressure between the wall and the stagnation point constant for all blockages tested. (Fig. 23-25). The absence of a gap makes the afterbody pressure distribution essentially uniform (Fig. 23-25) unlike its counterpart models for which the gap is finite. For comparable blockages, a wall body has a lower drag than a body with a finite gap. (See Tables 1 and 2). This characteristic of the wall bodies is linked to the deflection of the oncoming flow. Visual observations in a smoke tunnel confirmed this behaviour of the flow configuration (Fig. 22b) and c).

4.8 VORTEX SHEDDING FREQUENCY FOR MULTIPLE BODIES (SINGLE ROW)

The Strouhal numbers S, S_1 and S_j for the single rows of cylinders and prisms shown in Figures 26 to 28, are based respectively on the undisturbed mean velocity u, the gap velocity u_1 and the contracted jet velocity u_j. In all cases, S increased with blockage. In the lower range of blockage, S_1 is nearly constant for the single rows of prisms at 60^o and cylinders.

S_1 for the single rows of prisms at 0^o indicated a marked increase with blockage. S_j was nearly constant up to a blockage of 0.3 (Fig. 26). These trends are similar to the characteristics displayed by single-prisms subject to comparable blockage. As blockage is increased to 0.5, vortex shedding for single rows of cylinders and prisms occurs at more than one frequency (Figs. 26, 28). For single cylinder rows, Borges [37] too has reported the existence of multiple vortex shedding frequencies at higher blockages. Even for flow past twin cylinders of diameter d, the flow characteristics have been observed to change distinctly, when the gap between the cylinders is reduced to the order of d. In the present tests, the hot wire signals for single row bodies consisted of a larger number of harmonics when the blockage was increased beyond 0.5.

CHAPTER 5

CONCLUSIONS AND RECOMMENDATIONS

5.1 CONCLUSIONS

The experimental values of the empirical constant k, has been determined for the two prisms and the cylinder over a range of blockage. The experimental values of k for the prism at 0° agree closely with the theoretical values of k for normal plates when the blockage is at least moderate.

For flow past bluff shapes, solid boundary interference cannot be interpreted merely as an effective increase in the stream velocity. In particular, the forebody pressure distributions for all the shapes defied attempts to regroup and form a single distribution. However, the drag force for the two prisms and the cylinder yielded nearly constant values for the drag coefficient C_{Dj}. The fact that C_{D_1} and C_{Dj} are both nearly constant over a range of blockage for the prism at 60° and the cylinder (subcritical) indicates that C_c does not vary much with blockage.

For eccentrically mounted prisms and cylinders, C_D was independent of the gap (G/b or G/d) when the latter was more than unity. C_D for the circular cylinder displayed some erratic trend when the gap was reduced. For eccentrically mounted bodies, the flow was deflected towards the wider gap, and C_{Dj} was nearly constant for any one shape.

The Strouhal number S_1 for multiple prisms (single row) at 60^o attains nearly a constant value for blockage up to 0.5. In this range of blockage, S_1 for multiple cylinders is also constant. For multiple prisms at 0^o, S_j is nearly constant only up to a blockage of 0.3 and gradually increases beyond this blockage.

From the point of view of the drag force and the vortex shedding frequency, $(b/B < 0.5)$, the interference effect due to the side walls on a single body appears to be similar to that due to neighbouring bodies on a member of a multiple body configuration.

5.2 RECOMMENDATIONS FOR FURTHER STUDIES

The present study can be extended to cover the following situations:

(1) The effect of wall interference on the unsteady force coefficients for bluff shapes.

(2) The effect of wall interference including hydroelastic effects, and

(3) Detailed wake study under constrained flow condition.

REFERENCES

1. Leuthesser, H.J., "Static Wind Loading of Grouped Buildings". Intl. Conf. on Wind Effects on Buildings and Structures, Tokyo, 1971.

2. McLaren, F.G. et al. "The Interference Between Bluff Sharp-edged Cylinders in Turbulent Flows Representing Models of Two Tower Buildings Close Together", Tech. Note, Building Science, Vol. 6, 1971, pp.273-274.

3. Klenhofer, W.J., "Influence of a Neighbouring Building on Flat Roof Wind Loading", Intl. Conf. on Wind Effects on Buildings and Structures, Tokyo, 1971.

4. Glauert, H., "Wind Tunnel Interference of Wings, Bodies and Air Screws", A.R.C., R & M 1566, 1933.

5. Lock, C.M., "The Interference of a Wind Tunnel on a Symmetrical Body", A.R.C., R & M 1275, 1929.

6. Maskell, E.C., "A Theory of Blockage Effects on Bluff Bodies and Stalled Wings in a Closed Wind Tunnel", A.R.C., R & M 3400, 1957.

7. Fail, R. et al, "Low Speed Experiments on the Wake Characteristics of Flat Plates Normal to an Air Stream", A.R.C., R & M 3120, 1957.

8. Cowdrey, C.F., "Application of Maskell's Theory of Wind Tunnel Blockage to Some Large Solid Models", Paper No. 29.1, Proc. Symp. on Wind Effects on Buildings and Structures, Natl. Phy. Lab., U.K., 1969.

9. Toebes, G.H., "The Frequency of Oscillatory Forces Acting on Bluff Cylinders in Constricted Passages", Proc. 14th Congress of Intl. Hyd. Rsch. Vol. 2, 1971, pp.B-7-58.

10. Modi, V.J., and El-Sherbiny, S., "Effect of Wall Confinement on Aerodynamics of Stationary Circular Cylinder", Proc. Intl. Conf. on Wind Effects on Buildings

and Structures, Tokyo, 1971, pp. 11-19-1 to 11-19-12.

11. Plate, E.J., "The Drag on a Smooth Plate With a Fence Immersed in Its Boundary Layer", ASME Paper 64-FE-17, Fluids Engg. Conf., Philadelphia, 1964.

12. Rangaraju, K.G., and Garde, R.J., "Resistance of an Inclined Plate Placed on a Plane Boundary in Two-Dimensional Flow", ASME Paper 69-FE-3, Fluids Engg. Conf., Evanston, Ill., 1969.

13. Shaw, T.L., "Steady Flow Past Flat Plate in Channel", J. Hyd. Div. Proc. ASCE, Vol. 95, 1969, pp.2013-2018.

14. Shaw, T.L., "Effect of Side Walls on Flow Past Bluff Bodies", J. Hyd. Div. Proc. ASCE, Vol. 97, 1971, pp.65-79.

15. Ramamurthy, A.S., and Ng., C.P., "Steady Force Coefficients Including Blockage Effects", To appear in J.Eng. Mechs. ASCE, 1973.

16. Sarpakya, T., "Discussion on Butterfly Valve Flow Characteristics, J. Hyd. Div. Proc. ASCE, Vol. 83, 1957, pp.31-47.

17. Lin, C.A.C., "Effect of Channel Walls on Base Pressure and Flow About a Blunt Body", M.S. Thesis, Dept. of Engg. Mechs. and Hydraulics, Univ. of Iowa, 1966.

18. Lin, C.A.C., "A Free Streamline Model of a Two-Dimensional Wake", Ph.D. Thesis, Dept. of Engg. Mechs. and Hydraulics, Univ. of Iowa, 1970.

19. Arie, M., and Rouse, H., "Experiments on Two-Dimensional Flow Over a Normal Wall", J. Fl. Mechs., Vol. 1, 2, 1956, pp. 129-141.

20. Good, M.C., and Joubert, P.N., "The Form Drag of Two-Dimensional Bluff Plates Immersed in Turbulent Boundary Layers", J. Fl. Mechs., Vol. 31, 3, 1968, pp.547-582.

21. Laird, A.D.K., and Warren, W., "Group of Vertical Cylinders Oscillating in Water", J. Engg. Mechs.Div. Proc. ASCE, Vol. 89, 1963, pp.25-35.

22. Unrue, R.D., "Drag Coefficients of Circular Cylinders in an Infinite Single Row Array", M.S. Thesis, Washington State Univ., 1961.

23. Biermann, D., and Herrnstein, W.H., "The Interference Between Struts in Various Combinations", NACA Report, 468, 1933.

24. Abernathy, F.H., "Flow Over an Inclined Plate", Ph.D. Thesis, Div. of Appl. Physics, Harvard Univ. Mass.1958.

25. Robertson, J.M., Hydrodynamics in Theory and Application . Prentice-Hall, New Jersey, 1965.

26. Roshko, A., "On the Drag and Shedding Frequency of Two-Dimensional Bluff Bodies", Tech. Note 3169, NACA.

27. Chen, Y.S. "Effect of Confining Walls on the Periodic Wake of 90° Wedges", Dept. of Engg. Mechs. and Hydraulics, Univ. of Iowa, 1967.

28. Tozkas, A., "Effect of Confining Walls on the Periodic Wake of Cylinders and Plates", M.S. Thesis, Dept. of Engg. Mechs.,and Hydraulics, Univ. of Iowa, 1965.

29. Toebes, G.H., and Ramamurthy, A.S., "Lift and Strouhal Frequency for Bluff Shapes in Constricted Passages", Proc. Conf. on Flow Induced Vibration in Nuclear Reactors, Agronne Natl. Lab., Illinois, 1970, pp.225-247.

30. Harleman, R.F., and Daily, J.W., "Fluid Dynamics", Addison Wesley, 1966.

31. Toch, A., "Discharge Characteristics of Tainter Gates", Trans. ASCE, Vol. 120, 1955, p.290.

32. Shaw, T.L., "Wake Dynamics of Two-Dimensional Structures in Confined Flows", Proc. 14th Congress of Intl. Assn. of Hyd. Resch. Vol. 2, 1971, pp.41-48.

33. Chen, Y.N., "Fluctuating Lift Forces of the Karman Vortex Streets on Single Circular Cylinders and Tube Bundles", ASME Paper 17-Vibr-13, Vibration Conference, Toronto, 1971.

34. Owens, P.P., "Buffeting Excitation of Boiler Tube Vibration", J. Mech. Eng. Sci., Vol. 7, 1965, pp.431-439.

35. Putnam, A.A., "Flow Induced Noise and Vibration in Heat Exchangers", ASME Paper 64-WA/HT-21, 1964.

36. Mair, W.A., and Maull, D.J., "Bluff Bodies and Vortex Shedding - a Report on Euromech 17", J. Fl. Mechs. Vol. 4, 1971, pp.209-224.

37. Borges, A.R.J., "Vortex Shedding Frequencies of the Flow Through Two Row Banks of Tubes", J. Mech. Eng. Sci. Vol. 11, 1969, No. 5, pp.498-502.

38. Spivak, H.M., "Vortex Shedding Frequency and Flow Pattern in the Wake of Two Parallel Cylinders at Varied Spacing Normal to an Air Stream", J. Aero. Sci. Vol. 13, 1946, pp.289-301.

39. Livesey, J.L., and Dye, R.C.F., "Vortex Excited Vibration of a Heat Exchanger Tube Row", J. Mech. Engg. Sci. Vol.4, 1962, pp.349-352.

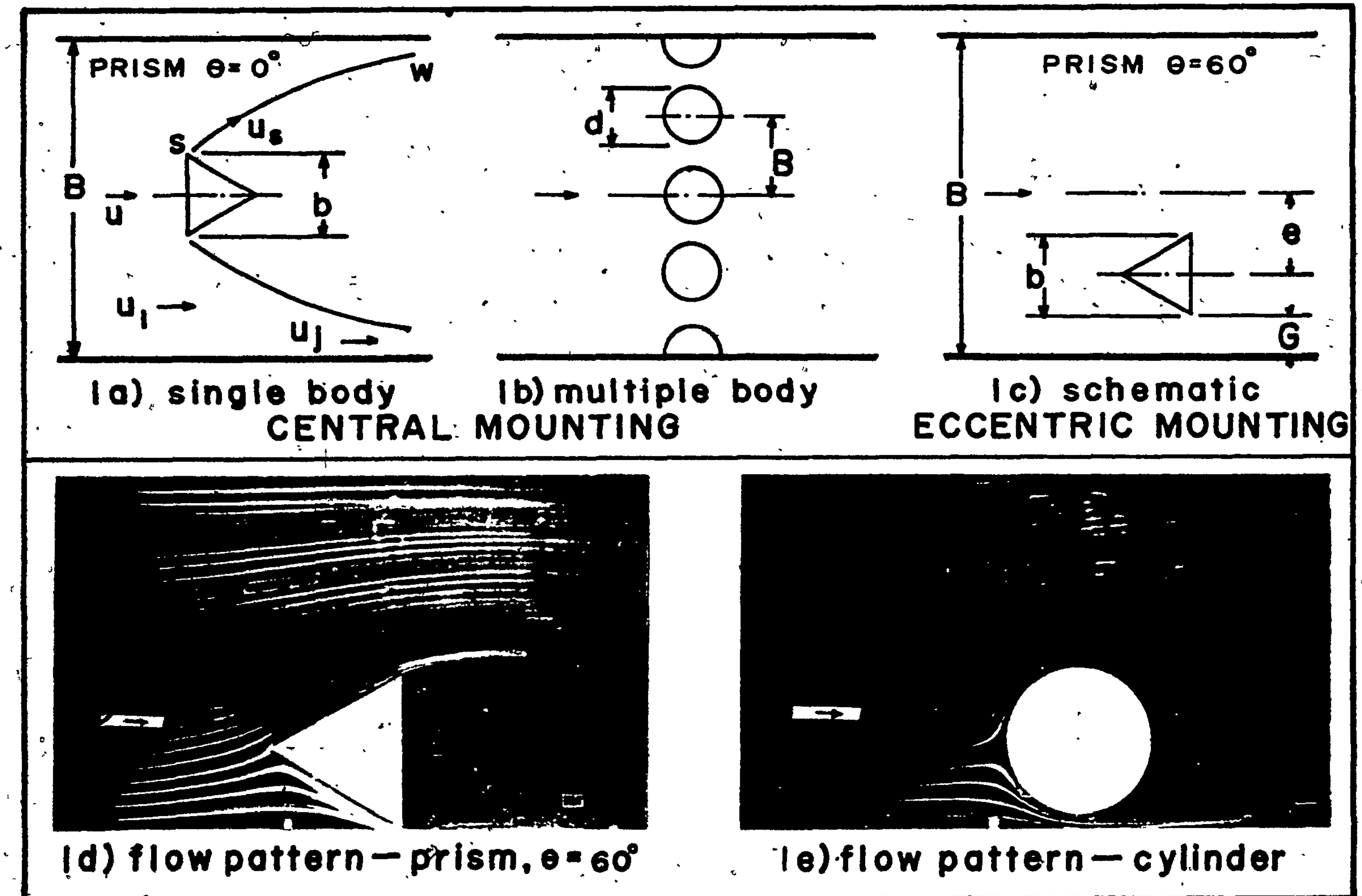

FIG. I CONSTRICTED FLOW

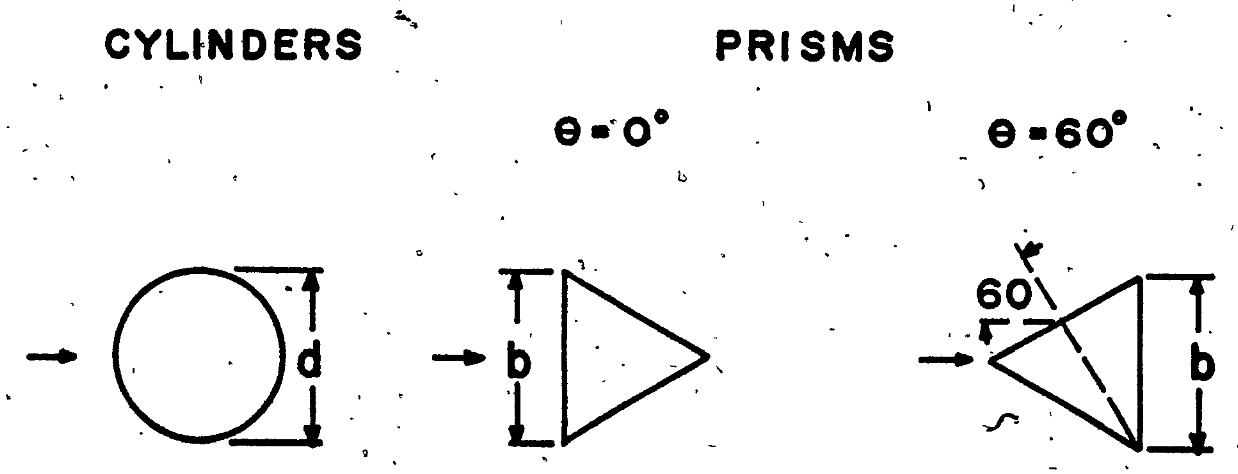

	GAGE MODELS	PRES. MODELS
b"	2 3 4 6 8	2·60 3·40 4·53
d"	2 3 4 6 8	1·96 3·20 4·28
b/B	·14 - ·56	·186 - ·324
d/B	·14 - ·56	·140 - ·611
G/b	·05 - 2·61	.0 - 1·88

FIG 2 TEST BODIES

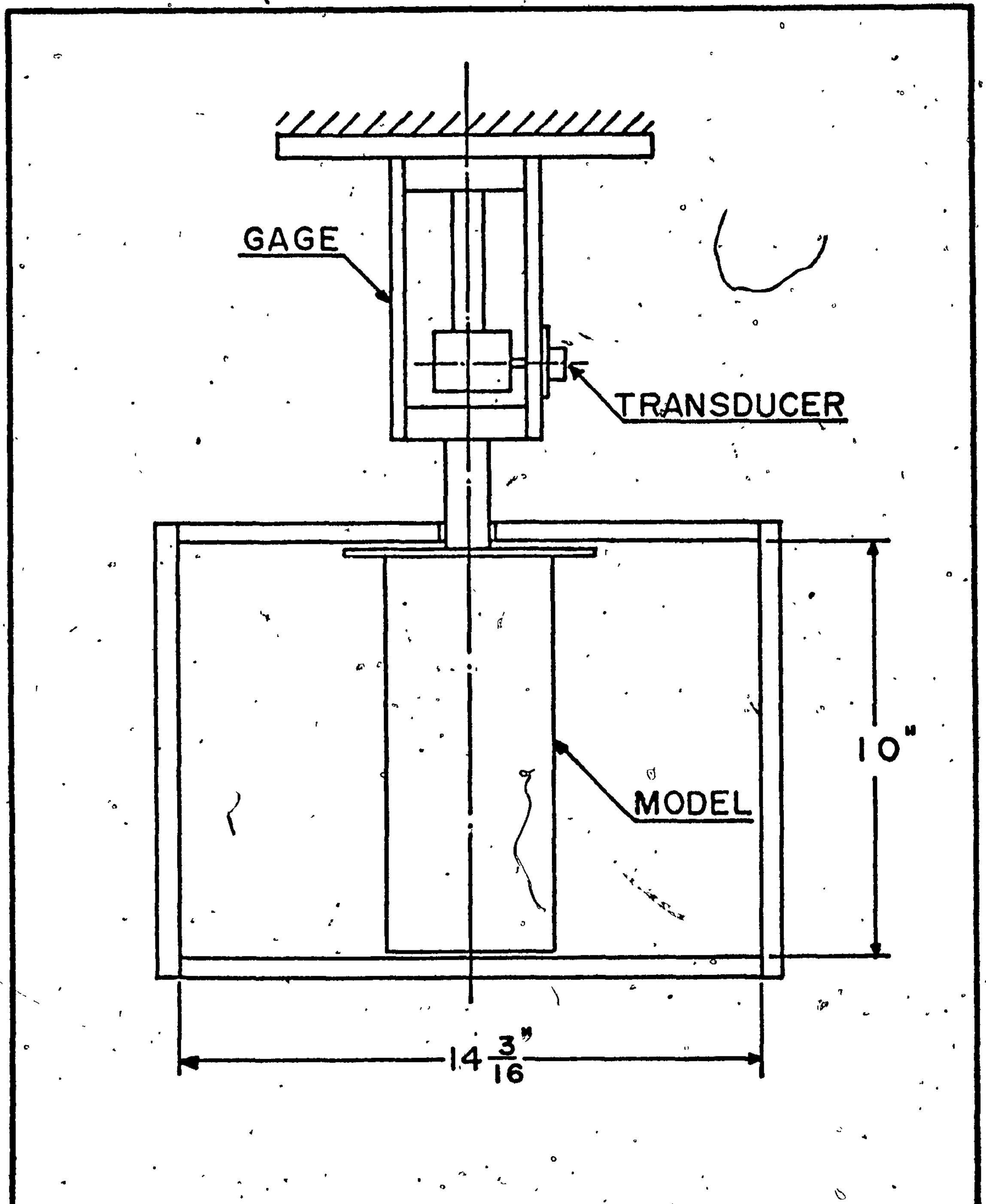

FIG 3 TEST SECTION

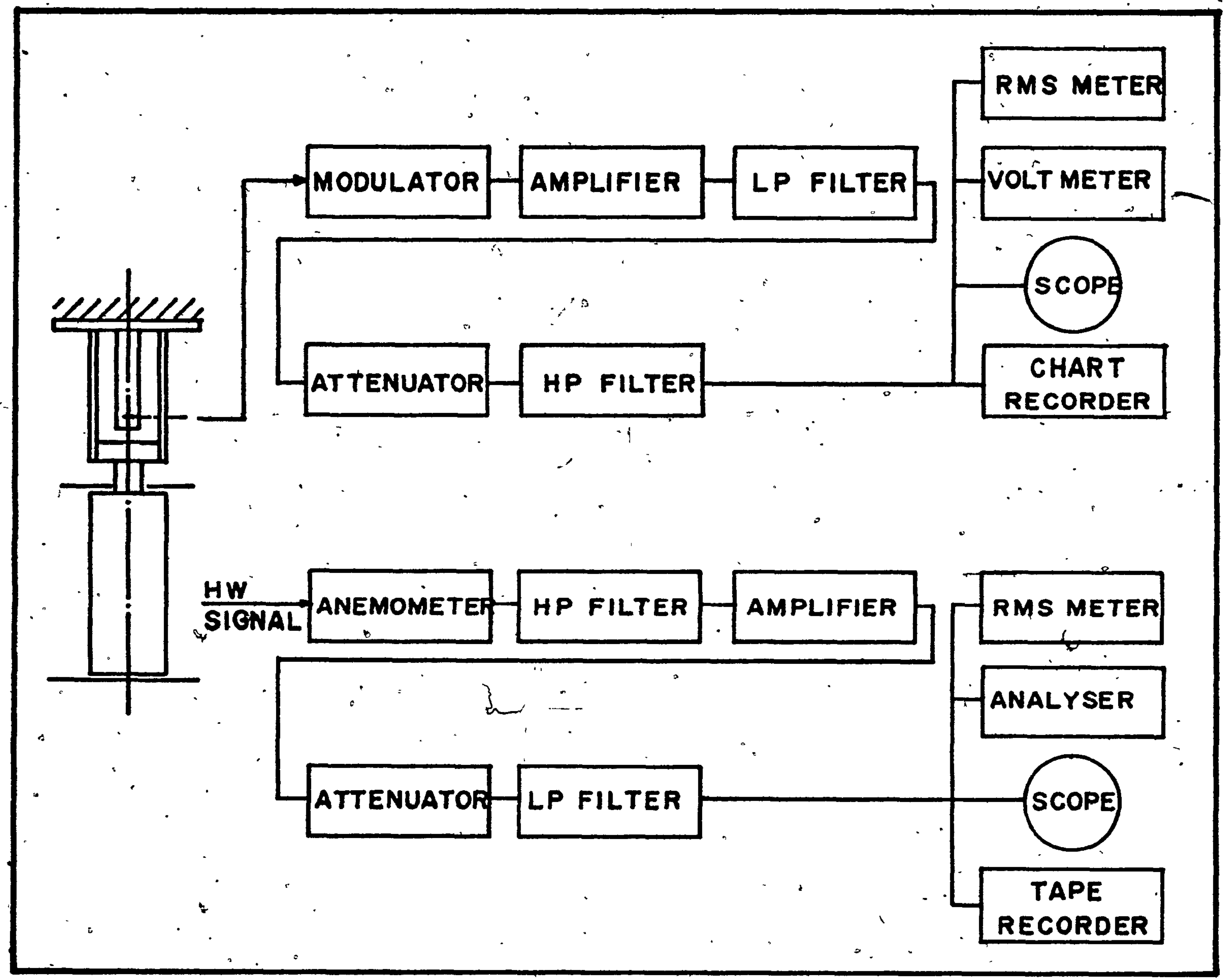

FIG 4 INSTRUMENTATION

FIG 5 k FOR BLUFF SHAPES

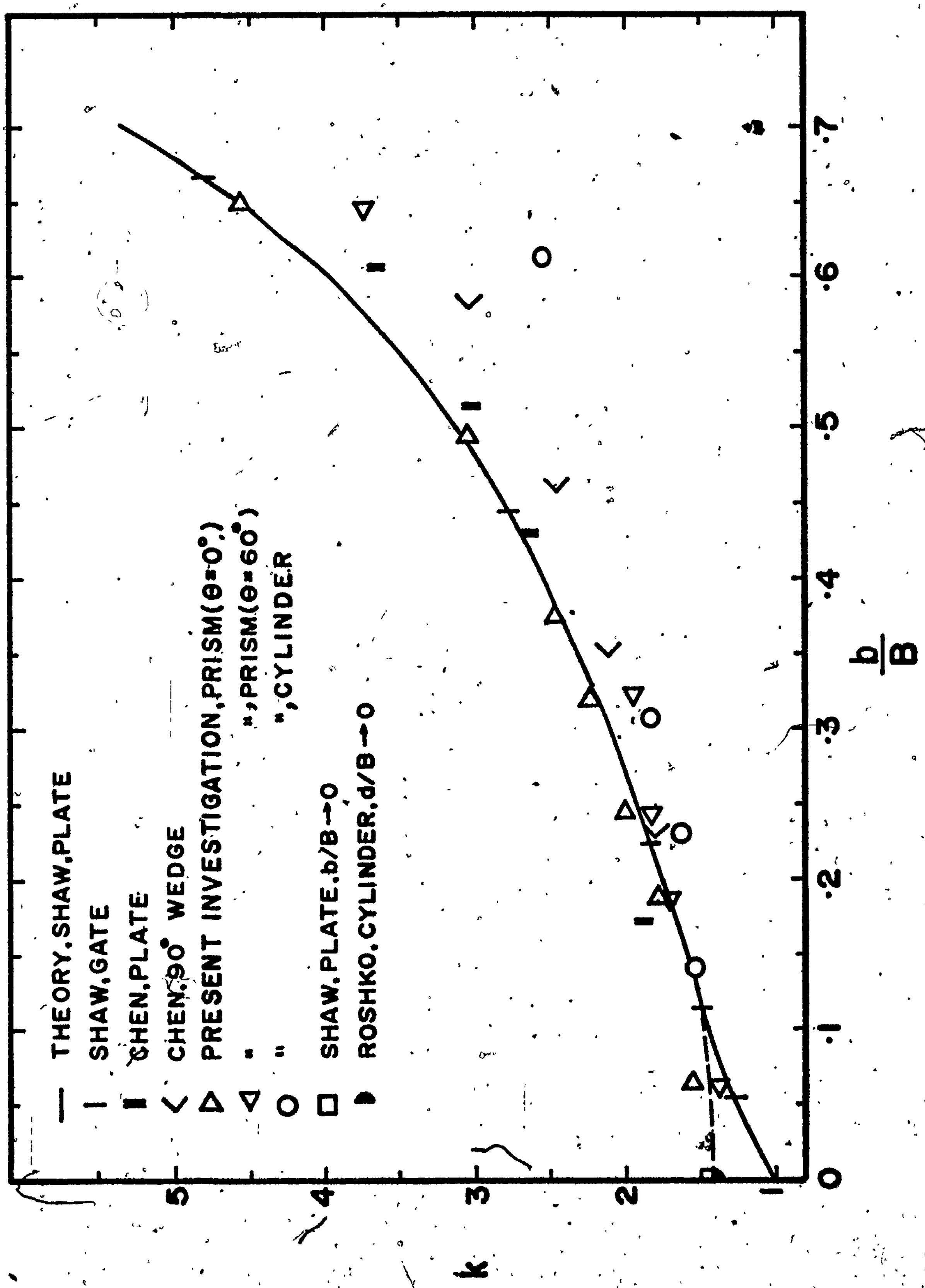

FIG 6 C_p, CENTRAL PRISM ($\theta = 0°$)

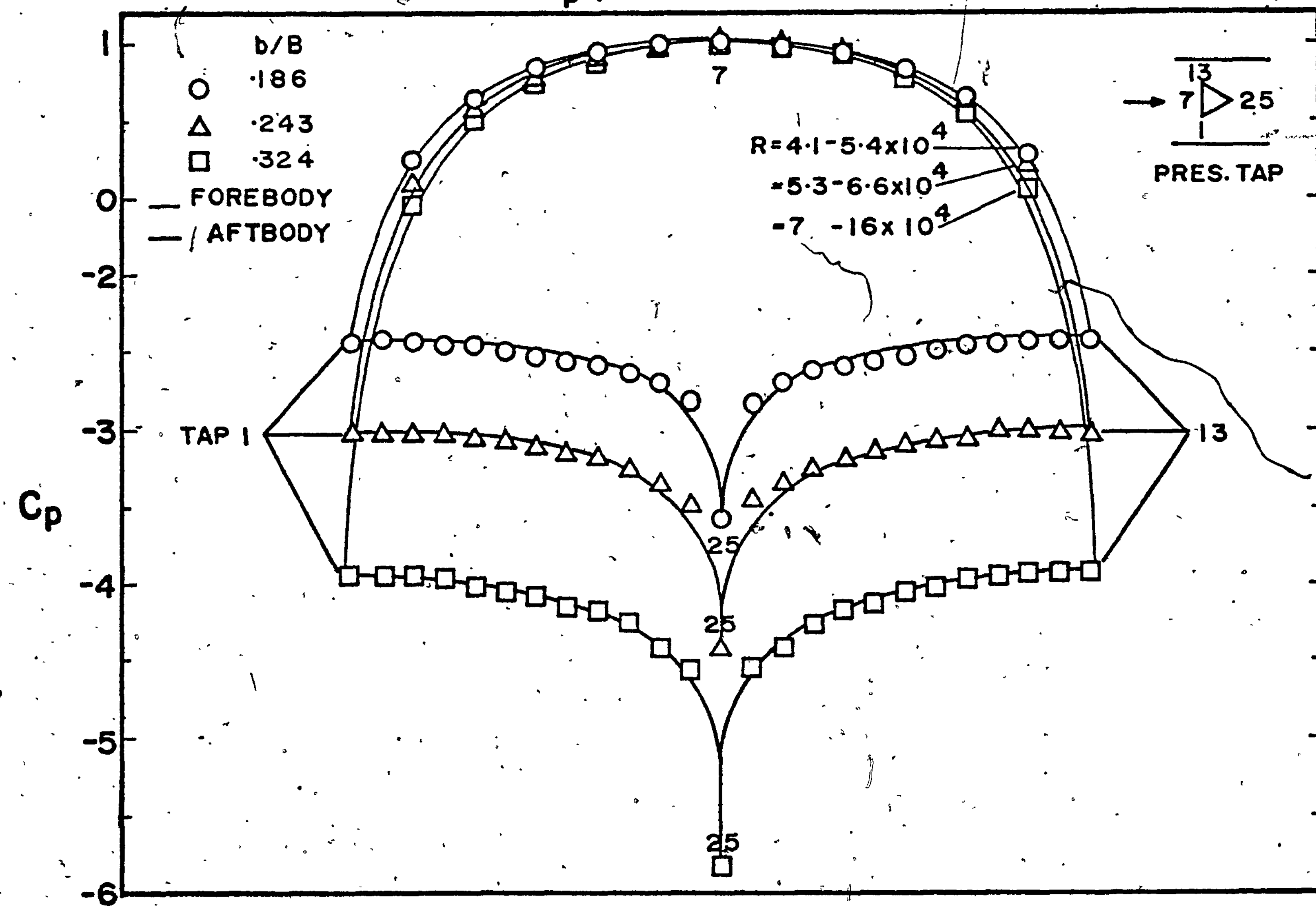

FIG 7 C_p, CENTRAL PRISM(θ=60°)

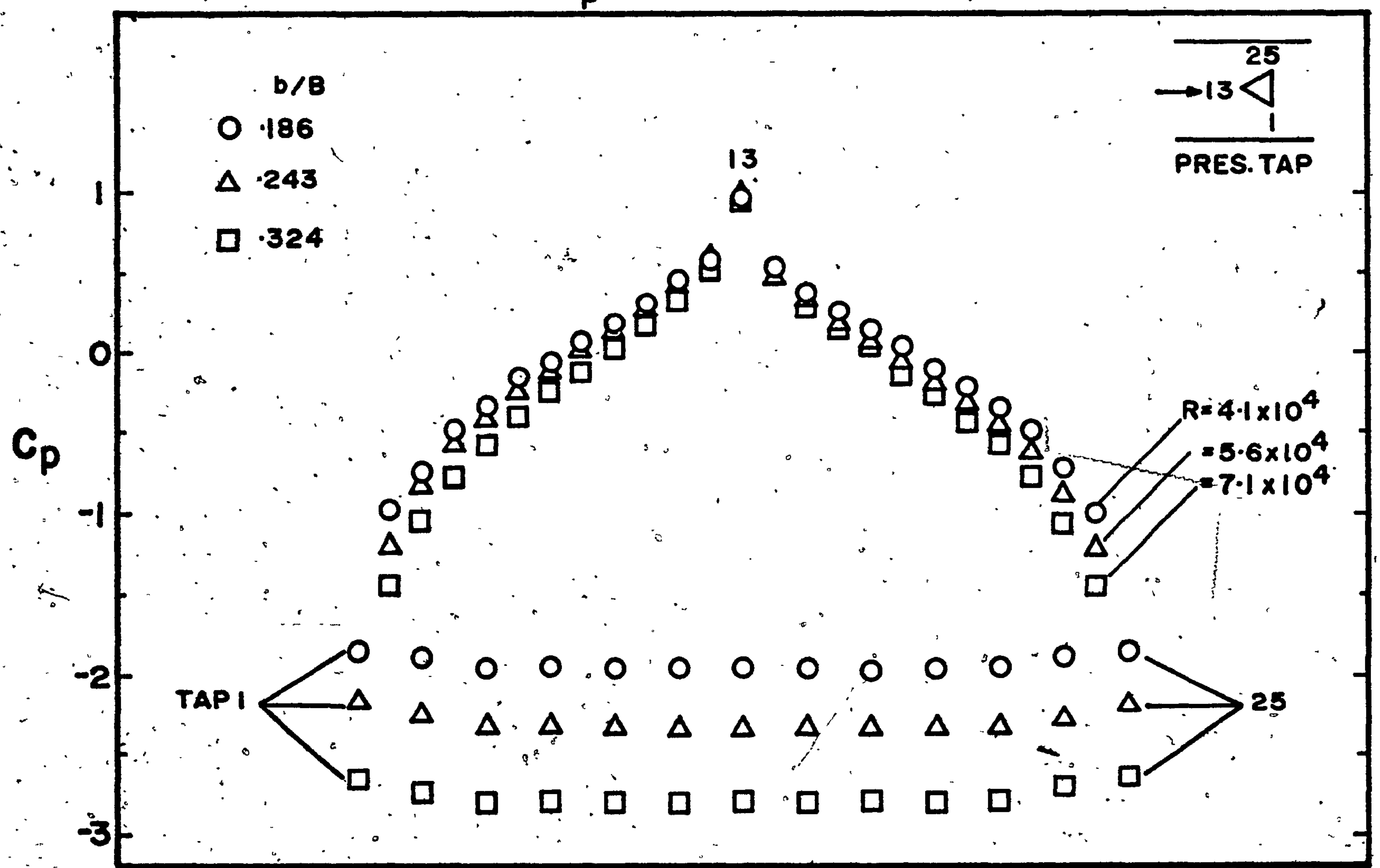

FIG 8 DISTRIBUTION OF C_{pb}/C_{ps}, PRISM ($\theta=0^{\circ}$)

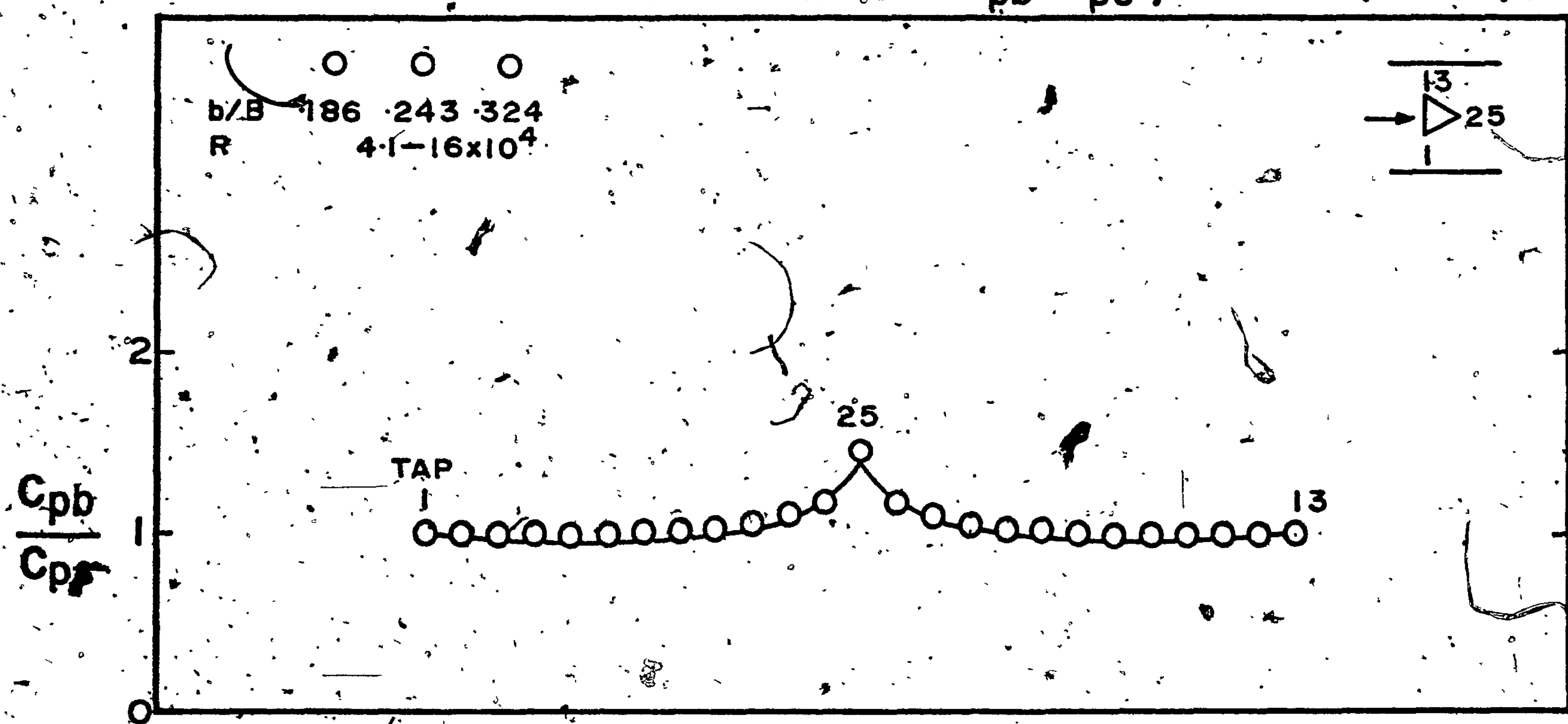

FIG 9 C_D, C_{DI}, C_{Dj}, Vs b/B CENTRAL PRISM ($\theta = 0°$)

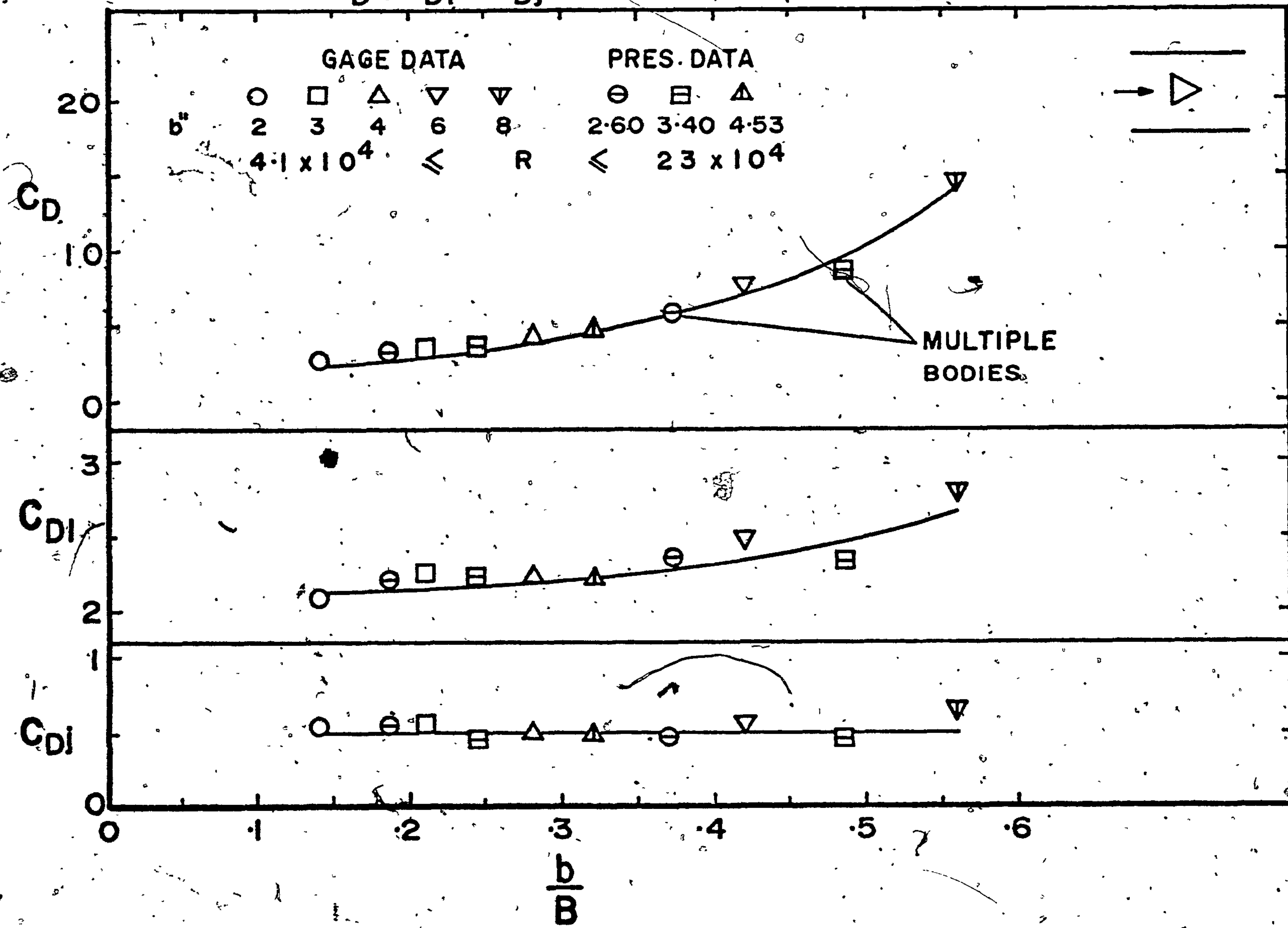

FIG 10 C_D, C_{DI}, C_{Dj}, Vs b/B CENTRAL PRISM (θ=60°)

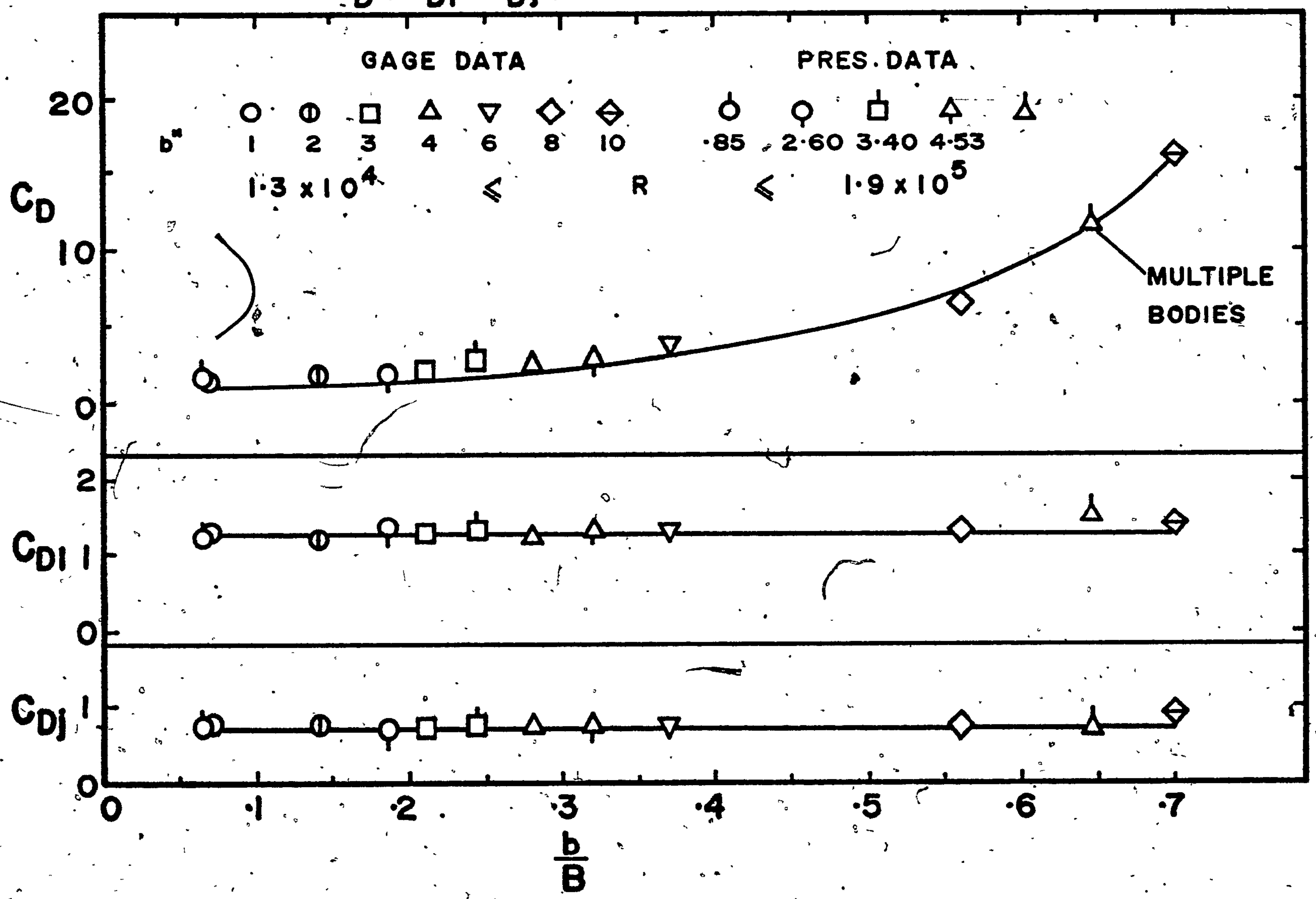

FIG 11 C_D, C_{DI}, C_{DJ} Vs R, CENTRAL CYLINDER

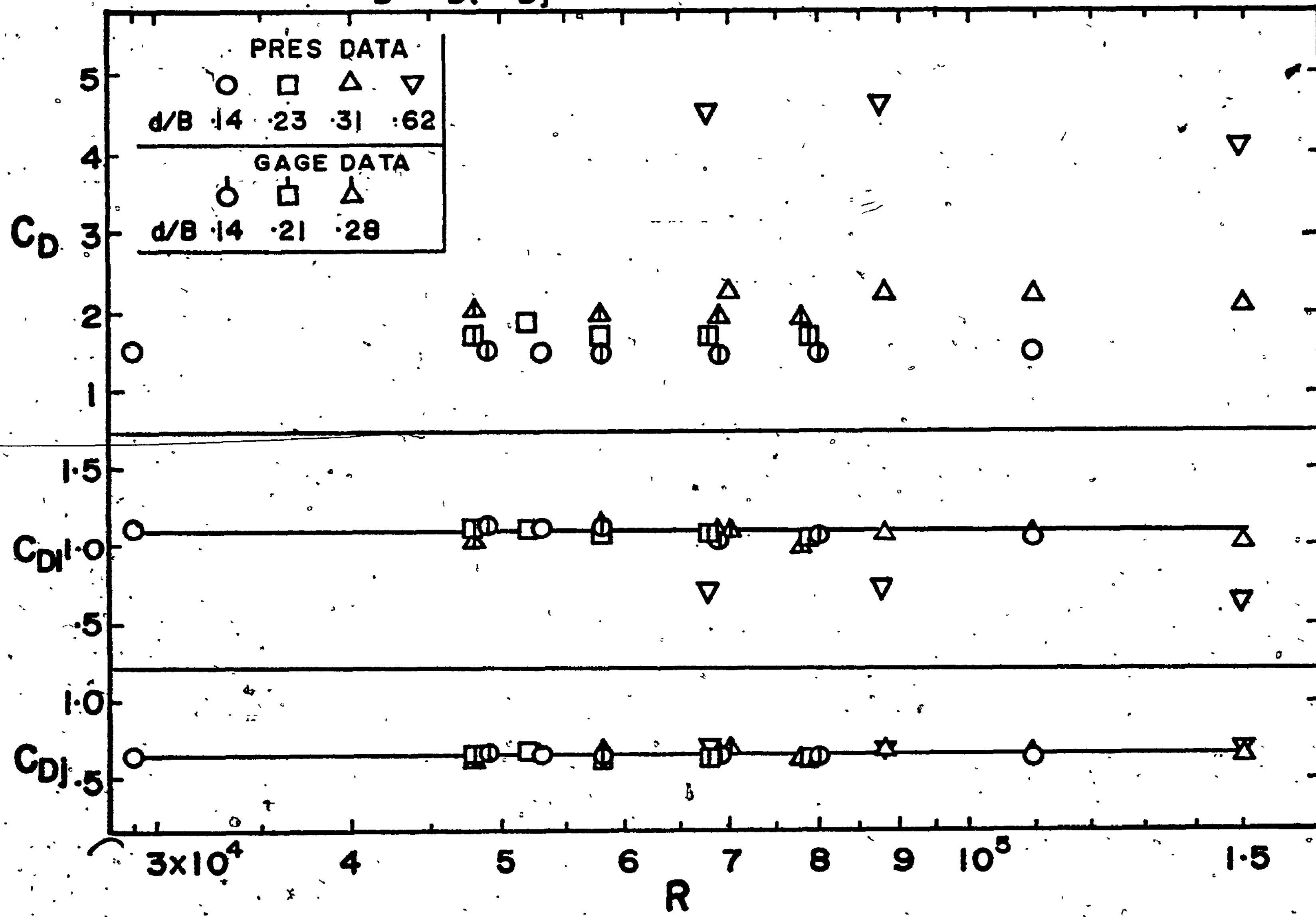

FIG 12 C_D, C_{DI}, C_{Dj} Vs d/B, CENTRAL CYLINDER

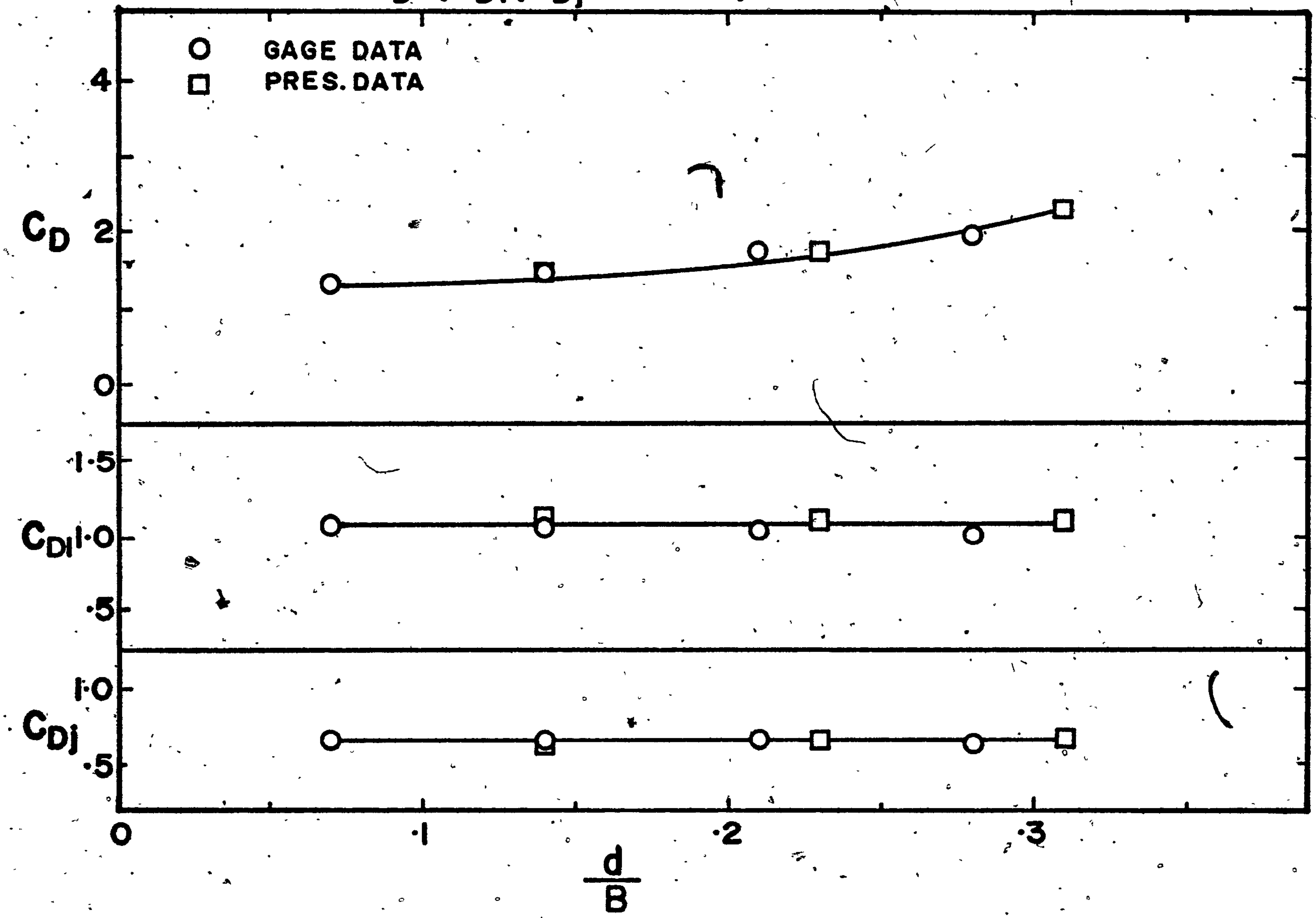

FIG 13 C_p FOR CYLINDER (d/B=·611, e/d=0)

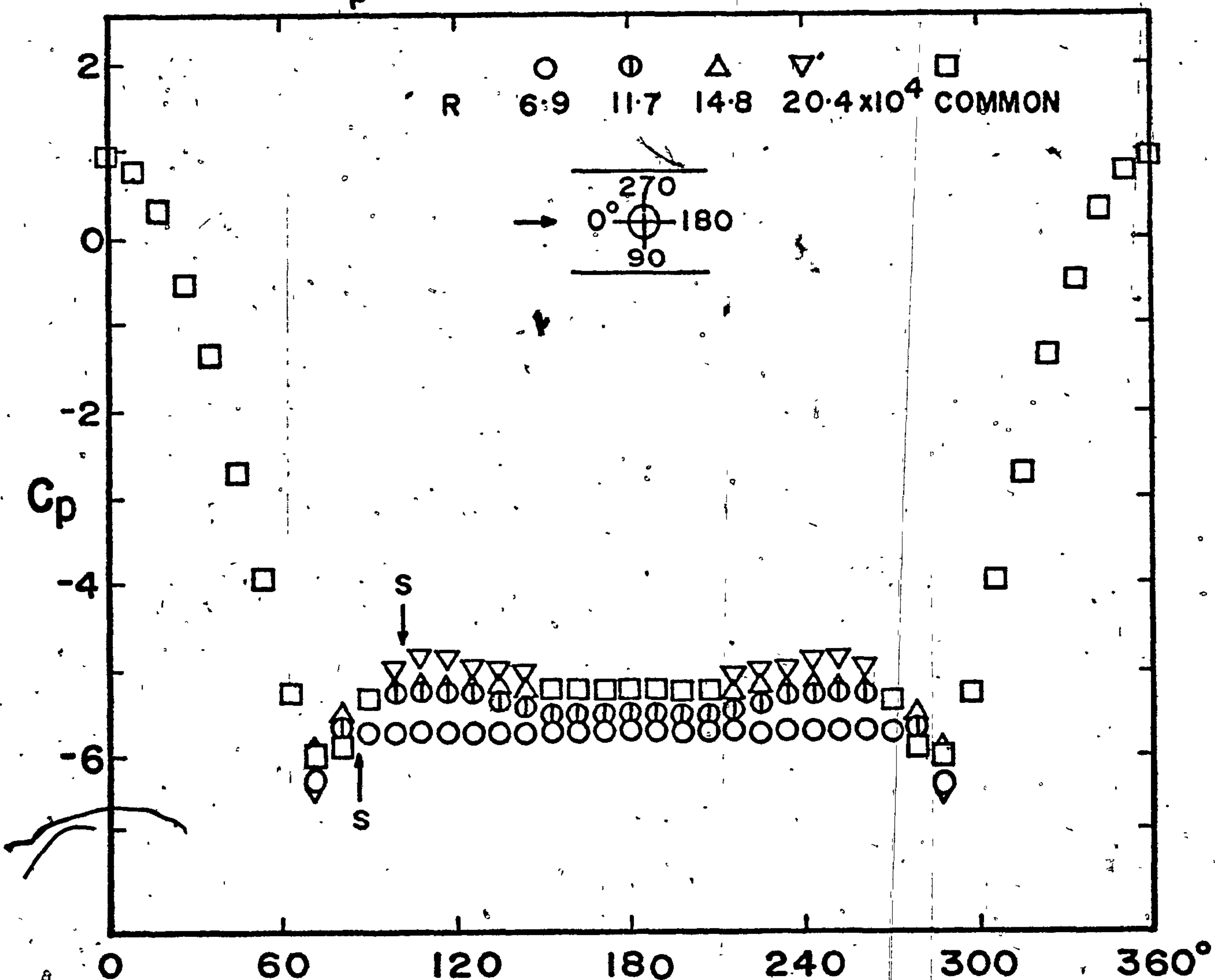

FIG 14 DRAG CONTRIBUTION, PRISMS, $\theta = 0^\circ$ & 60°

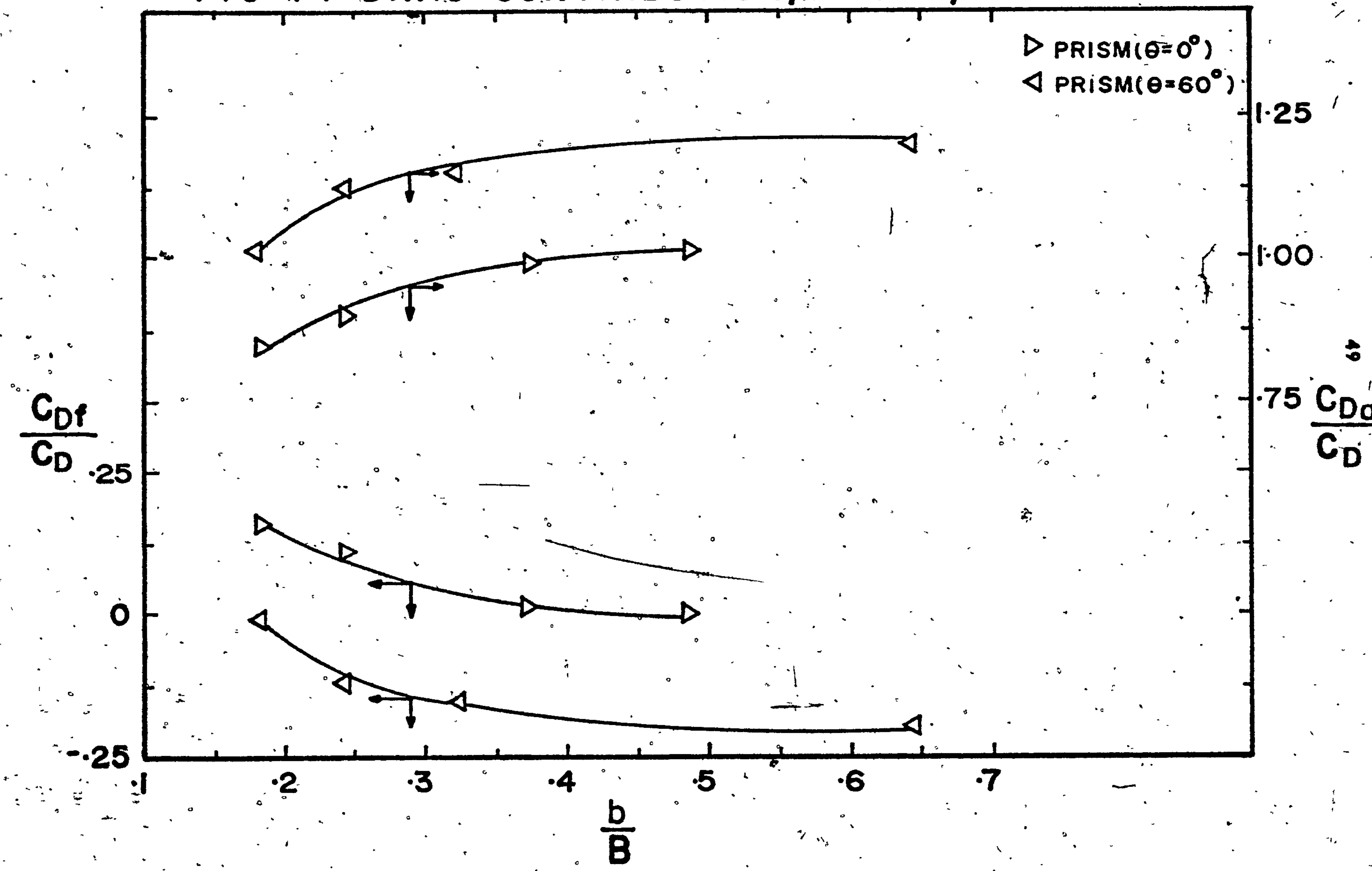

FIG 15 C_D, C_{DI}, C_{DI} Vs G/b, ECCENTRIC PRISM ($\theta=0°$)

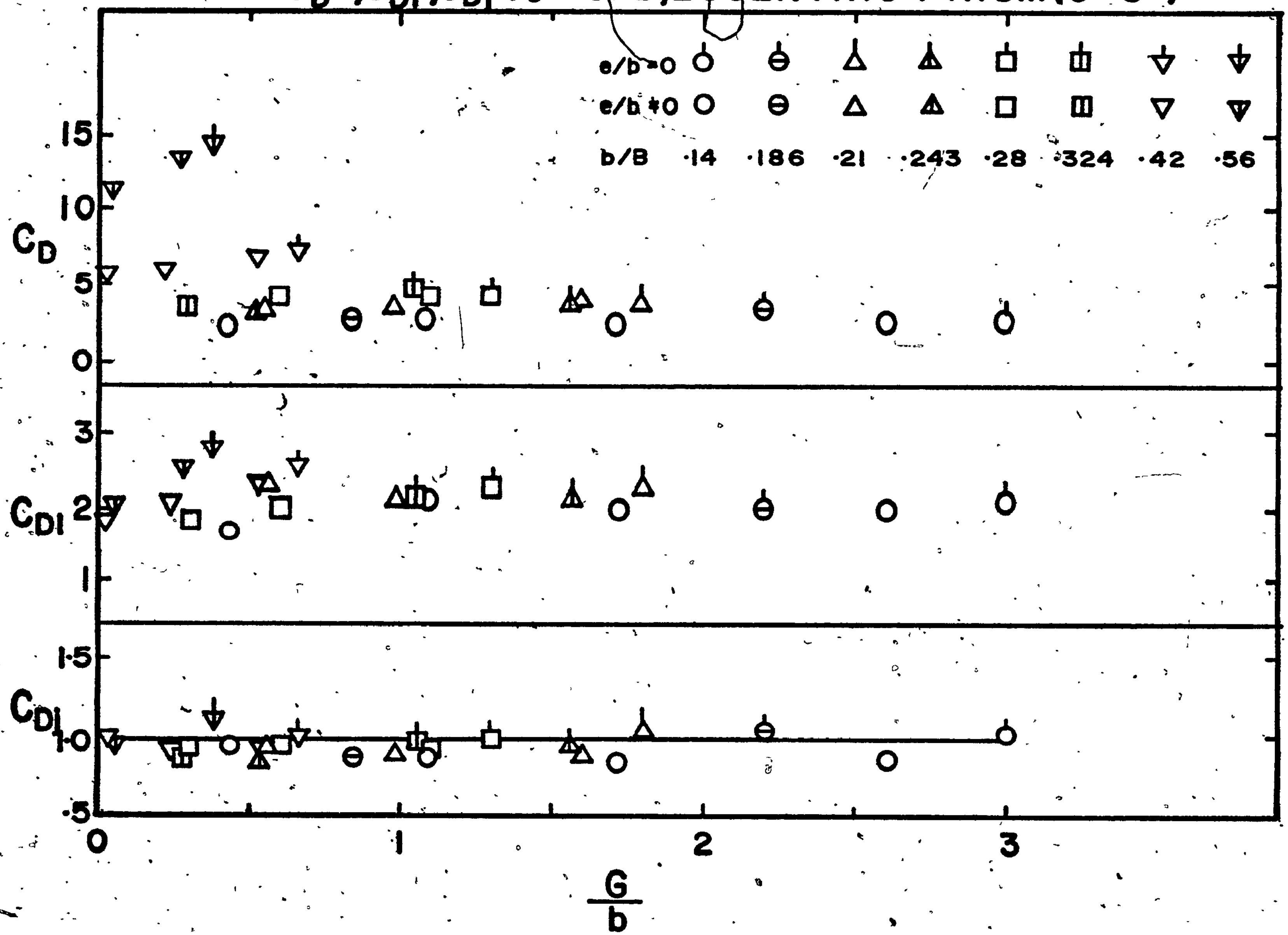

FIG 16 C_D, C_{DI}, C_{Dj} Vs G/b, ECCENTRIC PRISM (θ=60°)

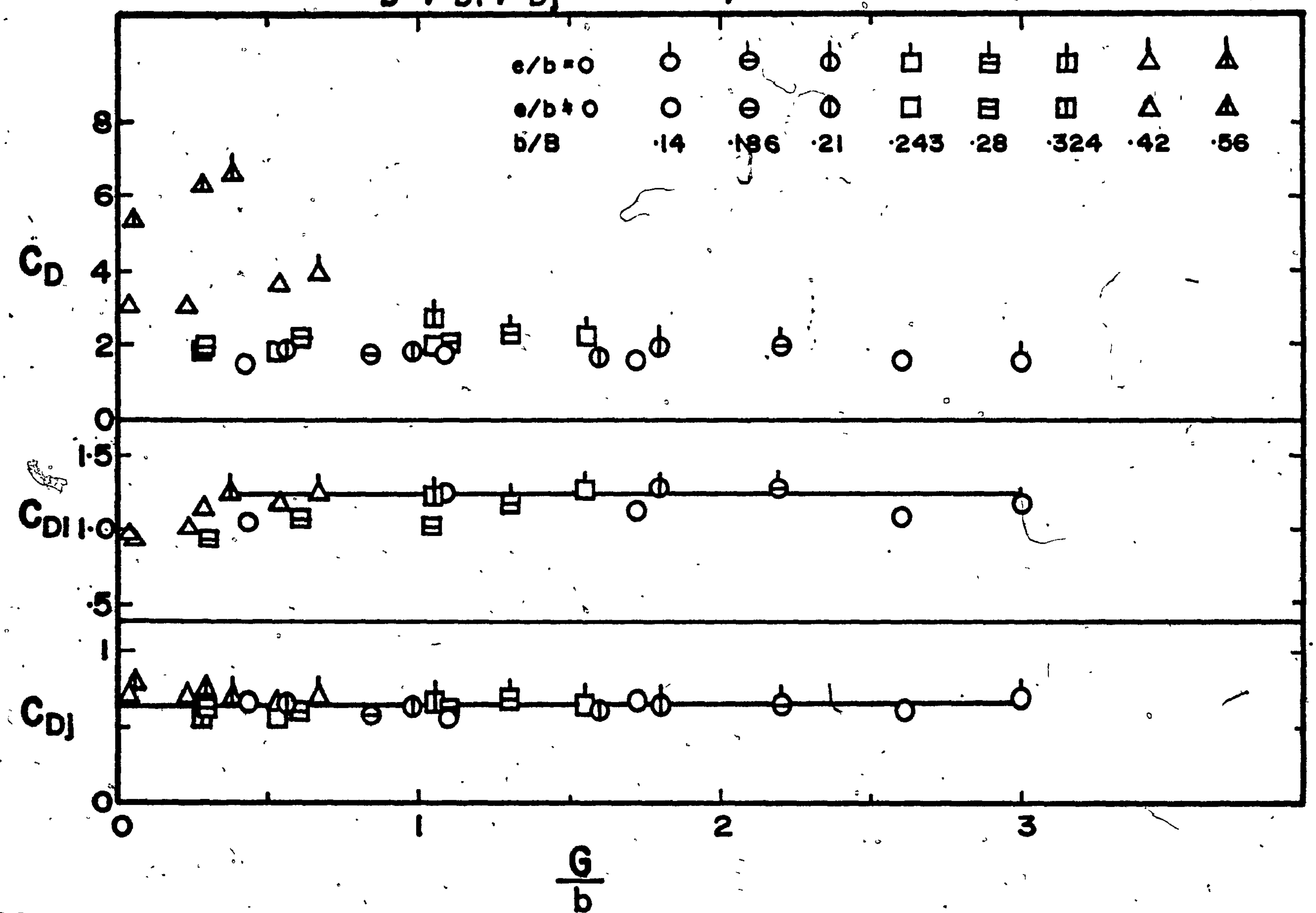

FIG 17 C_p FOR CYLINDER (d/B=·31, e/d=·82)

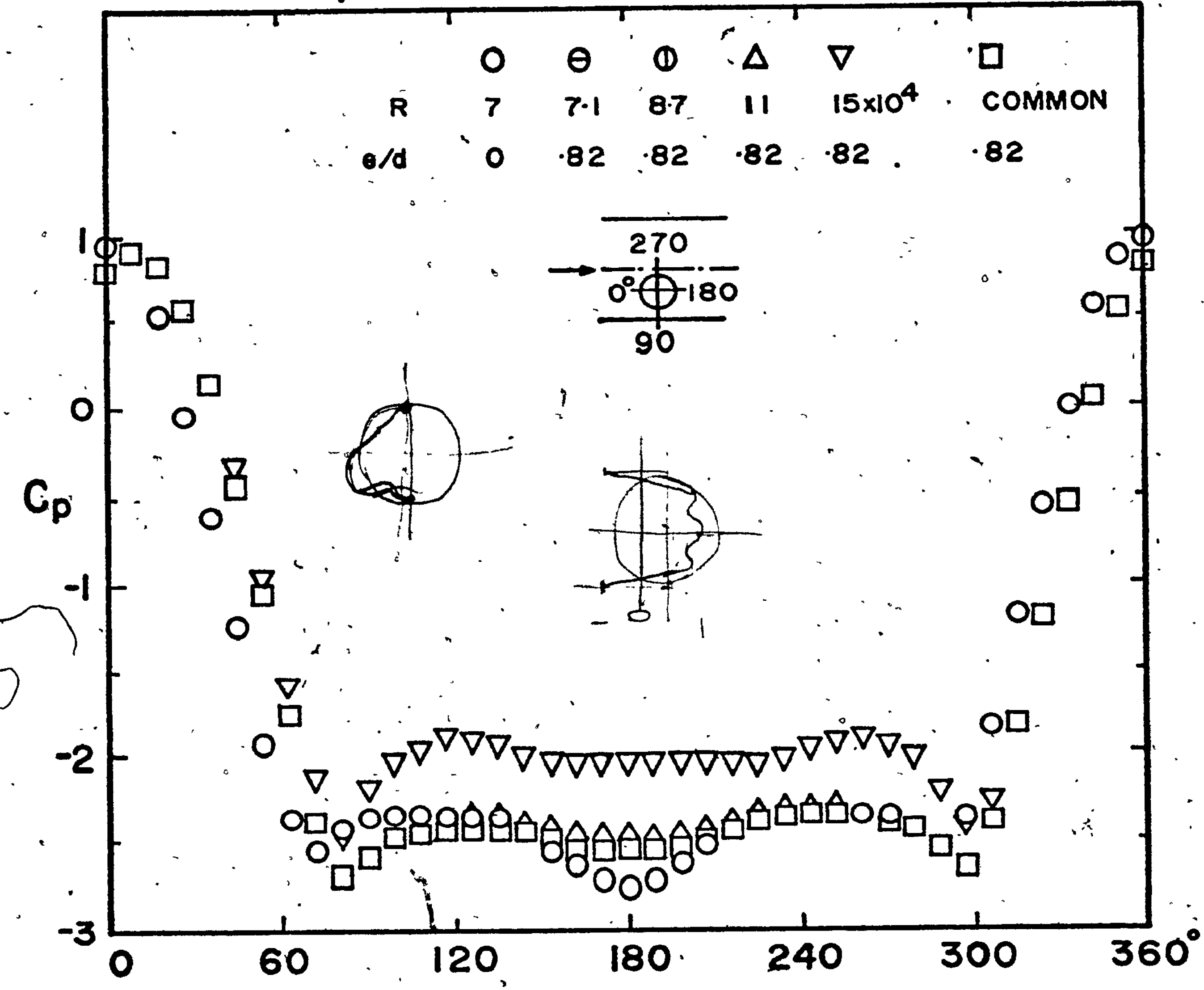

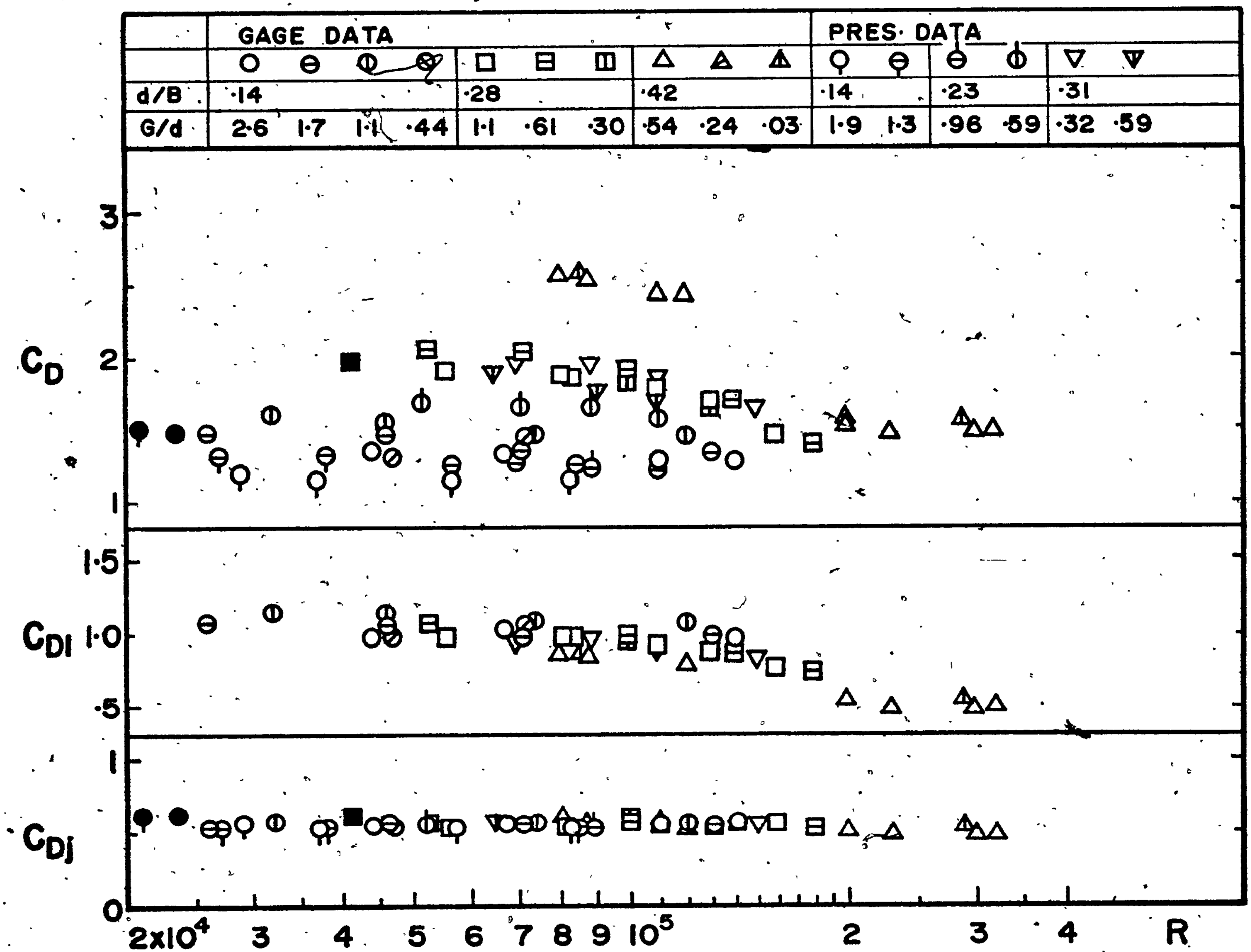

FIG 18 C_D, C_{DI}, C_{Dj}, Vs R, ECCENTRIC CYLINDER

FIG 19 C_D, C_{DI}, C_{Dj} Vs G/d, ECCENTRIC CYLINDER

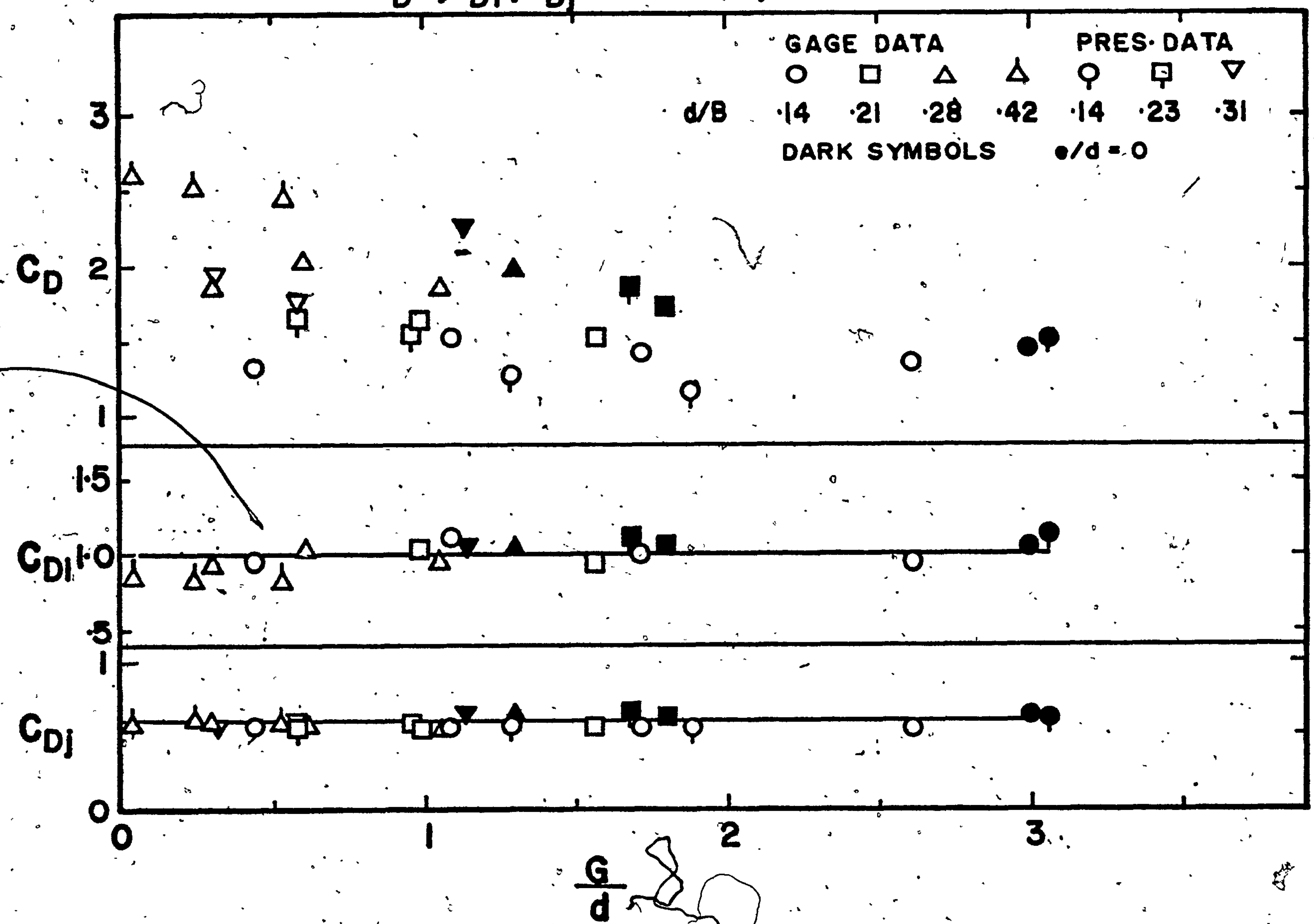

FIG 20 C_p, ECCENTRIC PRISM(θ=60°)

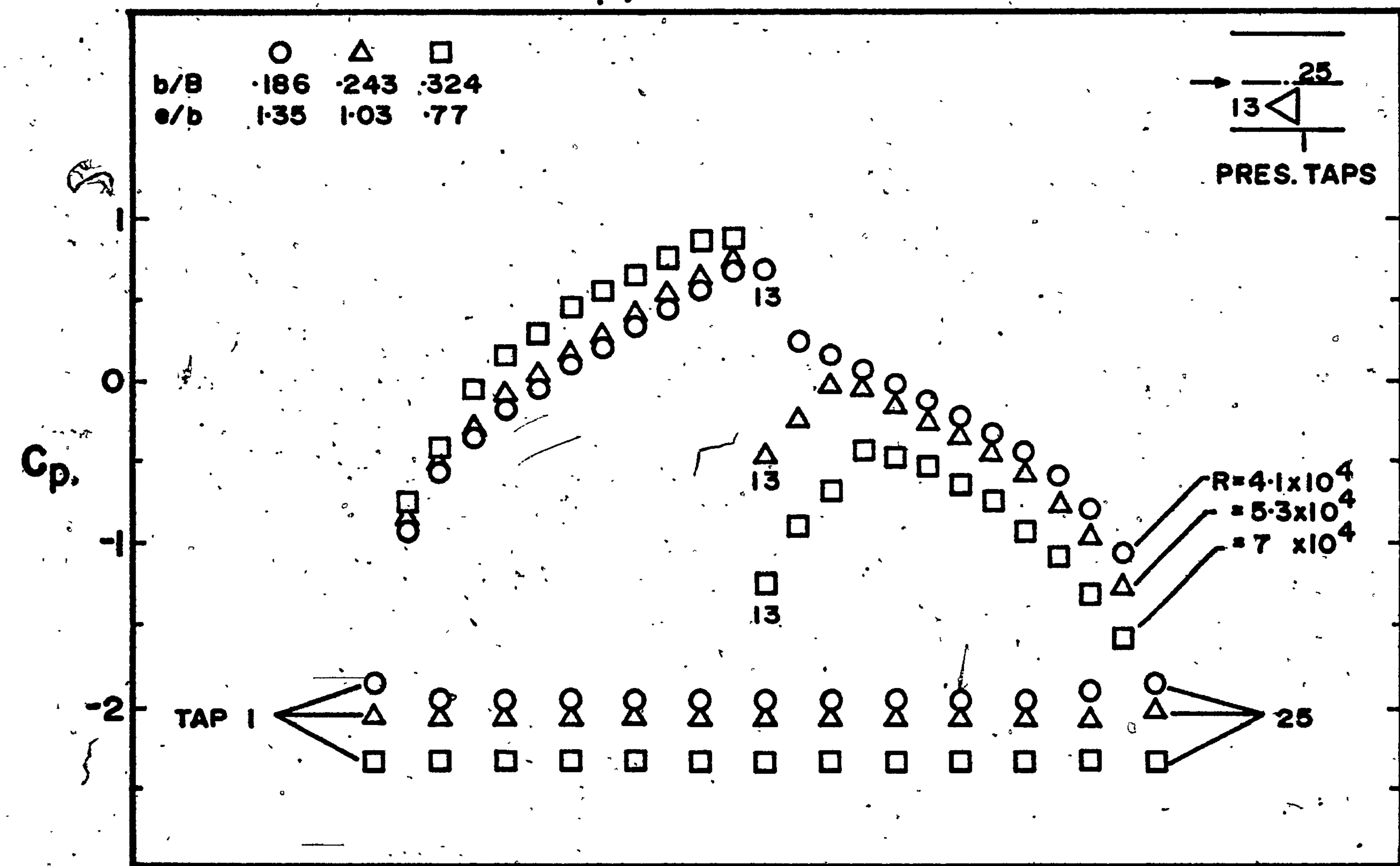

FIG 21 C_p, ECCENTRIC PRISM($\theta = 0°$)

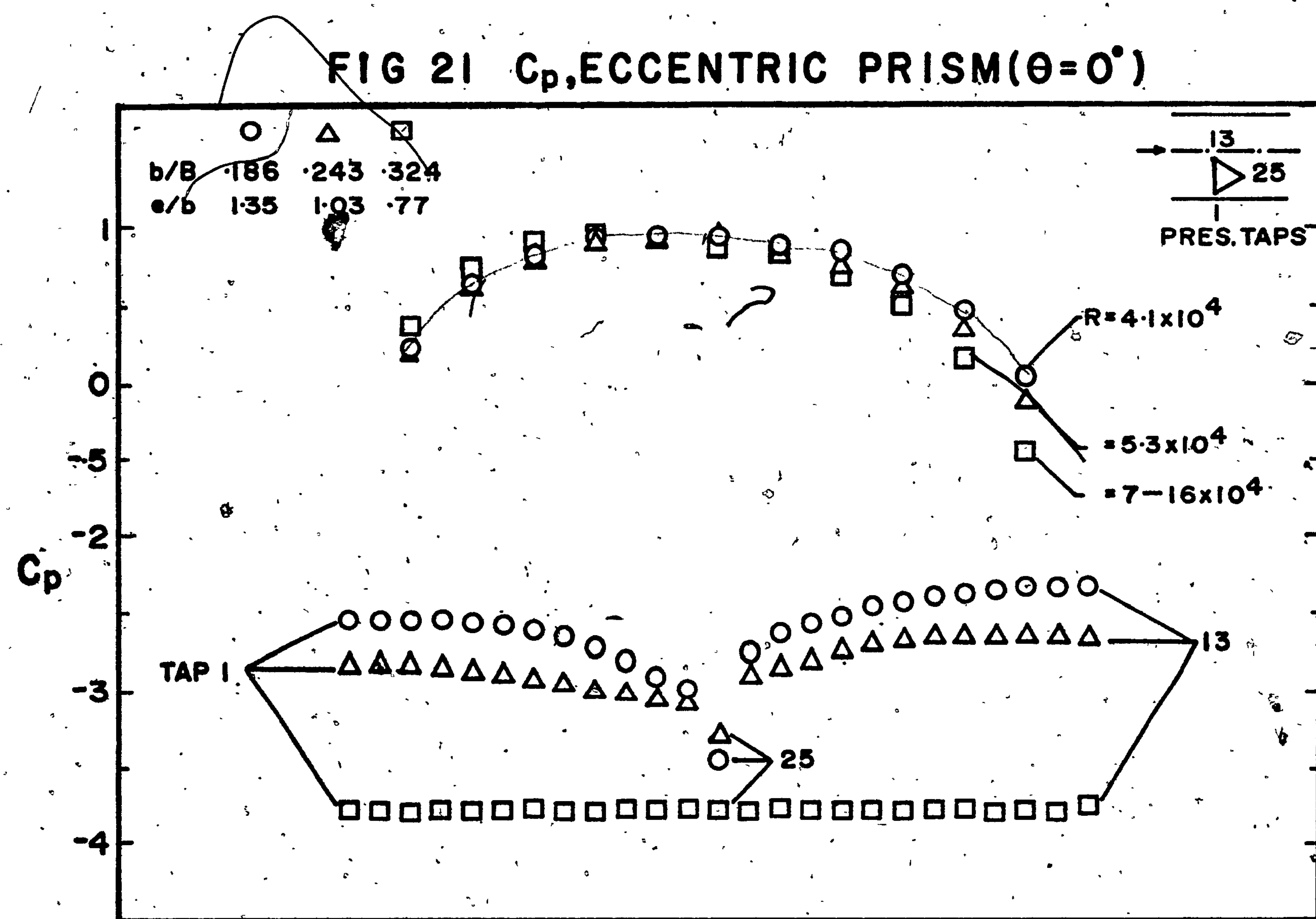

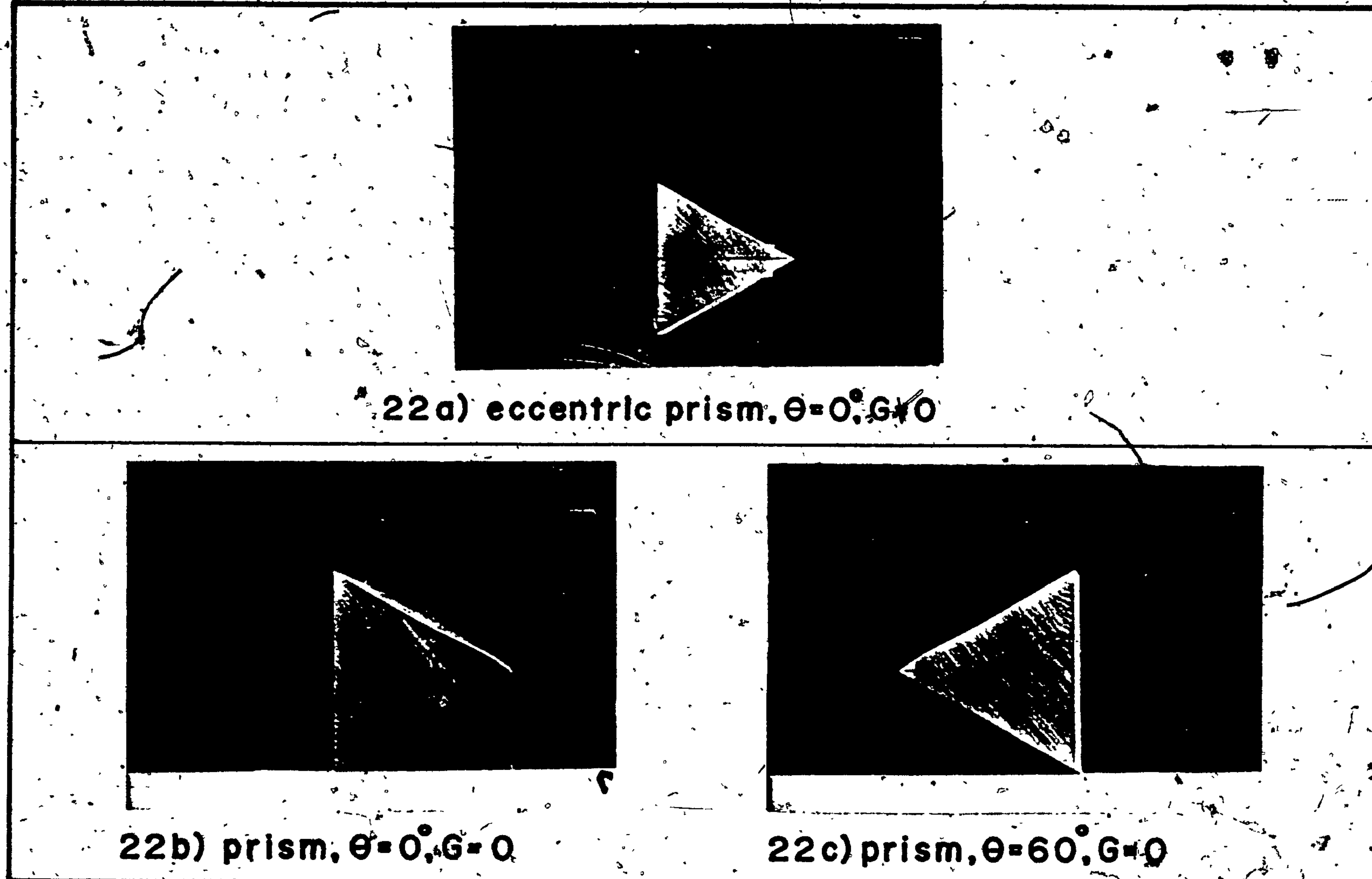

22a) eccentric prism, $\theta = 0°$, $G \neq 0$

22b) prism, $\theta = 0°$, $G = 0$

22c) prism, $\theta = 60°$, $G = 0$

FIG 22 FLOW PATTERN

FIG 23 Cp, PRISM(θ=0°), GAP=0

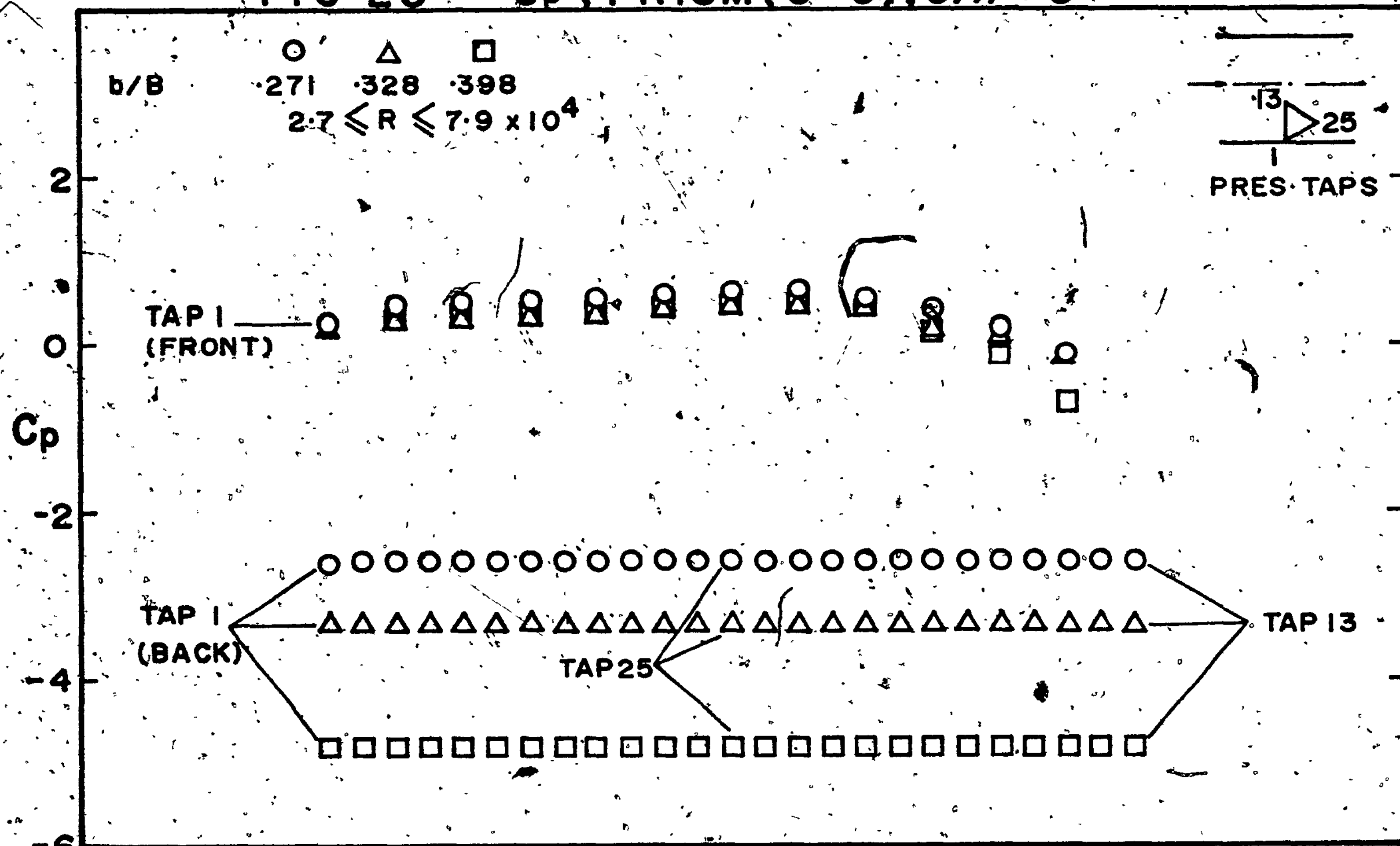

FIG 24 C_p, PRISM ($\theta=60^\circ$), GAP=0

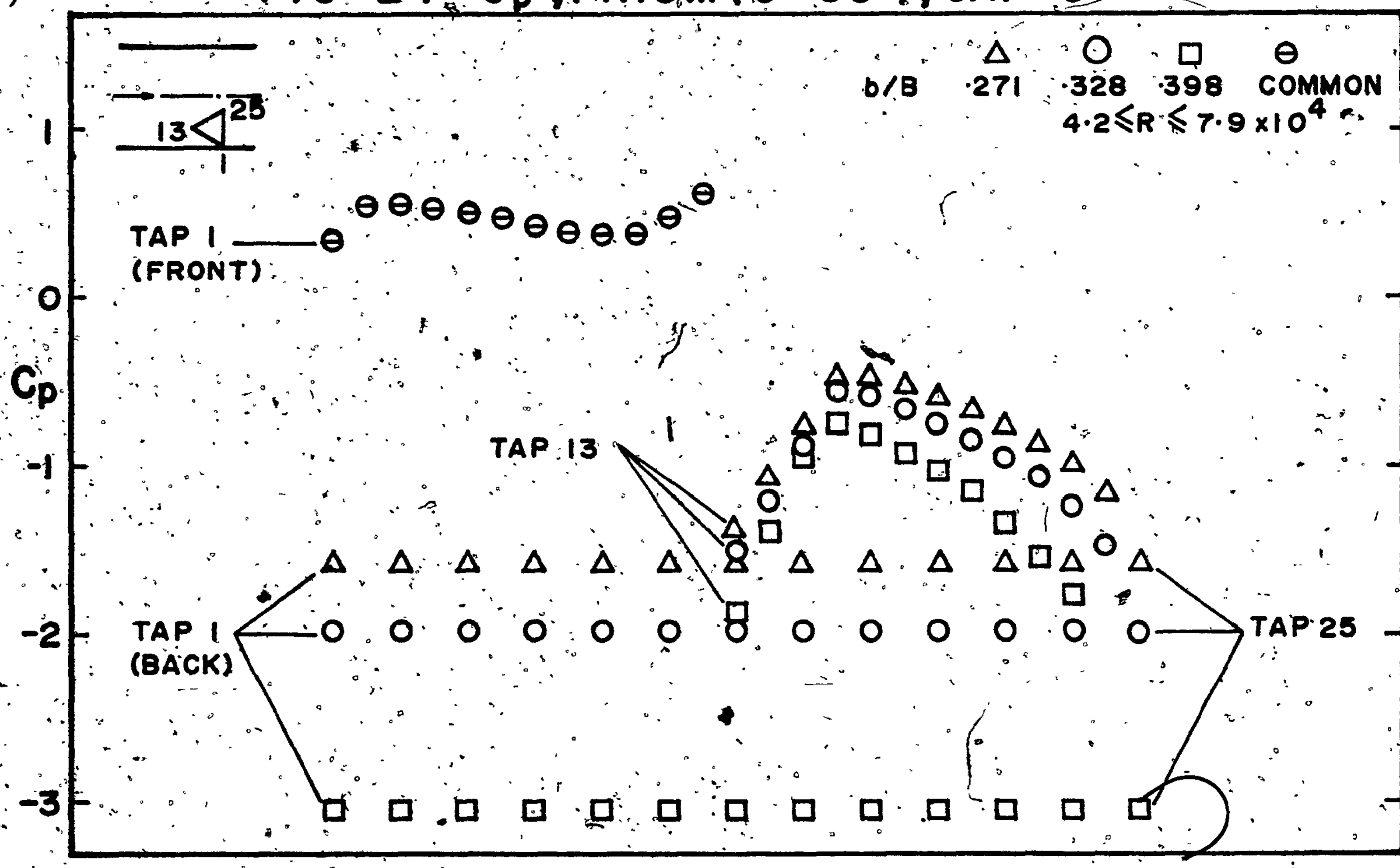

FIG 25 Cp , CYLINDER, GAP=0

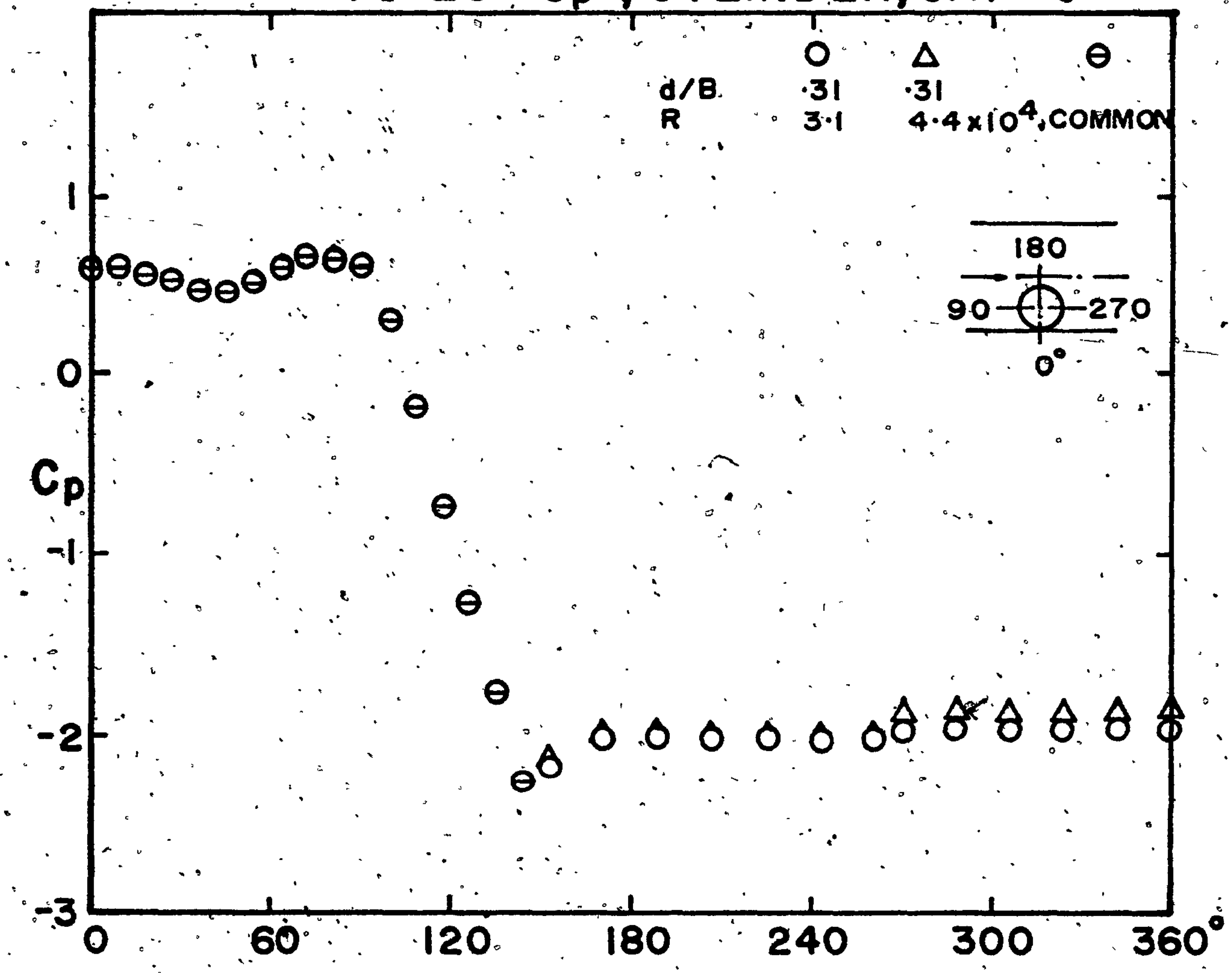

FIG 26 S, S_l, S_j Vs b/B, MULTIPLE PRISMS($\theta = 0°$)

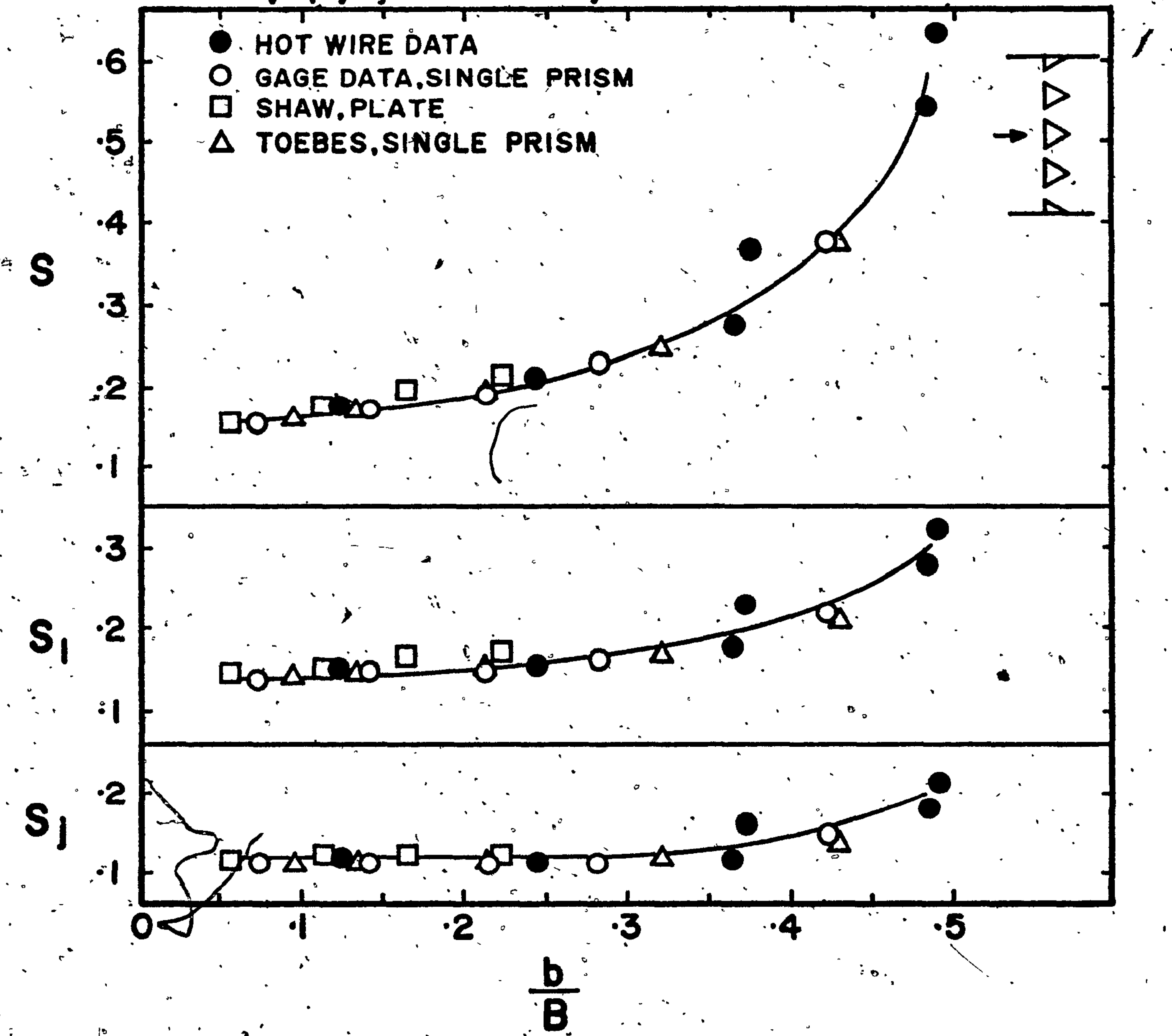

FIG 27 S, S_1 Vs b/B, MULTIPLE PRISMS (θ=60°)

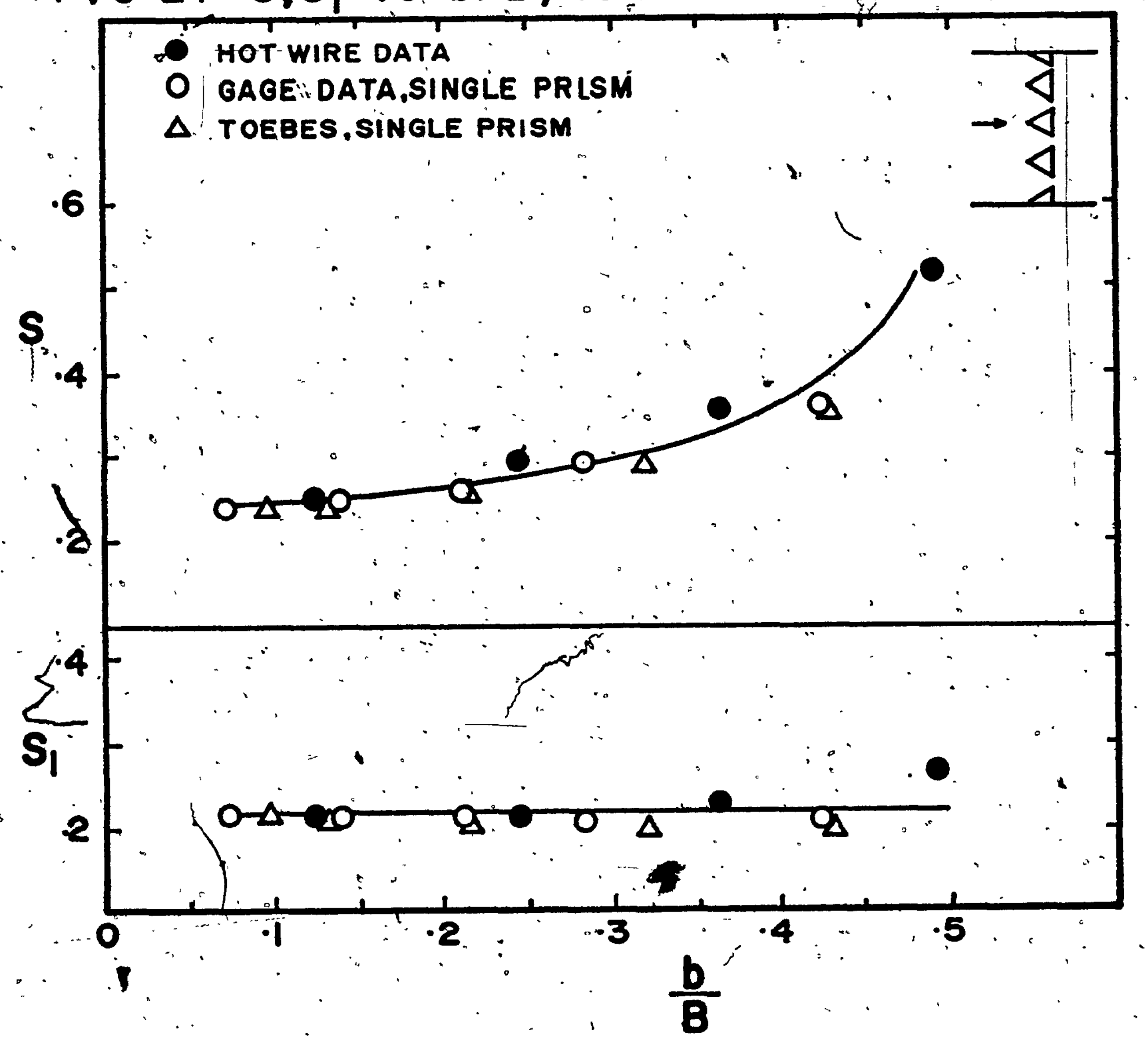

FIG 28 S, S_1 Vs d/B, MULTIPLE CYLINDERS

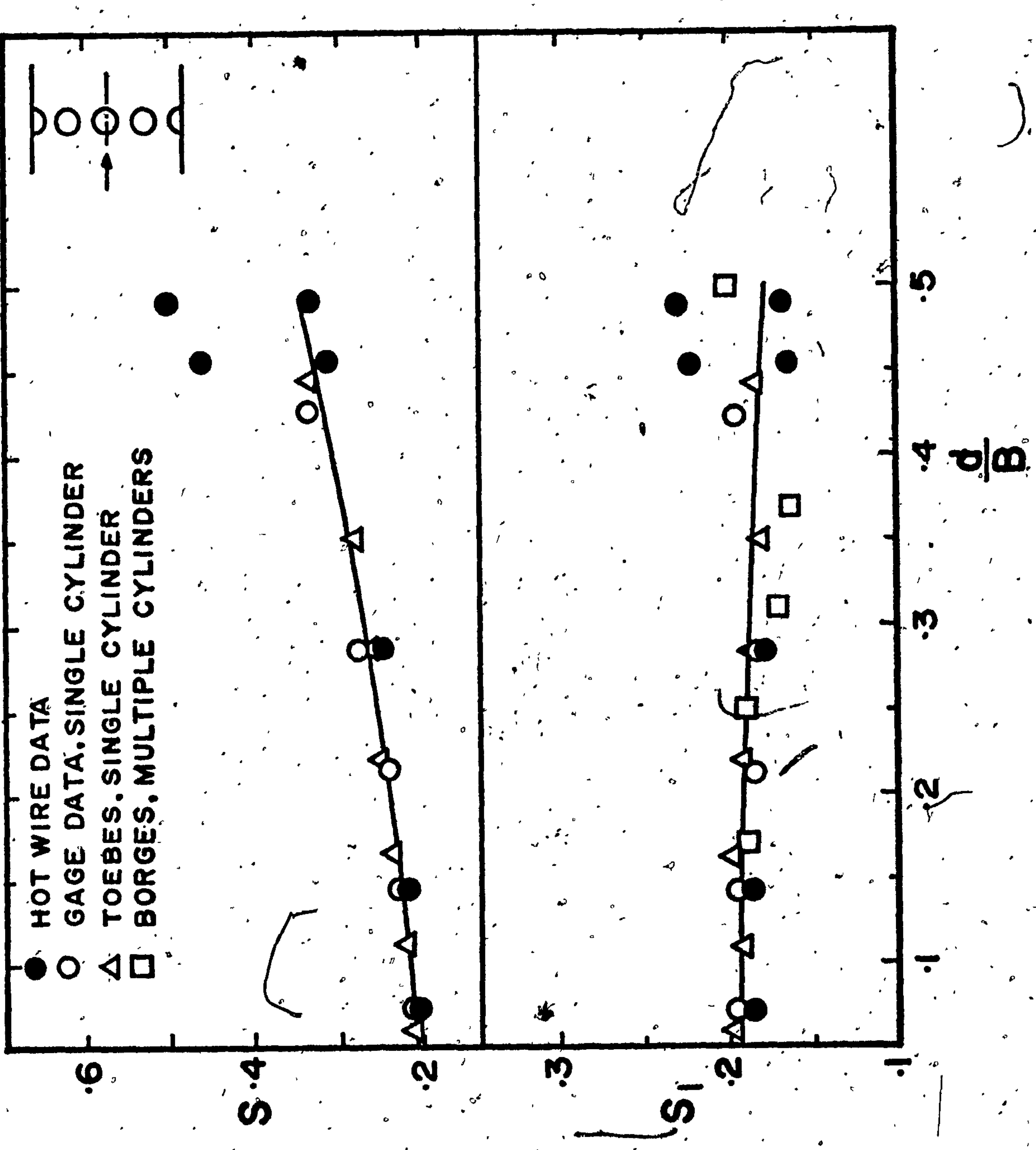

APPENDIX 1

COMPUTER PROGRAMS AND OUTPUT

```
C
C
C     PROGRAM 1   CD CD1 AND CDJ FOR TRIANGULAR PRISMS BASED UPON PRES
C                 SURE DISTRIBUTION.
C
C
      PROGRAM TRIAN(INPUT,OUTPUT)
      DIMENSION P(14,4),DG(4)
      REAL K
    1 FORMAT(5F10.4,I5/(8F10.4))
    2 FORMAT(8X,F5.3,F7.3,2F6.2,F8.3,F8.2,E9.2,F6.2,F7.2,3F6.2,F6.3,I8)
    3 FORMAT(8X,5HWIDTH,7H  BLOCK,6H   ECC,6H   GAP,8H  DELTAH,8H
     1U,9H        R,6H DRAG,7H    CPS,6H     K,6H    CD,6H   CD1,6H   C
     2DJ,8H   RUNNO,//)
    4 FORMAT(/)
   42 FORMAT(1H1,//////,13X,86HTABLE    CD CD1 CDJ FOR TRIANGULAR PRISMS
     1 AT 0 DEGREE,BASED UPON PRESSURE DISTRIBUTION,/)
   43 FORMAT(1H1,//////,13X,87HTABLE    CD CD1 CDJ FOR TRIANGULAR PRISMS
     1 AT 60 DEGREE,BASED UPON PRESSURE DISTRIBUTION,/)
      M=1
   11 READ 7,SHAPE
      IF(SHAPE.EQ.100.) GO TO 22
      IF(SHAPE.EQ.1..OR.SHAPE.EQ.2.) GO TO 6
      IF(SHAPE.EQ.3.) GO TO 40
      IF(SHAPE.EQ.4.) GO TO 41
      GO TO 8
   40 PRINT 42
      PRINT 3
      GO TO 8
   41 PRINT 43
      PRINT 3
      GO TO 8
    6 PRINT 4
    8 READ 1,D,H,E,CPB,W,N,((P(I,J),I=1,N),J=1,3)
      DO 17 J=1,3
      S=0.
      NN=N-1
      DO 10 I=1,NN
      A=P(I,J)+P(I+1,J)
      S=S+A
   10 CONTINUE
      IF(D.EQ.2.60) GO TO 12
      IF(D.EQ.3.40) GO TO 13
      IF(D.EQ.4.53) GO TO 70
      IF(J.EQ.3) GO TO 60
      DG(J)=.0144*S
      GO TO 17
   60 DG(J)=.0288*S
      GO TO 50
   70 IF(J.EQ.3) GO TO 14
      DG(J)=.0336*S
      GO TO 17
   14 DG(J)=.0672*S
      GO TO 50
   13 IF(J.EQ.3) GO TO 15
```

```
    7 FORMAT(F10.1)
      DG(J)=.0252*S
      GO TO 17
   15 DG(J)=.0504*S
      GO TO 50
   12 IF(J.EQ.3) GO TO 16
      DG(J)=.0193*S
   17 CONTINUE
   16 DG(J)=.0386*S
   50 IF(SHAPE.EQ.1..OR.SHAPE.EQ.3..OR.SHAPE.EQ.5.) GO TO 18
      DRAG=DG(2)+DG(1)-DG(3)
      GO TO 19
   18 DRAG=DG(3)-DG(2)-DG(1)
   19 DYNHD=5.194*H
      IF(E.EQ.0.) GO TO 32
      CD=14.49*DRAG/(DYNHD*D)
      GO TO 33
   32 CD=15.93*DRAG/(DYNHD*D)
   33 V=18.29*SQRT(H/.0753)
      RE=520.*V*D
      BR=D/W
      CD1=CD*(1.-BR)*(1.-BR)
      ECC=E/D
      IF(W.EQ.11.38.OR.W.EQ.10.38.OR.W.EQ.9.6) GO TO 34
      GAP=(W/2.-E-D/2.)/D
      GO TO 35
   34 GAP=0.
   35 K=SQRT(1.-CPB)
      CDJ=CD/(K*K)
      PRINT 2,D,BR,ECC,GAP,H,V,RE,DRAG,CPB,K,CD,CD1,CDJ,M
      M=M+1
      GO TO 11
   22 STOP
      END
```

TABLE 1 CD CD1 CDJ FOR TRIANGULAR PRISMS AT 0 DEGREE, BASED UPON PRESSURE DISTRIBUTION

WIDTH b	BLOCK b/B	ECC e/b	GAP G/b	DELTAH[1] in.	U fps	R	DRAG lbs	CPS	K	CD	CD1	CDJ	RUNNO
2.600	.186	0.00	2.19	.205	30.18	.44E+05	.59	-2.19	1.79	3.38	2.24	1.060	1
2.600	.186	0.00	2.19	.220	31.26	.42E+05	.62	-2.19	1.79	3.31	2.20	1.038	2
2.600	.371	0.00	.85	.217	31.05	.42E+05	1.10	-5.10	2.47	5.97	2.36	.979	3
2.600	.186	1.35	.85	.201	29.88	.40E+05	.56	-2.59	1.89	2.98	1.97	.830	4
2.600	.186	1.35	.85	.209	30.47	.41E+05	.57	-2.59	1.89	2.94	1.95	.818	5
2.600	.271	1.35	0.00	.420	43.20	.58E+05	1.08	-2.51	1.87	2.77	1.47	.789	6
3.400	.243	0.00	1.56	.203	30.03	.53E+05	.89	-3.03	2.01	3.95	2.27	.980	7
3.400	.243	0.00	1.56	.204	30.10	.53E+05	.86	-2.96	1.99	3.81	2.18	.962	8
3.400	.243	0.00	1.56	.314	37.35	.66E+05	1.34	-2.96	1.99	3.85	2.21	.973	9
3.400	.486	0.00	.53	.213	30.76	.54E+05	2.07	-8.04	3.01	8.77	2.32	.970	10
3.400	.243	1.03	.53	.204	30.10	.53E+05	.79	-2.85	1.96	3.20	1.83	.830	11
3.400	.328	1.03	0.00	.334	38.52	.68E+05	1.46	-3.34	2.08	3.5[illegible]	1.63	.828	12
4.530	.324	0.00	1.05	.201	29.88	.70E+05	1.46	-3.95	2.22	4.91	2.25	.992	13
4.530	.324	0.00	1.05	.219	31.19	.73E+05	1.56	-3.93	2.22	4.83	2.21	.980	14
4.530	.324	.77	.27	.201	29.88	.70E+05	1.31	-3.75	2.18	4.02	1.84	.847	15
4.530	.324	.77	.27	.342	38.98	.92E+05	2.25	-3.75	2.18	4.06	1.86	.854	16
4.530	.324	.77	.27	.600	51.63	.12E+06	3.89	-3.75	2.18	3.99	1.82	.840	17
4.530	.324	.77	.27	1.000	66.65	.14E+06	6.46	-3.75	2.18	3.98	1.82	.838	18
4.530	.398	.77	0.00	.252	33.46	.79E+05	1.91	-4.80	2.41	4.67	1.69	.805	19

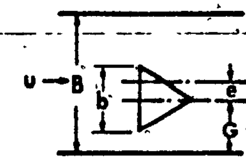

[1] DEFLECTION OF WATER COLUMN IN MANOMETRE

TABLE 1 CD CD1 CDJ FOR TRIANGULAR PRISMS AT 60 DEGREE BASED UPON PRESSURE DISTRIBUTION

WIDTH	BLOCK	ECC	GAP	DELTAH	U	R	DRAG	CPS	K	CD	CD1	CDJ	RUNNO
.850	.061	0.00	7.74	.190	29.05	.13E+05	.07	-.88	1.37	1.28	1.13	.677	20
.850	.061	0.00	7.74	.742	57.41	.25E+05	.27	-.86	1.37	1.30	1.15	.696	21
2.600	.186	0.00	2.19	.205	30.18	.41E+05	.34	-1.84	1.69	1.95	1.29	.686	22
2.600	.186	0.00	2.19	.220	31.26	.42E+05	.36	-1.84	1.69	1.91	1.27	.673	23
2.600	.186	1.35	.85	.204	30.10	.41E+05	.34	-1.95	1.72	1.77	1.17	.599	24
2.600	.186	1.35	.85	.210	30.54	.41E+05	.34	-1.95	1.72	1.74	1.15	.589	25
2.600	.271	1.35	0.00	.220	31.26	.42E+05	.28	-1.56	1.60	1.35	.72	.529	26
2.600	.271	1.35	0.00	.398	42.05	.57E+05	.50	-1.56	1.60	1.34	.71	.525	27
3.400	.243	0.00	1.56	.220	31.26	.55E+05	.52	-2.15	1.77	2.15	1.23	.683	28
3.400	.243	0.00	1.56	.225	31.62	.56E+05	.56	-2.15	1.77	2.25	1.29	.714	29
3.400	.243	1.03	.53	.205	30.18	.53E+05	.45	-2.10	1.76	1.81	1.04	.583	30
3.400	.243	1.03	.53	.214	30.83	.55E+05	.46	-2.10	1.76	1.77	1.01	.570	31
3.400	.328	1.03	0.00	.160	26.66	.47E+05	.33	-2.05	1.75	1.68	.76	.550	32
3.400	.328	1.03	0.00	.329	38.23	.68E+05	.70	-2.05	1.75	1.76	.79	.576	33
4.530	.324	0.00	1.05	.203	30.03	.71E+05	.80	-2.85	1.96	2.66	1.22	.692	34
4.530	.324	0.00	1.05	.210	30.54	.72E+05	.83	-2.85	1.96	2.69	1.23	.699	35
4.530	.324	.77	.27	.196	29.51	.70E+05	.61	-2.33	1.82	1.93	.88	.579	36
4.530	.324	.77	.27	.205	30.18	.71E+05	.64	-2.33	1.82	1.94	.89	.581	37
4.530	.398	.77	0.00	.085	19.43	.46E+05	.37	-3.04	2.01	2.71	.98	.671	38
4.530	.398	.77	0.00	.255	33.66	.79E+05	1.04	-3.04	2.01	2.52	.91	.623	39
4.530	.647	0.00	.27	.072	17.88	.42E+05	1.23	-12.80	3.71	11.57	1.44	.838	40
4.530	.647	0.00	.27	.173	27.72	.65E+05	3.04	-12.80	3.71	11.88	1.48	.861	41

```
C
C
C     PROGRAM 2   CD CD1 AND CDJ FOR CIRCULAR CYLINDERS BASED UPON PRES
C                 SURE DISTRIBUTION.
C
C
      PROGRAM CIRDRA(INPUT,OUTPUT)
      DIMENSION P(50)
      REAL LIFT,K
    1 FORMAT(5F10.4,I10/(8F10.4))
    2 FORMAT(8X,F5.3,F7.3,2F6.2,F8.3,F8.2,E9.2,F6.2,F7.2,3F6.2,F6.3,I8)
    3 FORMAT(8X,5HWIDTH,7H  BLOCK,6H   ECC,6H   GAP,8H  DELTAH,8H
     1U,9H         R,6H  DRAG,7H    CPS,6H     K,6H    CD,6H   CD1,6H   C
     2DJ,8H   RUNNO,//)
    4 FORMAT(/)
    5 FORMAT(1H1,//////,17X,76HTABLE    CD CD1 CDJ FOR CIRCULAR CYLINDER
     1S BASED UPON PRESSURE DISTRIBUTION,/)
    7 FORMAT(F10.1)
      N=1
   11 READ 7,SHAPE
      IF(SHAPE.EQ.100.) GO TO 22
      IF(SHAPE.EQ.10.) GO TO 6
      IF(SHAPE.EQ.1.) GO TO 40
      GO TO 8
   40 PRINT 5
      PRINT 3
      GO TO 8
    6 PRINT 4
    8 READ 1,D,H,E,CPB,W,J,(P(I),I=1,J)
      M=J-1
      DELTHE=6.283/M
      S=0.
      DO 10 I=1,M
      A=P(I)+P(I+1)
      B=A*COS((I-.5)*DELTHE)
      S=S+B
   10 CONTINUE
      R=D/2.
      DRAG=-.178*DELTHE*R*S
      SS=0.
      DO 20 I=1,M
      A=P(I)+P(I+1)
      C=A*SIN((I-.5)*DELTHE)
      SS=SS+C
   20 CONTINUE
      LIFT=-.178*DELTHE*R*SS
      DYNHD=5.194*H
      IF(E.EQ.0.) GO TO 30
      CD=14.49*DRAG/(DYNHD*D)
      CL=14.49*LIFT/(DYNHD*D)
      GO TO 31
   30 CD=15.93*DRAG/(DYNHD*D)
      CL=0.
   31 V=18.29*SQRT(H/.0753)
      RE=520.*V*D
```

```
      BR=D/W
      CD1=CD*(1.-BR)*(1.-BR)
      ECC=E/D
      IF(W.EQ.7.) GO TO 21
      IF(W.EQ.11.38.OR.W.FQ.10.25) GO TO 26
      GAP=(W/2.-E-D/2.)/D
      GO TO 23
   26 GAP=0.
      GO TO 23
   21 GAP=(3.5-E-D/2.)/D
   23 K=SQRT(1.-CPB)
      CDJ=CD/(K*K)
      PRINT 2,D,BR,ECC,GAP,H,V,RF,DRAG,CPB,K,CD,CD1,CDJ,N
      N=N+1
      GO TO 11
   22 STOP
      END
```

TABLE 2 CD CD1 CDJ FOR CIRCULAR CYLINDERS BASED UPON PRESSURE DISTRIBUTION.

WIDTH	BLOCK	ECC	GAP	DELTAH	U	R	DRAG	CPS	K	CD	CD1	CDJ	RUNNO
1.961	.140	0.00	3.07	.180	28.28	.29E+05	.17	-1.35	1.53	1.51	1.12	.645	1
1.961	.140	0.00	3.07	.609	52.01	.53E+05	.58	-1.35	1.53	1.50	1.11	.639	2
1.961	.140	1.19	1.88	.183	28.51	.29E+05	.15	-1.20	1.48	1.20	.89	.546	3
1.961	.140	1.19	1.88	.297	36.32	.37E+05	.24	-1.24	1.50	1.15	.85	.516	4
1.961	.140	1.19	1.88	.700	55.77	.57E+05	.56	-1.24	1.50	1.19	.85	.512	5
1.961	.140	1.19	1.88	1.500	81.63	.83E+05	1.21	-1.29	1.51	1.15	.85	.503	6
1.961	.140	1.78	1.28	.156	28.33	.27E+05	.14	-1.38	1.54	1.30	.96	.545	7
1.961	.140	1.78	1.28	.316	37.47	.38E+05	.29	-1.43	1.56	1.31	.97	.539	8
1.961	.140	1.78	1.28	.708	56.08	.57E+05	.63	-1.40	1.55	1.26	.94	.527	9
1.961	.140	1.78	1.28	1.570	83.52	.85E+05	1.38	-1.42	1.56	1.25	.93	.518	10
3.200	.229	0.00	1.69	.219	31.19	.52E+05	.43	-1.75	1.66	1.87	1.11	.681	11
3.200	.229	.73	.96	.192	29.21	.40E+05	.31	-1.40	1.55	1.42	.85	.592	12
3.200	.229	.73	.96	.397	42.00	.70E+05	.58	-1.44	1.56	1.28	.76	.525	13
3.200	.229	.73	.96	.642	53.41	.89E+05	.90	-1.40	1.55	1.22	.73	.510	14
3.200	.229	.73	.96	1.030	67.64	.11E+06	1.44	-1.40	1.55	1.21	.72	.506	15
3.200	.229	1.09	.59	.220	31.26	.52E+05	.43	-2.00	1.73	1.69	1.01	.565	16
3.200	.229	1.09	.59	.409	42.63	.71E+05	.77	-2.00	1.73	1.64	.98	.548	17
3.200	.229	1.09	.59	.649	53.70	.89E+05	1.23	-2.00	1.73	1.65	.98	.551	18
3.200	.229	1.09	.59	1.005	66.82	.11E+06	1.80	-2.00	1.73	1.57	.93	.522	19
3.200	.312	1.09	0.00	.068	17.38	.29E+05	.14	-1.94	1.71	1.77	.84	.603	20
3.200	.314	1.09	-.00	.160	26.66	.44E+05	.31	-1.94	1.71	1.70	.80	.578	21
3.200	.312	1.09	0.00	.341	38.92	.65E+05	.58	-1.70	1.64	1.49	.70	.550	22

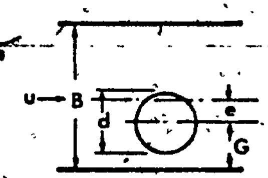

TABLE 2 CD CDI CDJ FOR CIRCULAR CYLINDERS BASED UPON PRESSURE DISTRIBUTION,

WIDTH	BLOCK	ECC	GAP	DELTAH	U	P	DRAG	CPS	K	CD	CDI	CDJ	RUNNO
4.280	.306	0.00	1.14	.220	31.26	.70E+05	.70	-2.30	1.82	2.28	1.10	.690	23
4.280	.306	0.00	1.14	.210	30.54	.68E+05	.66	-2.30	1.82	2.26	1.09	.686	24
4.280	.306	0.00	1.14	.355	39.71	.89E+05	1.11	-2.30	1.82	2.24	1.08	.678	25
4.280	.306	0.00	1.14	.590	51.20	.11E+06	1.83	-2.30	1.82	2.23	1.07	.674	26
4.280	.306	0.00	1.14	.990	66.32	.15E+06	2.91	-2.30	1.82	2.11	1.02	.639	27
4.280	.611	0.00	.32	.210	30.54	.68E+05	1.34	-5.75	2.60	4.97	.69	.677	28
4.280	.611	0.00	.32	.355	39.71	.89E+05	2.29	-5.58	2.57	4.63	.70	.704	29
4.280	.611	0.00	.32	.615	52.27	.12E+06	3.69	-5.26	2.50	4.30	.65	.687	30
4.280	.611	0.00	.32	.990	66.32	.15E+06	5.66	-5.05	2.46	4.10	.62	.677	31
4.280	.611	0.00	.32	1.860	90.90	.20E+06	10.23	-4.90	2.43	3.94	.60	.668	32
4.280	.306	.54	.59	.191	29.13	.65E+05	.53	-2.08	1.75	1.79	.86	.582	33
4.280	.306	.54	.59	.374	40.76	.91E+05	1.01	-2.08	1.75	1.76	.85	.571	34
4.280	.306	.54	.59	.600	51.63	.11E+06	1.57	-2.06	1.75	1.70	.82	.556	35
4.280	.306	.82	.32	.221	31.33	.70E+05	.65	-2.50	1.87	1.93	.93	.550	36
4.280	.306	.82	.32	.360	39.99	.89E+05	1.06	-2.50	1.87	1.92	.93	.549	37
4.280	.306	.82	.32	.585	50.98	.11E+06	1.69	-2.50	1.87	1.88	.91	.537	38
4.280	.306	.82	.32	.996	66.18	.15E+06	2.46	-2.00	1.73	1.63	.78	.542	39
4.280	.376	[illegible]	[illegible]	.067	17.25	.39E+05	.22	-2.40	1.84	2.10	.82	.618	40
4.280	.376	[illegible]	[illegible]	.069	19.88	.44E+05	.28	-2.40	1.84	2.04	.79	.600	41
4.280	.376	.82	0.00	.145	25.38	.56E+05	.42	-2.35	1.83	1.90	.74	.568	42
4.280	.376	.82	0.00	.223	31.48	.70E+05	.58	-2.10	1.76	1.69	.66	.545	43
4.280	.376	.82	0.00	.415	42.94	.96E+05	.89	-1.80	1.67	1.39	.54	.498	44

```
C
C
C     PROGRAM 3   CDT CD CDI AND CDJ FOR ECCENTRIC TRIANGULAR PRISMS
C                 AND CYLINDERS.
C
C
      PROGRAM ECCEN(INPUT,OUTPUT)
      REAL L,K
    1 FORMAT(8F10.4)
    4 FORMAT(10X,F5.1,F6.2,F5.2, F6.2,F8.3,F8.2,E9.2,F7.3,2F7.2,F6.2,4F7
     1.2,I8)
    5 FORMAT(10X,5HWIDTH,6H BLOCK,5H  ECC,6H   XAP,8H  DELTAH,8H       U
     1,9H        R,7H  VOLT,7H  DRAG,7H   CPS,6H     K,7H   CDT,7H
     2   CD,7H   CDI,7H   CDJ,8H   RUNNO,//)
    6 FORMAT(/)
    7 FORMAT(10X,5HWIDTH,6H BLOCK,5H  ECC,6H   XAP,8H  DELTAH,8H       U
     1,9H        R,7H  VOLT,7H  DRAG,7H   CPS,6H     K,7H    CD,7H
     2  CDI,7H   CDJ,8H   RUNNO,//)
   16 FORMAT(1H1,//////,32X,68HTABLE     CDT CD CDI CDJ FOR ECCENTRIC TR
     1IANGULAR PRISMS AT 0 DEGREE,/)
   17 FORMAT(1H1,//////,32X,69HTABLE     CDT CD CDI CDJ FOR ECCENTRIC TR
     1IANGULAR PRISMS AT 60 DEGREE,/)
   18 FORMAT(1H1,//////,36X,57HTABLE     CD CDI AND CDJ FOR ECCENTRIC CI
     1RCULAR CYLINDERS,/)
   51 FORMAT(10X,F5.1,F6.2,F5.2, F6.2,F8.3,F8.2,E9.2,F7.3,2F7.2,F6.2,3F7
     1.2,I8)
   55 FORMAT(32X,                         F8.3,F8.2,E9.2,F7.3,2F7.2,F6.2,4F7
     1.2,I8)
   57 FORMAT(32X,                         F8.3,F8.2,E9.2,F7.3,2F7.2,F6.2,3F7
     1.2,I8)
      N=1
   30 READ 1,SHAPE
      IF(SHAPE.EQ.0.) GO TO 20
      IF(SHAPE.EQ.20.) GO TO 11
      IF(SHAPE.EQ.30.) GO TO 12
      IF (SHAPE.EQ.40.) GO TO 13
      IF(SHAPE.EQ.50..OR.SHAPE.EQ.70.) GO TO 14
      GO TO 10
   11 PRINT 16
      PRINT 5
      GO TO 10
   12 PRINT 17
      PRINT 5
      GO TO 10
   13 PRINT 18
      PRINT 7
      GO TO 10
   14 PRINT 6
   10 READ 1,D,L,F,PATM,H,VOLT,PT,PR
      P=PATM*.489-PT*.0359
      GAMMA=.00508*P
      V=18.29*SQRT(H/GAMMA)
      RE=520.*V*D
      DRAG=VOLT/.1145
      AREA=D*L/144.
```

```
      RHO=GAMMA/32.2
      CD=2.*DRAG/(RHO*V*V*AREA)
      B=D/14.
      CD1=CD*(1.-B)*(1.-B)
      ECC=E/D
      GAP=(7.-E-D/2.)/D
      F=5.17*(PB-PT)
      K=SQRT(1.+2.*F/(RHO*V*V))
      CPB=1.-K*K
      CDJ=CD/(K*K)
C     COMPUTE THE THEORETICAL DRAG BY USING MOM BAL RELATION.
      CDT=(K-1.)*(K-1.)/B
      IF(SHAPE.EQ.20..OR.SHAPE.EQ.30..OR.SHAPE.EQ.50.) GO TO 53
      IF(SHAPE.EQ.60.) GO TO 54
      IF(SHAPE.EQ.40..OR.SHAPE.EQ.70.)                        GO TO 50
      PRINT 57,H,V,RE,VOLT,DRAG,CPB,K,CD,CD1,CDJ,N
      GO TO 52
   53 PRINT 4,D,B,ECC,GAP,H,V,RE,VOLT,DRAG,CPB,K,CDT,CD,CD1,CDJ,N
      GO TO 52
   54 PRINT 55,H,V,RE,VOLT,DRAG,CPB,K,CDT,CD,CD1,CDJ,N
      GO TO 52
   50 PRINT 51,D,B,ECC,GAP,H,V,RE,VOLT,DRAG,CPB,K,CD,CD1,CDJ,N
   52 N=N+1
      GO TO 30
   20 STOP
      END
```

TABLE 3 CDT CD CDI CDJ FOR ECCENTRIC TRIANGULAR PRISMS AT 0 DEGREE

WIDTH	BLOCK	ECC	GAP	DELTAH	U	R	VOLT	DRAG	CPS	K	CDT	CD	CDI	CDJ	RUNNO
1.0	.07	3.81	2.69	.700	56.50	.29E+05	.071	.62	-2.27	1.81	9.18	2.52	2.17	.77	1
				2.310	102.88	.53E+05	.230	2.01	-2.29	1.81	9.29	2.47	2.13	.75	2
				5.030	152.44	.79E+05	.500	4.37	-2.29	1.81	9.28	2.47	2.13	.75	3
2.0	.14	.39	2.61	.391	41.92	.44E+05	.084	.73	-2.27	1.81	4.56	2.67	1.96	.82	4
				.949	65.36	.69E+05	.207	1.81	-2.19	1.79	4.33	2.71	1.99	.85	5
				2.343	102.92	.11E+06	.519	4.53	-2.20	1.79	4.37	2.75	2.02	.86	6
				2.794	112.46	.12E+06	.617	5.39	-2.20	1.79	4.36	2.74	2.01	.86	7
2.0	.14	1.28	1.72	.152	26.24	.27E+05	.034	.30	-2.16	1.78	4.24	2.79	2.05	.88	8
				.443	44.81	.47E+05	.096	.84	-2.22	1.80	4.43	2.69	1.98	.83	9
				.932	65.05	.64E+05	.202	1.76	-2.30	1.82	4.66	2.69	1.98	.82	10
				1.942	94.04	.94E+05	.425	3.71	-2.35	1.83	4.83	2.72	2.00	.81	11
2.0	.14	1.91	1.09	.165	27.22	.28E+05	.038	.33	-2.41	1.85	5.03	2.86	2.10	.84	12
				.416	43.24	.45E+05	.095	.83	-2.58	1.89	5.58	2.85	2.09	.80	13
				.986	66.63	.69E+05	.229	2.00	-2.49	1.87	5.29	2.88	2.12	.83	14
2.0	.14	2.56	.44	.220	31.44	.33E+05	.039	.34	-1.45	1.56	2.23	2.22	1.63	.91	15
				.410	42.93	.45E+05	.075	.65	-1.46	1.57	2.25	2.26	1.66	.92	16
				.870	66.09	.69E+05	.176	1.54	-1.44	1.56	2.20	2.25	1.66	.92	17
				2.530	106.97	.11E+06	.464	4.05	-1.48	1.57	2.30	2.28	1.67	.92	18
				3.510	126.18	.13E+06	.642	5.61	-1.48	1.57	2.31	2.27	1.67	.92	19
3.0	.21	.26	1.57	.160	26.99	.42E+05	.066	.58	-3.05	2.01	4.78	3.41	2.11	.84	20
				.498	47.64	.74E+05	.203	1.77	-2.96	1.99	4.57	3.37	2.08	.85	21
				.910	64.44	.10E+06	.373	3.26	-2.91	1.98	4.46	3.39	2.09	.87	22
				1.958	94.67	.15E+06	.810	7.07	-2.95	1.99	4.55	3.42	2.11	.87	23
3.0	.21	.85	.98	.170	27.82	.43E+05	.069	.61	-2.81	1.95	4.23	3.38	2.09	.89	24
				.491	47.30	.74E+05	.202	1.76	-2.82	1.95	4.25	3.41	2.10	.89	25
				.916	64.65	.10E+06	.375	3.28	-2.85	1.96	4.31	3.39	2.09	.88	26
				1.340	78.25	.12E+06	.559	4.88	-2.93	1.98	4.50	3.45	2.13	.88	27
3.0	.21	1.27	.55	.181	28.70	.45E+05	.065	.57	-2.31	1.82	3.13	2.97	1.84	.90	28
				.489	47.20	.74E+05	.179	1.56	-2.36	1.83	3.24	3.03	1.87	.90	29
				.909	64.40	.10E+06	.337	2.94	-2.40	1.84	3.32	3.07	1.89	.90	30
				1.565	84.59	.13E+06	.601	5.25	-2.44	1.85	3.40	3.18	1.96	.93	31

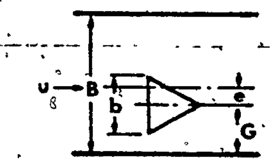

TABLE 3 CDT CD CDI CDJ FOR ECCENTRIC TRIANGULAR PRISMS AT 0 DEGREE

WIDTH	BLOCK	ECC	GAP	DELTAH	U	R	VOLT	DRAG	CPS	K	CDT	CD	CDI	CDJ	RUNNO
4.0	.29	.23	1.05	.149	25.89	.54E+05	.097	.85	-3.54	2.13	4.48	4.04	2.06	.89	32
				.268	34.73	.72E+05	.177	1.55	-3.57	2.14	4.52	4.10	2.09	.90	33
				.460	45.51	.95E+05	.310	2.71	-3.66	2.16	4.69	4.19	2.14	.90	34
				.890	63.35	.13E+06	.597	5.21	-3.56	2.13	4.51	4.16	2.12	.91	35
				1.235	74.66	.16E+06	.829	7.24	-3.55	2.13	4.49	4.17	2.13	.92	36
4.0	.29	.64	.61	.165	27.36	.57E+05	.111	.97	-3.38	2.09	4.18	4.16	2.12	.95	37
				.265	34.68	.72E+05	.170	1.49	-3.31	2.07	4.04	3.99	2.04	.93	38
				.550	49.98	.10E+06	.354	3.09	-3.29	2.07	4.02	3.99	2.04	.93	39
				.915	64.51	.13E+06	.591	5.17	-3.34	2.08	4.11	4.01	2.05	.92	40
				1.175	73.12	.15E+06	.762	6.65	-3.45	2.11	4.30	4.02	2.05	.90	41
4.0	.29	.95	.30	.160	26.83	.56E+05	.090	.78	-2.86	1.97	3.26	3.48	1.77	.90	42
				.270	34.86	.73E+05	.155	1.35	-2.95	1.99	3.41	3.57	1.82	.90	43
				.532	48.95	.10E+06	.304	2.65	-2.94	1.98	3.39	3.54	1.81	.90	44
				.911	64.09	.13E+06	.521	4.55	-2.92	1.98	3.36	3.55	1.81	.91	45
				1.690	87.40	.18E+06	.973	8.49	-2.96	1.99	3.42	3.57	1.82	.90	46
6.0	.43	.13	.54	.139	25.01	.79E+05	.226	1.97	-6.23	2.69	6.65	6.73	2.20	.93	47
				.320	37.95	.12E+06	.538	4.69	-6.38	2.72	6.87	6.95	2.27	.94	48
				.910	64.06	.20E+06	1.525	13.32	-6.45	2.73	6.98	6.94	2.26	.93	49
6.0	.43	.43	.24	.150	25.96	.81E+05	.225	1.97	-5.64	2.58	5.80	6.21	2.03	.93	50
				.355	39.94	.12E+06	.538	4.70	-5.75	2.60	5.96	6.27	2.05	.93	51
				.298	63.58	.20E+06	1.366	11.93	-5.92	2.63	6.20	6.30	2.06	.91	52
				1.310	76.84	.24E+06	1.966	17.17	-5.94	2.63	6.23	6.21	2.03	.89	53
6.0	.43	.63	.03	.312	37.47	.12E+06	.454	3.96	-4.88	2.43	4.74	6.02	1.97	1.02	54
				.879	62.95	.20E+06	1.717	10.63	-4.90	2.43	4.77	5.73	1.87	.97	55
				1.510	82.59	.26E+06	2.067	18.05	-5.01	2.45	4.92	5.67	1.85	.94	56
8.0	.57	.10	.28	.152	26.21	.11E+06	.654	5.71	-13.49	3.81	13.78	13.36	2.45	.92	57
				.230	32.25	.13E+06	.993	8.67	-13.41	3.80	13.69	13.40	2.46	.93	58
				.409	43.02	.18E+06	1.768	15.44	-13.65	3.83	13.99	13.42	2.46	.92	59
				.559	50.30	.21E+06	2.413	21.07	-13.76	3.84	14.14	13.40	2.46	.91	60
8.0	.57	.32	.05	.176	28.19	.12E+06	.637	5.56	-10.63	3.41	10.17	11.23	2.06	.97	61
				.251	33.67	.14E+06	.908	7.93	-10.63	3.41	10.16	11.23	2.06	.97	62
				.451	45.14	.19E+06	1.644	14.36	-10.81	3.44	10.39	11.31	2.08	.96	63

TABLE 3 CDT CD CDI CDJ FOR ECCENTRIC TRIANGULAR PRISMS AT 60 DEGREE

WIDTH	BLOCK	ECC	GAP	DELTAH	U	P	VOLT	DRAG	CPS	K	CDT	CD	CDI	CDJ	RUNNO
1.0	.07	3.81	2.69	.155	26.56	.14E+05	.010	.09	-2.05	1.75	7.83	1.60	1.38	.52	64
				.662	54.94	.29E+05	.040	.35	-1.88	1.70	6.80	1.50	1.29	.52	65
				2.196	100.29	.52E+05	.128	1.12	-1.79	1.67	6.32	1.45	1.25	.52	66
				5.380	156.54	.81E+05	.307	2.68	-1.76	1.66	6.10	1.44	1.24	.52	67
2.0	.14	.39	2.61	.168	27.47	.29E+05	.021	.18	-1.60	1.61	2.62	1.55	1.14	.60	68
				.349	39.60	.41E+05	.042	.37	-1.48	1.58	2.32	1.49	1.10	.60	69
				.919	64.32	.67E+05	.110	.96	-1.49	1.58	2.35	1.49	1.10	.60	70
				2.290	101.74	.11E+06	.274	2.39	-1.44	1.56	2.21	1.49	1.09	.61	71
				3.661	128.90	.13E+06	.438	3.83	-1.44	1.56	2.21	1.49	1.09	.61	72
2.0	.14	1.28	1.72	.165	27.34	.28E+05	.021	.18	-1.33	1.53	1.93	1.58	1.16	.68	73
				.330	41.50	.43E+05	.047	.41	-1.39	1.55	2.08	1.54	1.13	.64	74
				.955	65.85	.69E+05	.110	.96	-1.39	1.54	2.08	1.43	1.05	.60	75
2.0	.14	1.91	1.09	.180	28.43	.30E+05	.026	.23	-2.05	1.75	3.89	1.79	1.32	.59	76
				.368	40.67	.42E+05	.050	.44	-2.06	1.75	3.92	1.69	1.24	.55	77
				.810	60.38	.63E+05	.111	.97	-2.09	1.76	4.02	1.70	1.25	.55	78
				2.040	95.99	.10E+06	.276	2.41	-2.03	1.74	3.84	1.68	1.23	.55	79
2.0	.14	2.56	.44	.220	31.44	.33E+05	.025	.22	-1.27	1.51	1.79	1.41	1.04	.62	80
				.366	40.56	.42E+05	.042	.37	-1.31	1.52	1.88	1.42	1.05	.62	81
				.802	60.08	.62E+05	.092	.80	-1.25	1.50	1.76	1.42	1.05	.63	82
				2.190	99.48	.13E+06	.246	2.15	-1.18	1.4[illegible]	1.59	1.39	1.02	.64	83
				4.090	136.33	.14E+06	.446	3.90	-1.15	1.47	1.53	1.35	.99	.63	84

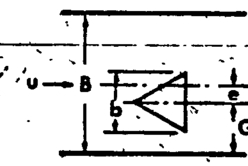

TABLE 3 CDT CD CD1-CDJ FOR ECCENTRIC TRIANGULAR PRISMS AT 60 DEGREE

WIDTH	BLOCK	ECC	GAP	DELTAH	U	R	VOLT	DRAG	CPS	K	CDT	CD	CD1	CDJ	RUNNO
3.0	.21	.26	1.57	.172	27.98	.44E+05	.036	.31	-1.79	1.67	2.10	1.71	1.05	.61	85
				.470	46.28	.72E+05	.092	.80	-1.74	1.65	2.00	1.62	1.00	.59	86
				.888	63.65	.99E+05	.173	1.51	-1.63	1.62	1.80	1.61	1.00	.61	87
				1.995	95.57	.15E+06	.383	3.34	-1.60	1.61	1.74	1.59	.98	.61	88
3.0	.21	.85	.98	.141	25.33	.40E+05	.031	.27	-2.05	1.75	2.59	1.83	1.13	.60	89
				.455	45.53	.71E+05	.097	.85	-1.88	1.70	2.27	1.76	1.09	.61	90
				.905	64.26	.10E+06	.195	1.70	-1.86	1.69	2.23	1.78	1.10	.62	91
				2.075	97.48	.15E+06	.440	3.84	-1.87	1.69	2.25	1.76	1.08	.61	92
3.0	.21	1.27	.56	.140	25.24	.30E+05	.033	.29	-2.13	1.77	2.77	1.95	1.20	.62	93
				.500	47.73	.74E+05	.112	.98	-1.85	1.69	2.21	1.85	1.14	.65	94
				.880	63.36	.99E+05	.197	1.72	-1.93	1.71	2.37	1.85	1.14	.63	95
4.0	.29	.20	1.05	.170	27.75	.59E+05	.058	.50	-2.40	1.84	2.49	2.10	1.07	.62	96
				.501	47.66	.99E+05	.164	1.43	-2.36	1.83	2.44	2.03	1.04	.60	97
				.890	63.56	.13E+06	.284	2.48	-2.08	1.76	2.00	1.98	1.01	.64	98
				1.480	82.04	.17E+06	.473	4.13	-2.25	1.80	2.25	1.98	1.01	.61	99
4.0	.29	.64	.64	.140	25.20	.52E+05	.048	.42	-2.56	1.89	2.75	2.13	1.09	.60	100
				.286	36.03	.75E+05	.099	.86	-2.63	1.90	2.86	2.15	1.10	.59	101
				.480	46.69	.97E+05	.165	1.44	-2.49	1.87	2.64	2.13	1.09	.61	102
				.900	63.97	.13E+06	.301	2.63	-2.42	1.85	2.53	2.08	1.06	.61	103

TABLE 3. CDT CD CDI CDJ FOR ECCENTRIC TRIANGULAR PRISMS AT 60 DEGREE

WIDTH	BLOCK	ECC.	GAP	DELTAH	U	R	VOLT	DRAG	CPS	K	CDT	CD	CDI	CDJ	RUNNO
4.0	.29	.95	.30	.310	37.32	.78E+05	.094	.82	-1.93	1.71	1.77	1.88	.96	.64	104
				.572	50.72	.11E+06	.170	1.48	-1.98	1.73	1.85	1.84	.96	.62	105
				.886	63.15	.13E+06	.261	2.28	-1.95	1.72	1.81	1.83	.93	.62	106
				1.840	91.14	.19E+06	.546	4.77	-1.92	1.71	1.76	1.84	.94	.63	107
6.0	.43	.13	.54	.151	26.13	.82E+05	.129	1.13	-4.28	2.30	3.94	3.54	1.15	.67	108
				.330	38.64	.12E+06	.284	2.48	-4.25	2.29	3.89	3.56	1.16	.68	109
				.870	62.79	.20E+06	.742	6.48	-4.32	2.31	3.99	3.53	1.15	.66	110
				1.050	69.00	.22E+06	.909	7.94	-4.30	2.30	3.96	3.58	1.17	.68	111
6.0	.43	.43	.24	.165	27.36	.85E+05	.117	1.02	-3.38	2.09	2.78	2.93	.96	.67	112
				.360	40.43	.13E+06	.261	2.28	-3.32	2.08	2.71	3.00	.98	.69	113
				.895	63.79	.20E+06	.644	5.62	-3.29	2.07	2.68	2.98	.97	.69	114
				1.819	91.07	.29E+06	1.312	11.46	-3.34	2.08	2.74	2.99	.97	.69	115
6.0	.43	.63	.03	.170	27.63	.86E+05	.123	1.07	-3.28	2.07	2.66	2.99	.98	.70	116
				.330	38.51	.12E+06	.234	2.04	-3.14	2.03	2.49	2.93	.96	.71	117
				.876	62.79	.20E+06	.617	5.39	-3.11	2.03	2.47	2.92	.95	.71	118
				2.005	95.16	.30E+06	1.411	12.32	-3.17	2.04	2.54	2.91	.95	.70	119
8.0	.57	.10	.28	.169	27.64	.11E+06	.326	2.85	-6.83	2.80	5.66	5.99	1.10	.76	120
				.230	32.25	.13E+06	.454	3.97	-6.97	2.82	5.81	6.13	1.13	.77	121
				.402	42.65	.18E+06	.802	7.00	-7.08	2.84	5.91	6.19	1.14	.77	122
				.7[illegible]0	57.89	.24E+06	1.485	12.97	-7.21	2.87	6.09	6.23	1.14	.76	123
8.0	.57	.32	.05	.151	26.11	.11E+06	.250	2.18	-5.67	2.58	4.38	5.14	.94	.77	124
				.222	31.66	.13E+06	.376	3.28	-5.87	2.62	4.60	5.26	.97	.76	125
				.469	46.03	.19E+06	.793	6.93	-5.77	2.60	4.49	5.25	.96	.77	126
				.690	55.85	.23F+06	1.165	10.17	-5.80	2.61	4.52	5.24	.96	.77	127

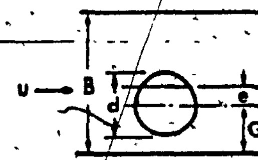

TABLE 3 GD CDI AND CDJ FOR ECCENTRIC CIRCULAR CYLINDERS

WIDTH	BLOCK	ECC	GAP	DELTAH	U	R	VOLT	DRAG	CRS	K	CD	CDI	CDJ	RUNNO
1.0	.07	3.81	2.69	.180	28.63	.15E+05	.009	.08	-1.55	1.60	1.30	1.12	.51	128
				.638	53.93	.29E+05	.033	.29	-1.62	1.56	1.28	1.11	.53	129
				2.221	100.87	.52E+05	.110	.96	-1.26	1.50	1.23	1.06	.54	130
				5.390	157.88	.82E+05	.252	2.20	-.97	1.40	1.16	1.00	.59	131
2.0	.14	.39	2.61	.400	42.40	.44E+05	.044	.38	-1.49	1.58	1.35	.99	.54	132
				.920	64.35	.67E+05	.102	.89	-1.49	1.58	1.37	1.01	.55	133
				2.630	109.09	.11E+06	.274	2.39	-1.25	1.50	1.29	.95	.57	134
				3.990	134.63	.14E+06	.408	3.56	-1.21	1.49	1.27	.93	.57	135
2.0	.14	1.28	1.72	.143	25.45	.26E+05	.017	.15	-1.88	1.70	1.48	1.08	.51	136
				.431	44.20	.44E+05	.050	.44	-1.43	1.56	1.44	1.06	.59	137
				1.030	68.39	.71E+05	.112	.98	-1.43	1.56	1.35	.99	.56	138
				3.192	120.79	.13E+06	.342	2.99	-1.48	1.58	1.33	.98	.54	139
2.0	.14	1.91	1.09	.210	30.71	.32E+05	.027	.24	-1.71	1.65	1.60	1.17	.59	140
				.439	44.42	.46E+05	.055	.48	-1.63	1.62	1.56	1.14	.59	141
				1.125	71.18	.74E+05	.133	1.16	-1.68	1.64	1.47	1.08	.55	142
				2.760	111.78	.12E+06	.321	2.80	-1.60	1.61	1.44	1.06	.56	143
2.0	.14	2.56	.44	.458	45.38	.47E+05	.048	.42	-1.30	1.52	1.30	.96	.56	144
				1.070	69.42	.72E+05	.123	1.07	-1.48	1.57	1.43	1.05	.58	145
				2.455	105.37	.11E+06	.251	2.19	-1.07	1.44	1.27	.93	.61	146
				4.150	137.33	.14E+06	.416	3.63	-1.07	1.44	1.24	.91	.60	147
3.0	.21	.26	1.57	.155	26.56	.41E+05	.029	.25	-1.80	1.67	1.55	.96	.55	148
				.464	45.98	.72E+05	.085	.74	-1.78	1.67	1.52	.94	.55	149
				.914	64.58	.10E+06	.171	1.49	-1.87	1.69	1.55	.96	.54	150
				2.064	97.21	.15E+06	.358	3.13	-1.67	1.64	1.44	.89	.54	151
3.0	.21	.85	.98	.161	27.07	.42E+05	.032	.28	-2.23	1.80	1.65	1.02	.51	152
				.472	46.38	.72E+05	.095	.83	-2.07	1.75	1.67	1.03	.54	153
				.931	65.18	.10E+06	.188	1.64	-2.14	1.77	1.67	1.03	.53	154
				2.079	97.57	.15E+06	.387	3.38	-1.91	1.71	1.54	.95	.53	155
4.0	.29	.20	1.08	.160	26.81	.56E+05	.049	.43	-2.61	1.90	1.90	.97	.53	156
				.338	38.97	.81E+05	.102	.89	-2.59	1.90	1.87	.96	.52	157
				.590	51.51	.11E+06	.170	1.48	-2.34	1.83	1.79	.91	.53	158
				.880	62.94	.13E+06	.241	2.10	-2.15	1.77	1.70	.87	.54	159
				1.380	78.87	.16E+06	.325	2.84	-1.72	1.65	1.46	.75	.54	160

TABLE 3 CD CDI AND CDJ FOR ECCENTRIC CIRCULAR CYLINDERS

WIDTH	BLOCK	ECC	GAP	DELTAH	U	R	VOLT	DRAG	CPS	K	CD	CDI	CDJ	RUNNO
4.0	.29	.64	.61	.144	25.56	.53E+05	.048	.42	-2.56	1.89	2.07	1.06	.58	161
				.264	34.61	.72E+05	.087	.76	-2.60	1.90	2.06	1.05	.57	162
				.514	48.32	.10E+06	.159	1.39	-2.42	1.85	1.92	.98	.56	163
				.945	65.56	.14E+06	.259	2.26	-2.14	1.77	1.70	.87	.54	164
				1.674	87.35	.19E+06	.376	3.28	-1.76	1.66	1.39	.71	.51	165
4.0	.29	.95	.30	.160	26.81	.56E+05	.049	.43	-2.30	1.82	1.90	.97	.58	166
				.359	40.17	.84E+05	.108	.94	-2.13	1.77	1.87	.95	.60	167
				.560	50.18	.10E+06	.163	1.42	-2.01	1.73	1.81	.92	.60	168
				.885	63.12	.13E+06	.233	2.03	-1.78	1.67	1.63	.83	.59	169
				1.685	87.20	.18E+06	.388	3.39	-1.51	1.58	1.43	.73	.57	170
6.0	.43	.13	.54	.178	28.28	.89E+05	.109	.95	-3.24	2.06	2.53	.83	.60	171
				.350	39.66	.12E+06	.205	1.79	-3.16	2.04	2.42	.79	.58	172
				.882	63.01	.20E+06	.323	2.82	-2.05	1.75	1.52	.49	.50	173
				2.032	95.81	.30E+06	.726	6.34	-2.00	1.73	1.48	.48	.49	174
6.0	.43	.43	.24	.145	25.65	.80E+05	.090	.79	-3.16	2.04	2.57	.84	.62	175
				.266	34.74	.11E+06	.157	1.37	-3.03	2.01	2.44	.80	.61	176
				1.146	72.21	.23E+06	.411	3.59	-2.01	1.73	1.48	.48	.49	177
				2.233	100.96	.32E+06	.806	7.04	-2.13	1.77	1.49	.49	.48	178
6.0	.43	.63	.03	.170	27.63	.86E+05	.107	.93	-2.93	1.98	2.60	.85	.66	179
				.900	63.65	.20E+06	.338	2.96	-1.82	1.68	1.56	.51	.55	180
				1.890	92.37	.29E+06	.718	6.27	-1.91	1.71	1.57	.51	.54	181
8.0	.57	.10	.28	.160	26.90	.11E+06	.230	2.01	-6.22	2.69	4.46	.82	.62	182
				.320	38.05	.16E+06	.314	2.74	-4.04	2.25	3.05	.56	.60	183
				.400	42.54	.18E+06	.385	3.36	-4.03	2.24	2.99	.55	.59	184
				.850	62.06	.26E+06	.820	7.16	-4.05	2.25	2.99	.55	.59	185
8.0	.57	.32	.05	.160	26.87	.11E+06	.196	1.71	-4.60	2.37	3.80	.70	.68	186
				.337	39.01	.16E+06	.296	2.59	-3.51	2.12	2.73	.50	.60	187
				.[illegible]30	44.08	.18E+06	.405	3.54	-3.63	2.15	2.92	.54	.63	188
				1.045	68.77	.29E+06	.970	8.47	-3.75	2.18	2.88	.53	.61	189

```
C
C
C     PPOGRAM 4   THEORETICAL CD FOR ECCENTRIC PRISMS AT 0 DEGREE
C
C
      PROGRAM ECCCD(INPUT,OUTPUT)
      REAL M,N
    1 FORMAT (4F .4)
    2 FORMAT(27X,4F6.2,3F7.3,4F7.2,F7.0)
    4 FORMAT(/)
    5 FORMAT(27X,6H WIDTH,6H BLOCK,6H   ECC,6H   GAP,7H      M,7H    CC1
     1,7H    CC2,7H    CD1,7H    CD2,7H    CDT,7H     CD,7H    DEV,/)
    6 FORMAT(1H1,//////,38X,57HTABLE     THEORETICAL CD FOR ECCENTRIC PR
     1ISMS AT 0 DEGREE,/)
   11 FORMAT(//,52X,29HNOTE DEV=PERCENTAGE DEVIATION/60X,22H=ABS(CDT-CD),
     1/CDT X100.)
   16 FORMAT(39X,2F6.2,3F7.3,4F7.2,F7.0)
      PRINT 6
      PRINT 5
   10 READ 1,E,W,U,CDE
      IF(E.EQ.50.) GO TO 7
      IF(E.EQ.90.) GO TO 8
      B=W/14.
      ECC=E/W
      G1=7.-E-W/2.
      G2=7.+E-W/2.
      G=G1/W
      Q=1.
      P=.5/((7.-W/2.)**Q)
      M=     P*G1**Q
      CC1=COEF(   W,M,G1)
      CD1=CDCF(W,G1,M,CC1,U      )
      N=1.-M
      CC2=COEF(   W,N,G2)
      CD2=CDCF(W,G2,N,CC2,U)
      IF(E.EQ.0.) GO TO 17
      CD=CD1*M+CD2*N
      DEV=ABS(CD-CDE)*100./CD
      GO TO 18
   17 CD=1.1*(CD1*M+CD2*N)
      DEV=ABS(CD-CDE)*100./CD
   18 IF(E.EQ.0.) GO TO 15
      PRINT 16,    ECC,G  ,M,CC1,CC2,CD1,CD2,CD,CDE,DEV
      GO TO 10
   15 PRINT 2,W,B,ECC,G  ,M,CC1,CC2,CD1,CD2,CD,CDE,DEV
      GO TO 10
    7 PRINT 4
      GO TO 10
    8 PRINT 11
      STOP
      END
```

```
      FUNCTION COEF(X,Y,Z)
      BD=1.+X*Y/Z
      CC=.6
      DO 10 J=1,100
      R=BD/CC-CC/BD
      A=1./(1.+R*ATAN(2./R)/3.1416)
      IF(ABS(CC-A).LE..005) GO TO 12
      CC=CC+.005
   10 CONTINUE
   12 COEF=CC
      RETURN
      END
```

```
      FUNCTION CDCF(W,X,Y,Z,V)
      PHI=3.1416
      DD=X*Z
      A=2.*DD/(PHI*Y*W*V)
      B=X+Y*W*V
      C=(PHI/(4.*B*DD))*(B*B/(DD*DD)+1.)*(B-DD)*(B-DD)
      D=(B*B/(DD*DD)-1.)*(B*B-DD*DD)/(2.*B*DD)*ATAN((B*B-DD*DD)/(2.*B*DD
     1))
      F=B*B/(DD*DD)-1.
      CDCF=A*(C-D)+F
      RETURN
      END
```

TABLE 4 THEORETICAL CD FOR ECCENTRIC PRISMS AT 0 DEGREE

WIDTH	BLOCK	ECC	GAP	M	CC1	CC2	CD1	CD2	CDT	CD	DEV
2.00	.14	0.00	3.00	.500	.745	.745	2.34	2.34	2.57	2.83	10.
		.39	2.61	.435	.745	.745	2.34	2.34	2.34	2.71	16.
		1.28	1.72	.287	.745	.745	2.34	2.34	2.34	2.70	16.
		1.91	1.09	.182	.745	.745	2.34	2.34	2.34	2.85	22.
		2.55	.45	.075	.745	.745	2.34	2.34	[illegible]	2.26	3.
2.60	.19	0.00	2.19	.500	.725	.725	2.65	2.65	2.91	3.31	14.
		1.35	.85	.193	.725	.725	2.65	2.65	2.65	2.96	12.
3.00	.21	0.00	1.83	.500	.710	.710	3.11	3.11	3.42	3.63	6.
		.26	1.57	.429	.710	.710	3.11	3.11	3.11	3.40	9.
		.85	.98	.267	.710	.710	3.11	3.11	3.11	3.40	9.
		1.27	.56	.154	.710	.710	3.11	3.11	3.11	3.00	4.
3.40	.24	0.00	1.56	.500	.700	.700	3.20	3.20	3.52	3.90	11.
		1.03	.53	.170	.700	.700	3.20	3.20	3.20	3.20	0.
4.00	.29	0.00	1.25	.500	.685	.685	3.98	3.98	4.37	4.31	1.
		.20	1.05	.422	.685	.685	3.98	3.98	3.98	4.15	4.
		.64	.61	.244	.685	.685	3.98	3.98	3.98	4.00	1.
		.95	.30	.119	.685	.685	3.98	3.98	3.98	3.57	10.
4.53	.32	0.00	1.05	.500	.675	.675	4.33	4.33	4.76	4.87	2.
		.77	.27	.130	.675	.675	4.33	4.33	4.33	4.03	7.
6.00	.43	0.00	.67	.500	.655	.655	7.09	7.09	7.80	7.50	4.
		.13	.54	.403	.655	.655	7.09	7.09	7.09	6.94	2.
		.43	.24	.180	.655	.655	7.09	7.09	7.09	6.25	12.
		.63	.03	.024	.655	.655	7.09	7.09	7.09	5.84	18.
8.00	.57	0.00	.38	.500	.630	.630	12.73	12.73	14.00	14.46	3.
		.10	.28	.370	.630	.630	12.73	12.73	12.73	13.40	5.
		.32	.05	.073	.630	.630	12.73	12.73	12.73	11.20	12.

NOTE: DEV=PERCENTAGE DEVIATION =ABS(CDT-CD)/CDT X100.

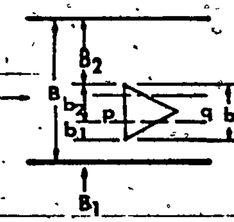

pq–stagnation streamline

$m = b_1 / b$

```
C
C
C     PROGRAM  5  STROUHAL NUMBERS FOR MULTIPLE BODIES CONFIGURATIONS.
C
C
      PROGRAM STROU(INPUT,OUTPUT)
      REAL NU
    1 FORMAT(6(F10.4),F10.6,F10.4)
    2 FORMAT(F10.4)
    3 FORMAT(12X,8H   WIDTH,6H BLOCK,8H  DELTAH,6H     F,6H    CC,8H
     1     U,9H        R,7H     S,7H    S1,7H    SJ,8H      U1,8H
     2UJ,8H  RUNNO,///)
    4 FORMAT(12X,F8.3,F6.3,F8.3,F6.0,F6.3,F8.2,E9.2,3F7.3,2F8.2,5X,I3)
    5 FORMAT(/)
    6 FORMAT(12X,F8.3,F6.3,F8.3,F6.0,F14.2,E9.2,2F7.3,F15.2,13X,I3)
   16 FORMAT(1H1,//////,26X,64HTABLE       S S1 AND SJ FOR MULTIPLE TRIANG
     1ULAR PRISMS AT 0 DEGREE,/)
   17 FORMAT(1H1,//////,27X,62HTABLE      S AND S1 FOR MULTIPLE TRIANGULA
     1R PRISMS AT 60 DEGREE,/)
   18 FORMAT(1H1,//////,32X,50HTABLE      S AND S1 FOR MULTIPLE CIRCULAR
     1CYLINDERS,/)
      N=1
   10 READ 2,SHAPE
      IF(SHAPE.EQ.0.) GO TO 20
      IF (SHAPE.EQ.1.) GO TO 11
      IF(SHAPE.EQ.2.) GO TO 12
      IF(SHAPE.EQ.3.) GO TO 13
      IF(SHAPE.EQ.4.  .OR.SHAPE.EQ.14.) GO TO 30
      GO TO 19
   11 PRINT 16
      PRINT 3
      GO TO 19
   12 PRINT 17
      PRINT 3
      GO TO 19
   13 PRINT 18
      PRINT 3
   19 READ 1,D,BR,H,PT,PATM,GAMMAA,NU,FREQ
      IF(SHAPE.EQ.1..OR.SHAPE.EQ.14..OR.SHAPE.EQ.16.) GO TO 21
      GO TO 50
   21 READ 2 ,CC
      GO TO 50
   30 PRINT 5
      GO TO 19
   50 P=PATM*.488+PT*.0292
      GAMMA=(GAMMAA*P)/14.7
      IF(D.EQ.2.6.OR.D.EQ.3.4.OR.D.EQ.3.412.OR.D.EQ.4.28) GO TO 51
      V=20.3*(SQRT(H/GAMMA))
      GO TO 52
   51 V=18.29*(SQRT(H/GAMMA))
   52 S=.0876*FREQ*D/V
      ETA=1.-BR
      V1=V/ETA
      S1=ETA*S
      RE=(V*D)/(12.*NU)
```

```
      IF(SHAPE.EQ.1..OR.SHAPE.EQ.14..OR.SHAPE.EQ.16.) GO TO 32
      GO TO 34
   32 VJ=V1/CC
      SJ=S1*CC
      PRINT 4,D,BR,H,FREQ,CC,V,RE,S,S1,SJ,V1,VJ,N
      N=N+1
      GO TO 10
   34 PRINT 6,D,BR,H,FREQ,V,RE,S,S1,V1,N
      N=N+1
      GO TO 10
   20 STOP
      END
```

TABLE 5 S SI AND SJ FOR MULTIPLE TRIANGULAR PRISMS AT 0 DEGREE

WIDTH	BLOCK	DELTAH	F	CC	U	R	S	SI	SJ	UI	UJ	RUNNO
.858	.123	.210	79.	.760	34.45	.14E+05	.171	.150	.114	39.49	51.96	1
.858	.123	1.175	188.	.760	82.17	.34E+05	.172	.151	.115	93.64	123.21	2
.858	.123	5.185	400.	.760	175.05	.70E+05	.172	.151	.115	199.49	262.48	3
.858	.245	.240	105.	.700	38.38	.16E+05	.206	.155	.109	50.84	72.62	4
.858	.245	1.175	224.	.700	81.49	.34E+05	.207	.156	.109	107.95	154.22	5
.858	.245	5.325	480.	.700	174.35	.70E+05	.207	.156	.109	230.96	329.94	6
.639	.365	.240	181.	.665	37.37	.11E+05	.271	.172	.114	58.86	88.52	7
.639	.365	1.178	400.	.665	82.72	.25E+05	.271	.172	.114	130.29	195.92	8
.639	.365	1.786	492.	.665	101.89	.31E+05	.270	.172	.114	160.48	241.32	9
.639	.365	.050	89.	.665	16.00	.52E+04	.295	.187	.124	26.62	40.03	10
.639	.365	.210	170.	.665	34.70	.11E+05	.274	.174	.116	54.65	82.19	11
.639	.365	.790	340.	.665	67.32	.21E+05	.283	.179	.119	106.03	159.44	12
.639	.365	2.560	600.	.665	120.02	.37E+05	.278	.176	.117	190.46	286.40	13
2.600	.371	.054	25.	.665	15.87	.20E+05	.359	.226	.150	25.24	37.96	14
2.600	.371	.180	45.	.665	28.97	.36E+05	.354	.222	.148	46.08	69.30	15
2.600	.371	1.200	120.	.665	74.82	.93E+05	.365	.230	.153	119.03	179.00	16
2.600	.371	5.050	247.	.665	152.47	.19E+06	.369	.232	.154	242.55	364.74	17
.858	.490	.038	120.	.645	14.63	.61E+04	.608	.310	.200	29.09	45.10	18
.858	.490	.120	212.	.645	26.34	.11E+05	.605	.308	.199	51.67	80.11	19
.858	.490	.580	468.	.645	57.70	.24E+05	.609	.310	.200	113.35	175.74	20
.858	.490	1.880	830.	.645	103.53	.42E+05	.603	.307	.198	203.07	314.84	21
.858	.490	.030	110.	.645	13.10	.54E+04	.631	.322	.208	25.70	39.84	22
.858	.490	.610	490.	.645	58.03	.24E+05	.625	.319	.206	115.55	179.15	23
.858	.490	2.000	880.	.645	106.23	.43E+05	.623	.318	.205	208.30	322.95	24
3.412	.485	.036	23.	.645	12.00	.21E+05	.533	.274	.177	25.05	38.84	25
3.412	.485	.150	47.	.645	26.36	.44E+05	.533	.274	.177	51.18	79.35	26
3.412	.485	.830	112.	.645	61.85	.10E+06	.541	.279	.180	120.10	186.21	27
3.412	.485	3.360	224.	.645	123.18	.20E+06	.544	.280	.181	239.19	370.84	28

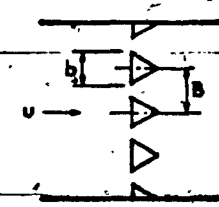

TABLE 5 . S SI AND SJ FOR MULTIPLE TRIANGULAR PRISMS AT 0 DEGREE

WIDTH	BLOCK	DELTAH	F	CC	U	R	S	SI	SJ	UI	UJ	RUNNO
4.280	.610	.040	90.	.630	13.62	.28E+05	2.477	.966	.609	34.93	55.44	29
4.280	.610	.180	140.	.630	28.86	.60E+05	1.819	.709	.447	74.01	117.47	30
4.280	.610	.180	250.	.630	28.86	.60E+05	3.247	1.267	.798	74.01	117.47	31
4.280	.610	.600	220.	.630	52.49	.11E+06	1.571	.613	.386	134.59	213.64	32
4.280	.610	.600	750.	.630	52.49	.11E+06	5.357	2.089	1.316	134.59	213.64	33
2.600	.743	.070	0.	.615	9.72	.12E+05	0.000	0.000	0.000	37.78	61.42	34
2.600	.743	.280	0.	.615	36.29	.45E+05	0.000	0.000	0.000	141.11	229.44	35
2.600	.743	.440	110.	.615	45.41	.56E+05	.552	.142	.087	176.54	287.05	36
2.600	.743	1.120	0.	.615	71.34	.87E+05	0.000	0.000	0.000	277.36	450.99	37

TABLE 5, S AND SI FOR MULTIPLE TRIANGULAR PRISMS AT 60 DEGREE

WIDTH	BLOCK	DELTAH	F	CC	U	R	S	SI	SJ	U1	UJ	RUNNO
.858	.123	.215	115.		35.39	.15E+05	.244	.214		40.33		38
.858	.123	1.024	250.		77.26	.32E+05	.243	.213		88.05		39
.858	.123	5.135	564.		174.08	.70E+05	.244	.214		198.38		40
.858	.245	.221	133.		35.53	.15E+05	.281	.212		47.07		41
.858	.245	1.031	288.		76.76	.31E+05	.282	.213		101.68		42
.858	.245	4.260	586.		156.29	.63E+05	.282	.213		207.03		43
.858	.245	6.210	710.		189.26	.76E+05	.282	.213		250.71		44
.639	.365	.220	213.		35.72	.11E+05	.334	.212		56.26		45
.639	.365	1.200	498.		83.37	.26E+05	.334	.212		131.32		46
.639	.365	5.010	1015.		170.40	.52E+05	.333	.212		268.39		47
.639	.365	6.500	1160.		194.57	.58E+05	.334	.212		306.45		48
2.600	.371	.059	28.		16.61	.21E+05	.377	.237		26.43		49
2.600	.371	.10	52.		31.34	.39E+05	.378	.238		49.86		50
2.600	.371	1.300	130.		78.06	.98E+05	.379	.238		124.17		51
2.600	.371	6.950	304.		180.56	.22E+06	.383	.241		287.23		52
.858	.490	.058	120.		18.32	.76E+04	.492	.251		35.93		53
.858	.490	.230	240.		36.46	.15E+05	.495	.252		71.52		54
.858	.490	1.000	500.		76.12	.31E+05	.494	.252		149.32		55
.858	.490	4.960	1110.		168.25	.68E+05	.496	.253		330.04		56
3.412	.485	.052	28.		15.55	.26E+05	.538	.277		30.19		57
3.412	.485	.220	57.		32.02	.53E+05	.532	.274		62.17		58
3.412	.485	1.020	120.		68.94	.11E+06	.520	.268		133.86		59
3.412	.485	5.150	275.		154.06	.25E+06	.534	.275		299.15		60
4.280	.610	.040	27.		13.44	.28E+05	.742	.289		34.97		61
4.280	.610	.160	55.		27.27	.56E+05	.756	.295		69.93		62
4.280	.610	.700	115.		56.82	.12E+06	.759	.296		145.70		63
4.280	.610	3.130	240.		118.19	.24E+06	.761	.297		303.06		64

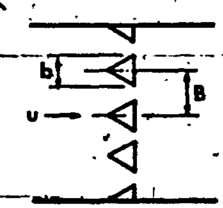

TABLE 5 S AND SI FOR MULTIPLE TRIANGULAR PRISMS AT 60 DEGREE

WIDTH	BLOCK	DELTAH	F	CC	U	R	S	SI	SJ	UI	UJ	RUNNO
.639	.730	.030	195.		13.10	.40E+04	.833	.225		48.51		65
.639	.730	.130	410.		27.23	.84E+04	.843	.228		100.86		66
.639	.730	.030	157.		13.10	.40E+04	.671	.181		48.51		67
.639	.730	.165	300.		30.67	.94E+04	.548	.148		113.59		68
.639	.730	.600	700.		58.44	.18E+05	.670	.181		216.45		69
.639	.730	1.800	1200.		99.37	.30E+05	.676	.183		368.04		70
.639	.730	.030	190.		13.09	.40E+04	.813	.219		48.47		71
.639	.730	.130	260.		27.21	.84E+04	.535	.144		100.79		72
.639	.730	.130	400.		27.20	.84E+04	.823	.222		100.73		73
.639	.730	.650	950.		60.74	.18E+05	.876	.236		224.96		74
.639	.730	1.620	1580.		99.85	.30E+05	.886	.239		369.83		75
2.600	.743	.018	26.		9.20	.12E+05	.656	.169		35.76		76
2.600	.743	.101	63.		21.76	.27E+05	.659	.170		84.61		77
2.600	.743	.440	130.		45.23	.56E+05	.655	.168		175.84		78
2.600	.743	1.660	250.		86.42	.11E+06	.659	.169		336.00		79
3.412	.730	.050	33.		15.35	.25E+05	.642	.173		56.86		80
3.412	.730	.200	70.		30.68	.50E+05	.682	.184		113.65		81
3.412	.730	.630	0.		54.17	.89E+05	0.000	0.000		200.63		82
3.412	.730	1.550	0.		91.59	.15E+06	0.000	0.000		339.21		83
3.412	.970	.080	0.		19.21	.32E+05	0.000	0.000		640.49		84
3.412	.970	.200	0.		30.51	.51E+05	0.000	0.000		1016.90		85
3.412	.970	.520	40.		48.27	.79E+05	.248	.007		1608.90		86

TABLE 5 S AND SI FOR MULTIPLE CIRCULAR CYLINDERS

WIDTH	BLOCK	DELTAH	F	CC	U	R	S	SI	SJ	UI	UJ	RUNNO
.250	.071	.255	355.		38.50	.46E+04	.202	.188		41.46		87
.250	.071	1.840	950.		103.51	.12E+05	.201	.187		111.46		88
.250	.071	7.220	1900.		206.37	.24E+05	.202	.187		222.24		89
.250	.071	9.080	2140.		232.31	.27E+05	.202	.187		250.17		90
.500	.071	.270	182.		39.48	.95E+04	.202	.188		42.51		91
.500	.071	1.400	420.		89.96	.22E+05	.204	.190		96.87		92
.500	.071	5.660	836.		181.56	.43E+05	.202	.187		195.52		93
.500	.071	8.900	1050.		228.57	.54E+05	.201	.187		246.14		94
.500	.143	.250	180.		37.99	.91E+04	.208	.178		44.32		95
.500	.143	1. 30	430.		91.01	.22E+05	.207	.177		106.18		96
.500	.143	5.700	860.		182.93	.43E+05	.206	.176		213.43		97
.500	.143	8.750	1070.		227.51	.53E+05	.206	.177		265.44		98
1.000	.143	.092	60.		22.80	.11E+05	.230	.197		26.72		99
1.000	.143	.300	108.		41.43	.20E+05	.228	.196		48.35		100
1.000	.143	1.380	235.		88.92	.43E+05	.232	.198		103.76		101
1.000	.143	9.010	600.		228.98	.11E+06	.230	.197		267.19		102
.500	.290	.240	200.		37.29	.90E+04	.235	.167		52.52		103
.500	.286	1.400	480.		90.06	.22E+05	.233	.167		126.09		104
.500	.286	5.710	973.		182.74	.43E+05	.233	.167		255.84		105
.500	.286	7.650	1140.		212.09	.50E+05	.235	.168		296.92		106
1.000	.286	.090	65.		22.67	.11E+05	.251	.179		31.74		107
1.000	.286	.260	110.		38.55	.18E+05	.250	.178		53.99		108
1.000	.286	1.300	250.		86.26	.41E+05	.254	.181		120.82		109
1.000	.286	7.900	600.		213.76	.10E+06	.246	.176		299.39		110
.800	.456	.070	130.		20.01	.77E+04	.455	.248		36.78		111
.800	.456	.180	200.		32.15	.12E+05	.436	.237		59.10		112
.800	.456	1.280	380.		85.51	.33E+05	.311	.169		157.18		113
.800	.456	5.840	800.		182.40	.68E+05	.307	.167		335.30		114
.800	.456	.060	120.		18.57	.72E+04	.453	.246		34.14		115
.800	.456	.190	210.		33.13	.13E+05	.444	.242		60.91		116
.800	.456	1.230	375.		84.30	.32E+05	.312	.170		154.97		117

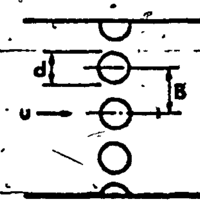

TABLE 5 S AND S1 FOR MULTIPLE CIRCULAR CYLINDERS

WIDTH	BLOCK	DELTAH	F	CC	U	R	S	S1	SO	U1	UJ	RUNNO
3.400	.490	.060	28.		16.70	.27E+05	.499	.255		32.74		118
3.400	.490	.110	37.		22.61	.37E+05	.487	.249		44.34		119
3.400	.490	.260	44.		34.78	.57E+05	.377	.192		68.20		120
3.400	.490	.570	57.		51.49	.84E+05	.330	.168		100.97		121
.500	.571	.215	300.		35.14	.84E+04	.374	.160		81.99		122
.500	.571	.570	490.		57.19	.14E+05	.375	.161		133.43		123
.500	.571	1.280	730.		85.54	.21E+05	.374	.160		199.58		124
1.000	.570	.060	140.		18.62	.90E+04	.659	.283		43.30		125
1.000	.570	.190	250.		33.12	.16E+05	.661	.284		77.03		126
1.000	.570	.750	500.		65.70	.32E+05	.667	.287		152.80		127
.375	.850	.100	24.		[illegible]	.43E+04	.033	.005		158.76		128
.375	.850	.100	340.		23.31	.43E+04	.469	.070		158.76		129
.375	.850	.420	32.		48.30	.87E+04	.022	.003		321.98		130
.375	.850	.420	60.		48.30	.87E+04	.041	.006		321.98		131
.375	.850	.420	90.		48.30	.87E+04	.061	.009		321.98		132
.375	.850	.420	400.		48.30	.87E+04	.272	.041		321.98		133
.375	.850	.750	200.		63.94	.11E+05	.103	.015		425.57		134
.375	.850	.750	400.		63.94	.11E+05	.206	.031		425.57		135
.750	.850	.020	21.		10.49	.38E+04	.132	.020		69.94		136
.750	.850	.020	70.		10.49	.38E+04	.438	.066		69.94		137
.750	.850	.020	230.		10.49	.38E+04	1.440	.216		69.94		138
.750	.850	.140	60.		27.72	.10E+05	.142	.021		184.81		139
.750	.850	.140	200.		27.72	.10E+05	.474	.071		184.81		140
.750	.850	.420	120.		47.72	.17E+05	.165	.025		318.16		141
.750	.850	.420	400.		47.72	.17E+05	.551	.083		318.16		142
.750	.850	.730	200.		62.26	.22E+05	.211	.032		415.06		143
.750	.850	.730	400.		62.26	.22E+05	.422	.063		415.06		144

APPENDIX 2

WIND TUNNEL CALIBRATION

APPENDIX 2

WIND TUNNEL CALIBRATION

Open-circuit tunnels are by far, the most common type among wind tunnels used for research in universities and industry. In some designs, flow measurement is done by the built-in flow meters, such as venturi tubes, nozzles, or orifices. In this chapter, the discussion will be restricted to the velocity calibration of subsonic wind tunnels equipped with flow venturis.

The velocity calibration used in the experimental program calls for the determination of two main characteristics in the test section. (Fig. 1):

(i) The mean flow velocity in terms of the pressure difference across the venturi, and

(ii) The level of free turbulence.

From a technical point of view, determining the turbulence level is a standard procedure [1,2,3,4] and will not be discussed here. Instead, a detailed procedure is outlined for determining the mean flow velocity in the test section of a subsonic wind tunnel with built-in venturi tubes. The working formulas, computing algorithms and programs are also included to assist the user of this test facility.

CALIBRATION PROCEDURE

The following will describe a procedure for determining the mean flow velocity in the test section in terms of the pressure difference across the venturi. With slight modifications, the same procedure may be applied to other types of flow meter. The particular wind tunnel referred to is shown schematically in Fig. 1. Its major dimensions are listed below:

Test Section:

14 in. wide x 10 in. high x 20 in. long

Venturi Tubes:

(The shape of the venturi tubes follows the standard specification. [5])

Venturis	Pipe Dia.D	Throat Dia,	$\beta = \frac{d}{D}$
Large	16 in.	10 in.	.625
Small	12 in.	8 in.	.667

STEP I

Check leakage, leveling, vibration and motor overheating, etc. Emphasis is made here, that in checking leakage, one should pay particular attention to the connections of the duct work downstream of the venturis, all the way to the exit of the diffuser. One should also check carefully, the fittings, connections, and tubings of flow measurement instruments,such as manometers, pitot tubes, etc. Overlooking these "minor" points is often the cause of erroneous readings.

STEP II

Set up the instruments, as shown in Fig. 2. It is to be noted that the manometers used in conjunction with the measurements of h_t and h_v is preferably of the micro projection type [6],[7], particularly at low speed. The reasons for this will be clear after seeing Eqs. (1) and (2). p_t is read by branching off the static of the pitot tube, as shown in Fig. 2. Two thermometers were used to record t_t and t_v.

STEP III

Take readings of h_v, p_v, t_v, h_t, p_t and t_t, at locations, as shown in Fig. 2.

STEP IV

Calculate the mean flow velocity in the test section,

V_t, by substituting the above readings as taken in STEP III into the following formulas:

For large venturi operating alone

$$V_t = 11.1 \frac{y_a \sqrt{h_v \gamma_v}}{\gamma_t} \text{ fps} \qquad (1)$$

For small venturi operation alone

$$V_t = 7.21 \frac{y_a \sqrt{h_v \cdot \gamma_v}}{\gamma_t} \text{ fps} \qquad (2)$$

where y_a = expansion factor taken from Fig.90 [5].

γ_t, γ_v = specific weight of the flowing fluid in the test section and venturi pipe, respectively.

For derivation of these formulas, see the following sections.

MEAN FLOW VELOCITY IN THE TEST SECTION

From continuity,

$$W_t = W_v$$

where W_t and W_v are mass flow rates, lbs/hr, through the test section and venturi, respectively. Following the procedure in [5], one gets

$$W_t = 3600 \; V_t A_t \gamma_t \quad \text{lbs/hr} \qquad (3)$$

A_t being the cross-sectional area of the test section and

$$W_v = y_a \frac{359C_d\beta^2D^2}{\sqrt{1-\beta^4}} \sqrt{h_v \gamma_v} \text{ lbs/hr} \quad (4)$$

C_d being the discharge coefficient of the venturi.

Hence

$$V_t = \frac{359y_aC_d\beta^2D^2}{3600A_t\gamma_t\sqrt{1-\beta^4}} \sqrt{h_v \gamma_v} \text{ fps} \quad (5)$$

Upon substituting the values of A_t and venturi dimensions, the following working formulas are obtained:

For large venturi operating alone

$$V_t = 11.1 \; y_a \frac{\sqrt{h_v \gamma_v}}{\gamma_t} \text{ fps} \quad (1)$$

For small venturi operating alone

$$V_t = 7.21 \; y_a \frac{\sqrt{h_v \gamma_v}}{\gamma_t} \text{ fps} \quad (2)$$

To calculate γ_t and γ_v one proceeds as follows, [5] :

$$\gamma_v = \frac{\gamma_a \, p_v}{14.7} \text{ lbs/cu.ft.} \quad (6)$$

where γ_a is the specific weight of dry air at 14.7 psia and at the actual air temperature, and p_v in psia. The values of γ_a are taken from Table A.4 [8].

$$\gamma_t = \frac{\gamma_a \, p_t}{14.7} \quad \text{lbs./cu.ft.} \qquad (7)$$

The value of C_d has been found to be .98.

For the experimental determination of C_d see the following section.

EXPERIMENTAL DETERMINATION OF DISCHARGE COEFFICIENT, C_d

ASME Research Committee on Fluid Meters calibrated a great number of Herschel-type venturi tubes ([5] Fig.18), for pipe sizes from 2 to 32 in. and diameter ratios from .27 to .75. It was established that the mean discharge coefficient curve is a function of the pipe Reynolds number (see Fig. 88, [5]). However, in this graph, the range of variation of C_d for a given Reynolds number in the upper range of the latter was considered to be large. As such, a direct calibration of the specific venturi in question was contemplated to include effects local to the venturis of the wind tunnel. The following procedure indicates the details about the determination of C_d. To do this, V_t has to be determined first (see Eq. (5)).

In Fig. 3, an imaginary grid system is superimposed on the cross-sectional area of the test section normal to the flow. The grid divides the x- and y-axis into 8 and 6 segments, respectively. The physical width and height are shown corresponding to i and j designations. Pitot tube readings are taken at each node ($x_i, y_j, i = 2...8$ and $j = 2...6$). The local flow velocity $v_{i,j}$ at the walls must be zero, i.e., $V_{i,1} = 0$, $V_{i,7} = 0$, $V_{1,j} = 0$, and $V_{9,j} = 0$.

The expression for the total volume flow rate per unit height normal to the flow can be set as:

$$Q' = \sum_{i=1}^{8} \tfrac{1}{2}(V_{i,j}+V_{i+1,j})(x_{i+1,j}-x_{i,j}),$$

j remaining fixed

Hence, the mean flow velocity on a hor-zontal plane located at y_j is

$$V_j = \frac{Q'}{14}$$

Similarly, the total flow across the test section is

$$Q = \sum_{j=1}^{6} 14(y_{j+1}-y_j)[\tfrac{1}{2}(V_{j+1}+V_j)]$$

Hence, the mean flow velocity of the test section is given by

$$V_t = \frac{Q}{10 \times 14}$$

Thus C_d in Eq. (5) can be determined. The experimental values of C_d are shown in Fig. 4. Further, to facilitate the calculation of V_t, a computer program is attached.

It is to be noted that in the program, use was made of the formula

$$V_t = 18.29 \sqrt{\frac{h_t}{\gamma_t}}$$

This equation is based on Bernoulli's equation.

It is also interesting to note that the central velocity taken at the central point of the test section bears a fixed ratio to the mean velocity over the entire section. Denote

$$r = \frac{\text{Mean Velocity}}{\text{Central Velocity}}$$

For both venturis, $r \approx .95$ (See Table 1).

BIBLIOGRAPHY

1. Hinze, J.O., Turbulence, An Introduction to its Mechanism and Theory. 1959, McGraw-Hill.

2. Instruction and Service Manual for Type 55D05 Battery-Operated CTA. DISA.

3. Instruction and Service Manual for Type 55D01 Anemometer Unit. DISA.

4. Rasmussen, C.G., and Madsen, B.B., Hot-Wire and Hot-Film Anemometry. DISA.

5. Fluid Meters. Fifth Edition, 1959, ASME Research Committee on Fluid Meters.

6. Bradshaw, P., Experimental Fluid Mechanics. Second Edition, 1970, Pergamon Press.

7. Instruction Manual for Micro Projection Manometer, Model 513. TEM Instruments Ltd.

8. Flowmeter Computation Handbook. 1961. ASME Research Committee on Fluid Meters.

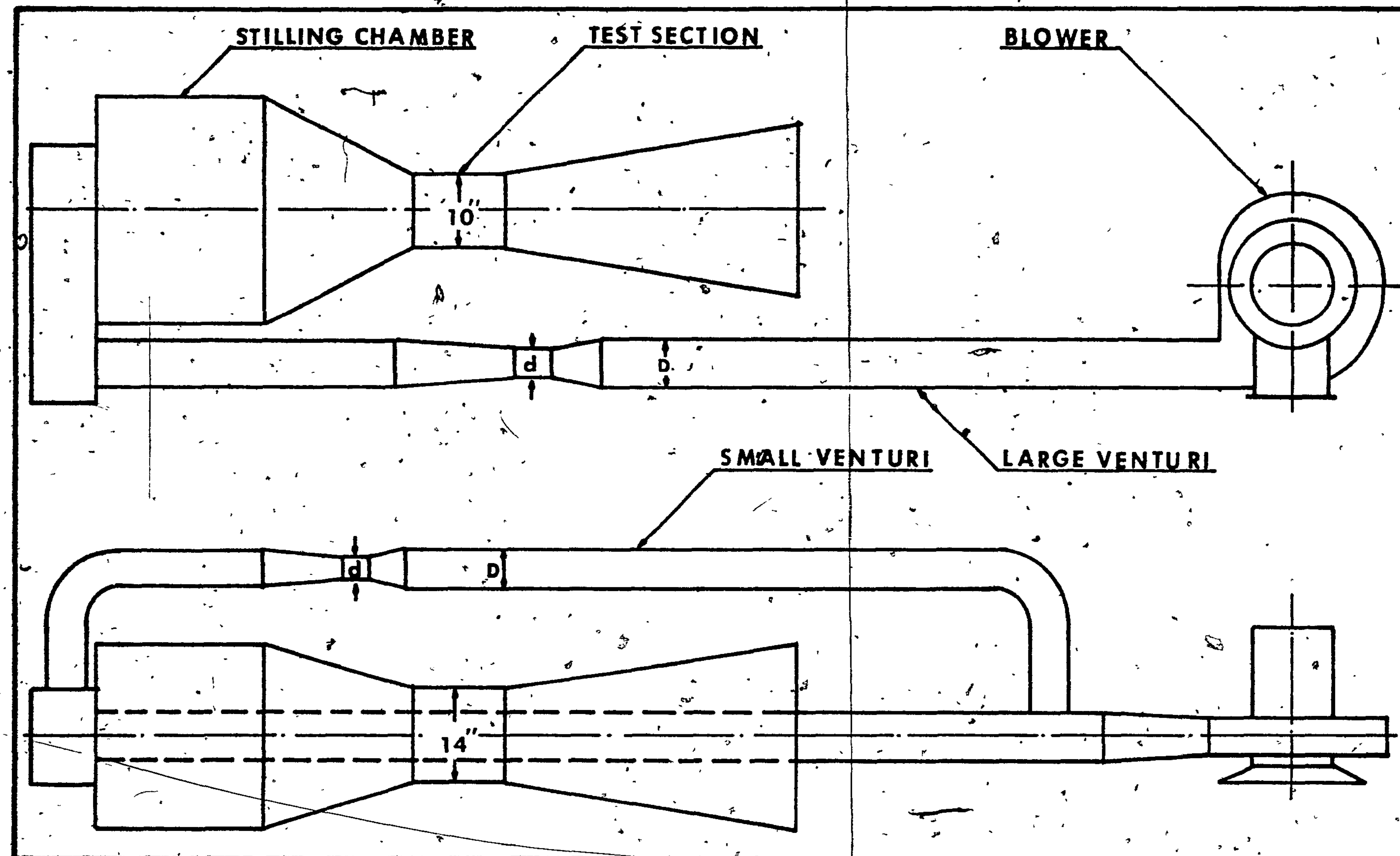

FIG I WIND TUNNEL

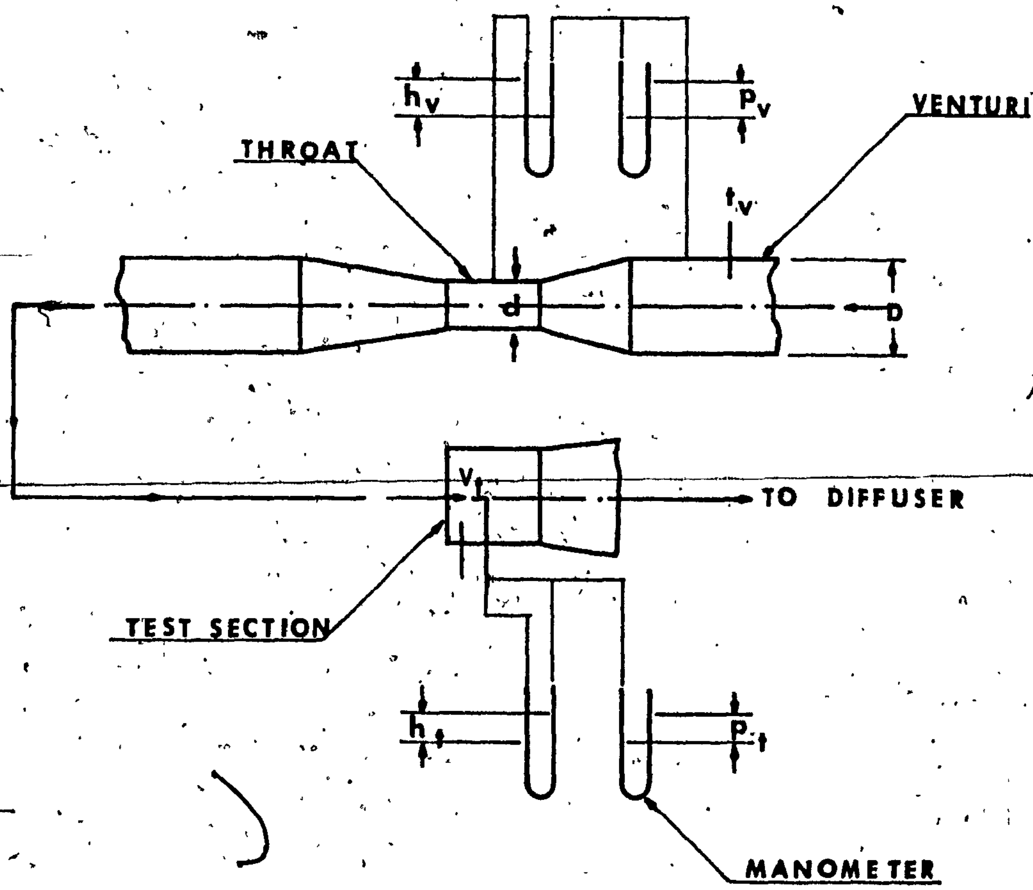

Notations: Subscripts v and t denote venturi and test section respectively.

p_v static pressure upstream of throat, psig.

h_v pressure difference across venturi, in. of water at 68F.

t_v temperature of flowing fluid upstream of throat, F.

p_t Static pressure at test section, psig.

h_t pitot reading, in. of water at t_t.

t_t temperature of flowing fluid at test section, F.

FIG. 2 INSTRUMENT SET-UP FOR DETERMINING THE MEAN FLOW VELOCITY, V_t, AND THE DISCHARGE CO-EFFICIENT C_d

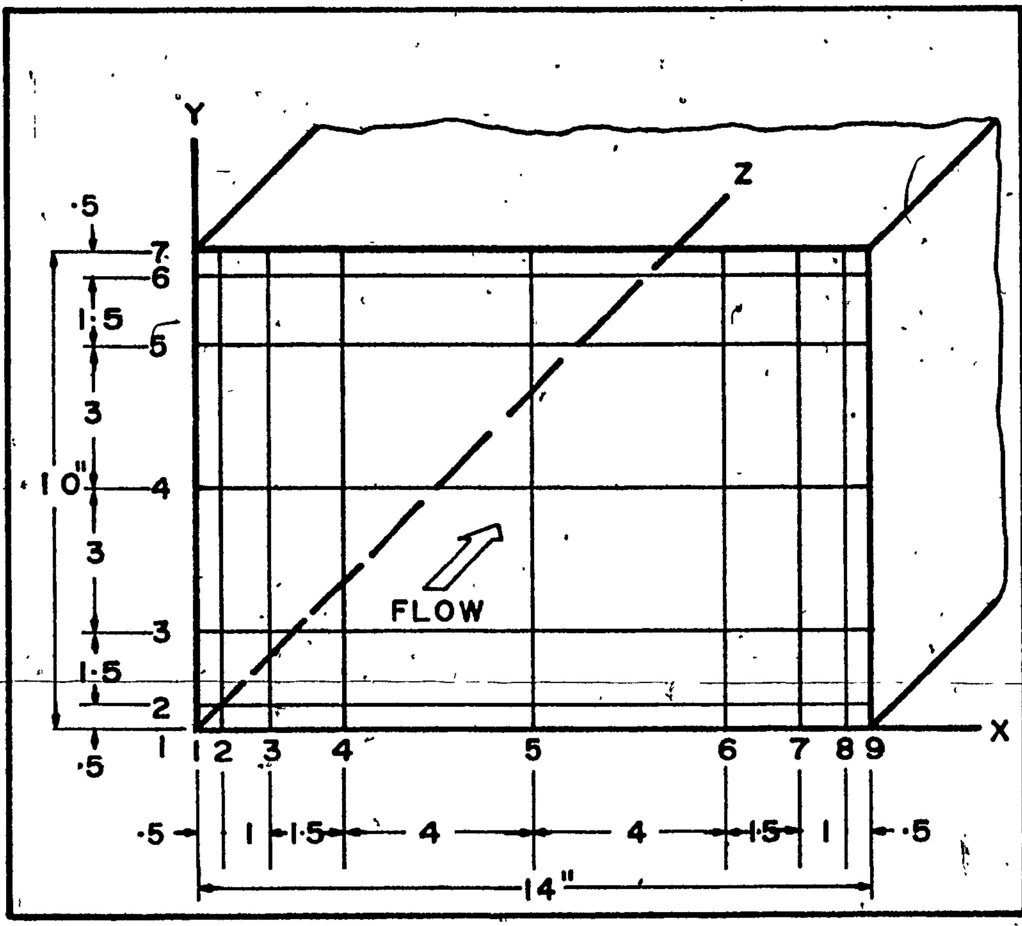

FIG 3 GRID SYSTEM

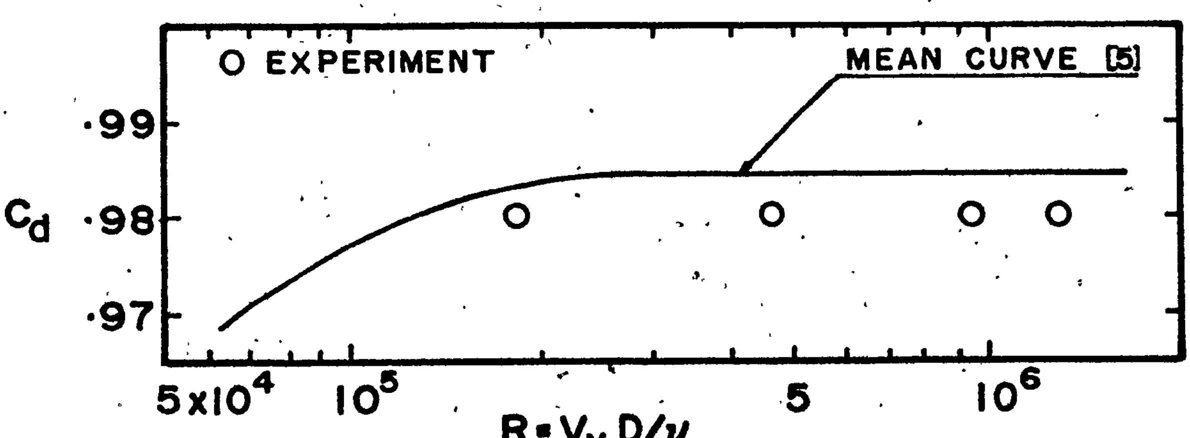

FIG 4 C_d vs R, VENTURI

TABLE 1

RATIO OF CENTRAL VELOCITY TO MEAN VELOCITY

Large Venturi			Small Venturi		
Mean Vel. fps	Central Vel. fps	Ratio	Mean Vel. fps	Central Vel. fps	Ratio
33.21	34.90	.951	30.52	32.40	.943
126.29	132.20	.958	100.92	106.0	.940
173.90	182.10	.946	120.72	127.50	.948
199.67	210.0	.950	126.80	134.0	.949
206.35	216.0	.950	129.42	136.10	.948

```
C
C
C     PROGRAM      MEAN FLOW VELOCITY FOR SMALL VENTURI OPERATING ALONE.
C
C
      PROGRAM PROFILE (INPUT,OUTPUT)
      DIMENSION H(9,7),X(8),Y(6),RHO(5) ,GAMMA(5) ,DELTAH(5)
      DATA(X(I),I=1,8)/.5,1.0,1.5,4.0,4.0,1.5,1.0,.5/
      DATA(Y(I),I=1,6)/.5,1.5,2.75,3.188,1.563,.5/
      DATA(RHO(I),I=1,5)/.0719,.0717,.0717,.0714,.0711/
      DATA(DELTAH(I),I=1,5)/1.17,13.75,19.,22.9,24.0/
      DATA(GAMMA(I),I=1,5)/.0719,.0729,.0735,.0735,.0731/
    1 FORMAT(1H1)
    2 FORMAT(///,45X,7HTEST NO,I5,2X,10HINPUT DATA,/)
    3 FORMAT(9F8.3)
    4 FORMAT(19X,I1,4X,9F8.3)
    5 FORMAT(    44X,19HMEAN FLOW VELOCITY=,F6.2,2X,6HFT/SEC)
    6 FORMAT(19X,1HJ,3X,1HI,8H       1,8H       2,8H       3,8H       4,
     18H       5,8H       6,8H       7,8H       8,8H       9,/)
    7 FORMAT(/,59X,6HRESULT,/)
      DO 10 K=1,5
      IF(K.EQ.1 .OR.K.EQ.4) GO TO 13
      GO TO 12
   13 PRINT 1
   12 PRINT 2,K
      PRINT 6
      READ 3,((H(I,J),I=1,9),J=1,7)
      DO 11 J=1,7
      PRINT 4,J, (H(I,J),I=1,9)
   11 CONTINUE
      D=AVGH(H,X,Y)
      V=18.29  *SQRT(D/RHO(K))
      PRINT 7
      PRINT 5,V
   10 CONTINUE
      END

      FUNCTION AVGH(A,B,C)
      DIMENSION A(9,7),B(8),C(6),AAVG(7)
      DATA AAVG(1),AAVG(7)/0.,0./
      DO 10 J=2,6
      SUM=0.
      DO 15 I=1,8
      AVG=(A(I,J)+A(I+1,J))/2.0
      FLOW=AVG*B(I)
      SUM=SUM+FLOW
   15 CONTINUE
      AAVG(J)=SUM/14.0
   10 CONTINUE
      SUM=0.
      DO 20 J=1,6
      AVG=(AAVG(J)+AAVG(J+1))/2.0
      FLOW=AVG*C(J)
      SUM=SUM+FLOW
   20 CONTINUE
      AVGH=SUM/10.0
      RETURN
      END
```

TEST NO 1 INPUT DATA

J	I	1	2	3	4	5	6	7	8	9
1		0.000	0.000	0.000	0.000	0.000	0.000	0.000	0.000	0.000
2		0.000	.198	.204	.194	.224	.204	.204	.204	0.000
3		0.000	.216	.216	.218	.220	.224	.224	.218	0.000
4		0.000	.210	.218	.222	.224	.228	.228	.216	0.000
5		0.000	.204	.222	.222	.226	.226	.224	.206	0.000
6		0.000	.160	.214	.188	.216	.204	.208	.194	0.000
7		0.000	0.000	0.000	0.000	0.000	0.000	0.000	0.000	0.000

RESULT

MEAN FLOW VELOCITY= 30.51 FT/SEC

TEST NO 2 INPUT DATA

J	I	1	2	3	4	5	6	7	8	9
1		0.000	0.000	0.000	0.000	0.000	0.000	0.000	0.000	0.000
2		0.000	2.320	2.180	2.200	2.380	2.240	2.260	2.390	0.000
3		0.000	2.350	2.400	2.410	2.420	2.450	2.460	2.440	0.000
4		0.000	2.300	2.420	2.400	2.410	2.440	2.450	2.350	0.000
5		0.000	2.320	2.400	2.410	2.420	2.440	2.440	2.350	0.000
6		0.000	1.950	2.370	2.040	2.310	2.260	2.340	2.240	0.000
7		0.000	0.000	0.000	0.000	0.000	0.000	0.000	0.000	0.000

RESULT

MEAN FLOW VELOCITY=100.87 FT/SEC

TEST NO 3 INPUT DATA

J	I	1	2	3	4	5	6	7	8	9
1		0.000	0.000	0.000	0.000	0.000	0.000	0.000	0.000	0.000
2		0.000	3.340	3.250	3.020	3.425	3.070	3.320	3.410	0.000
3		0.000	3.400	3.445	3.450	3.475	3.515	3.520	3.505	0.000
4		0.000	3.335	3.446	3.440	3.460	3.500	3.515	3.405	0.000
5		0.000	3.355	3.430	3.440	3.440	3.470	3.460	3.365	0.000
6		0.000	2.830	3.410	2.980	3.290	3.245	3.325	3.080	0.000
7		0.000	0.000	0.000	0.000	0.000	0.000	0.000	0.000	0.000

RESULT

MEAN FLOW VELOCITY=120.65 FT/SEC

TEST NO 4 INPUT DATA

J	I	1	2	3	4	5	6	7	8	9
1		0.000	0.000	0.000	0.000	0.000	0.000	0.000	0.000	0.000
2		0.000	3.640	3.350	3.290	3.690	3.300	3.570	3.670	0.000
3		0.000	3.730	3.820	3.815	3.820	3.850	3.854	3.840	0.000
4		0.000	3.610	3.750	3.790	3.815	3.850	3.850	3.710	0.000
5		0.000	3.670	3.770	3.795	3.790	3.835	3.820	3.690	0.000
6		0.000	3.270	3.760	3.270	3.650	3.620	3.730	3.510	0.000
7		0.000	0.000	0.000	0.000	0.000	0.000	0.000	0.000	0.000

RESULT

MEAN FLOW VELOCITY=126.73 FT/SEC

TEST NO 5 INPUT DATA

J	I	1	2	3	4	5	6	7	8	9
1		0.000	0.000	0.000	0.000	0.000	0.000	0.000	0.000	0.000
2		0.000	3.830	3.635	3.460	3.880	3.435	3.760	3.879	0.000
3		0.000	3.739	3.800	3.890	3.926	3.980	3.990	3.945	0.000
4		0.000	3.730	3.940	3.950	3.966	4.010	4.015	3.860	0.000
5		0.000	3.830	3.905	3.940	3.970	3.980	3.970	3.850	0.000
6		0.000	3.250	3.870	3.370	3.820	3.680	3.815	3.670	0.000
7		0.000	0.000	0.000	0.000	0.000	0.000	0.000	0.000	0.000

RESULT

MEAN FLOW VELOCITY=12[illegible].35 FT/SEC

APPENDIX 3

DESIGN FORMULAS FOR FORCE GAGES

DESIGN FORMULAS FOR FORCE GAGES

Flow-induced vibrations caused by flow past structural members tend to be random. These signals are to be registered by force gages which should possess the following major characteristics:

(i) Sufficiently high natural frequency to encompass and at the same time render minimum distortion to the input signals, and

(ii) the required damping characteristic

Sophisticated gages which meet these requirements are available commercially. However, for a comparatively small project, it is usually financial-wise prohibitive for the experimenter to seek expensive equipment. Under these restrictions, one will explore the possibilities of designing some devices that will meet the above requirements. To this end, the Force Gage was proposed.

The objective of this section is to present analytic formulas for predicting the natural frequencies in terms of dimensions and properties of the gage materials.

ANALYSIS

Three typical gages will be discussed in this chapter, i.e. the Rectangular, (Fig. 3, p. 38), the Trapezoidal and the composite types. They are of similar construction except that the side plates are of rectangular, trapezoidal contours and hollow rectangular cross-sections, respectively. The two side plates are rigidly fastened to a central piece whose stiffness can be considered as infinite in comparison with that of the plates. With this and the built-in feature at the upper fixed end, it can be assumed that the two plates always displace in parallel and with zero slope at both ends. It is this parallel movement feature that ensures that the test structural member attached underneath the central piece stays in its original orientation and further the gage always registers the correct responses regardless of the position of application of the resultant signal acting on the member.

For the Rectangular type, each plate can be considered as a cantilever beam of uniform width and height, with rectangular cross-section and with zero slope at both ends.

Hence $$\delta = \frac{PL^3}{12EI}$$

The spring constant of the gage (consisting of 2 plates) is therefore

$$K = \frac{24EI}{L^3} \qquad (1)$$

For the Trapezoidal type, each plate can be considered as a cantilever beam of uniform height but of uniformly varying width, with rectangular cross-section and zero slope at both ends. The deflection at the free end due to a concentrated load is given by [1,p.194]

$$\delta_p = \frac{12P}{Eh^3} \int_0^L \frac{x^2 dx}{b} \qquad (2)$$

By using the relation $b = b_1 + \frac{x}{L}(b_o - b_1)$, one obtains

$$\delta_p = \frac{12PL}{Eh^3} \int_0^L \frac{x^2 dx}{Lb_1 + x(b_o - b_1)}$$

$$= \frac{12PL^3}{Eh^3 b_1 (r-1)} \left[\tfrac{1}{2} - \frac{1}{r-1} + \frac{1}{(r-1)^2} \ln r\right] \qquad (3)$$

where $r \equiv$ width ratio

$= b_o/b_1$, $r > 1$.

To find the deflection at the free end due to a bending moment, one may apply the area-moment method and obtain

$$\delta_M = \int_0^L \frac{12Mxdx}{Ebh^3}$$

$$= \frac{12ML^2}{Eh^3} \cdot \frac{1}{b_1(r-1)} [1 - \frac{1}{r-1} \ln r] \quad (4)$$

Hence, the net resultant deflection at the free end due to P and M acting simultaneously is given by

$$\delta = \delta_P - \delta_M$$

$$= \frac{12L^2}{Eh^3 b_1(r-1)} \{PL[\tfrac{1}{2} - \frac{1}{r-1} + \frac{1}{(r-1)^2} \ln r]$$

$$- M [1 - \frac{1}{r-1} \ln r]\} \quad (5)$$

To simplify (5), use is made of one of the boundary conditions at the free end, i.e.

at $x = 0$, $\theta = 0$.

The angular deflection at the free end due to a bending moment is

$$\theta_M = \int_0^L \frac{Mdx}{EI}$$

$$= \frac{12ML}{Eh^3} \cdot \frac{\ln r}{b_1(r-1)} \quad (6)$$

Similarly, that due to a concentrated load is

$$\theta_P = \int_0^L \frac{Pxdx}{EI}$$

$$= \frac{12PL^2}{Eh^3} \frac{1}{b_1(r-1)}[1 - \frac{1}{r-1} \ln r] \tag{7}$$

Equating θ_m and θ_P a relationship between M and P is attained,

$$M = (\frac{1}{\ln r} - \frac{1}{r-1}) PL \tag{8}$$

With the aid of (8), (5) can be reduced to

$$\delta = \frac{12PL^3}{Eh^3b_1(r-1)} \{[\tfrac{1}{2} - \frac{1}{r-1} + \frac{1}{(r-1)^2} \ln r] - \frac{1}{\ln r} [1 - \frac{1}{r-1} \ln r]^2\} \tag{9}$$

From (9) it can be seen that the spring constant for a Trapezoidal Type gage is

$$K = \frac{2P}{\delta}$$

$$= \frac{Eh^3b_1(r-1)}{6AL^3} \tag{10}$$

where $A = [\tfrac{1}{2} - \frac{1}{r-1} + \frac{1}{(r-1)^2} \ln r] - \frac{1}{\ln r} [1 - \frac{1}{r-1} \ln r]^2$

The spring constant for a composite type gage can be readily computed by replacing I in (1) with that of a composite section. However, it is to be noted that from a stiffness point of view, an actual composite (built-up) section differs from its theoretical counterpart. The latter is considered as an integral section (such as extruded hollow structural sections); whereas, the former is generally built up using screws and rivets. Due to these assembly methods, considerable amount of slippage will inevitably take place between component plates joined together. Secondly, the weakening effect of screw or rivet holes also reduce the stiffness of the composite section. Altogether, the combined effects of slippage and weakening by the holes make the theoretical model describe the built-up section less accurately than the previous two cases. We will perceive the differences in the numerical example that follows.

EXPERIMENTAL RESULTS AND DISCUSSIONS

The rectangular type gage tested has the following dimensions:

width of plates,	b = 3 in.
thickness of plates,	h = 1/16 in.
length of equivalent cantilever beam,	L = 5 in.

Except for screws, LVDT, core-pin, and core-pin housing all other components are made of aluminum. The spring constant, K, is computed by using (2),

$$K = \frac{2\ Ebh^3}{L^3}$$

$$= 117.1 \text{ lbs/in.}$$

To compute the frequency, f, it is to be noted that a vibrating plate (idealized as a cantilever beam) has an infinite number of degrees of freedom. f is to be found from eq. $\omega_n = n^2 \sqrt{gEI/w}$ [2,p. 275.]

However, for the present case, it can be readily seen that much of the mass which vibrates with large amplitudes is located at the lower end of each plate. This is due to the fact that the vibration amplitudes of the upper portion (adjacent to the fixed end) of each plate are negligibly small as compared with that of the lower portion. Recall also, that the system has a considerably large mass in the form of the central piece.

Hence, the cantilever can be approximated by a mass-spring system of one degree of freedom. Therefore, f can be calculated from

$$f = \tfrac{1}{2}\pi\sqrt{\frac{K}{m}} \quad [2,(1.2\text{-}8),p.5] \qquad (11)$$

As a close approximation, m can be taken as the sum of the following masses:

(1) mass of the central piece

(2) one third of the mass of the side plates [3,p.34]

For the present case, $m = .017$ slugs, hence

$$f = 45.8 \text{ cps}$$

Experimental values are:

$$K = 116 \text{ lbs/in},$$

$$f = 45 \text{ cps}$$

For the Trapezoidal type gage, the theoretical and experimental values for K and f are compared as follows:

	Theoretical	Experimental	% Diff.
K, lbs/in	1144	1146	.2
f, cps	129	131.5	2

The experimental value of f is determined directly from the Logrithmic Decrement Curve, as shown in Figure 1. It can be readily verified that the damping ratio, ζ, based on mean logrithmic decrement, is almost equal to .01. Hence, the damping circular frequency ω_d can be taken as the natural circular frequency, ω_n[2, p.44].

The composite type gage has the following f values

	Theoretical	Experimental	% Diff
f, cps	247	260	5

The Logrithmic Decrement Curve is shown in Figure 2. The probable causes of discrepancy have already been explained earlier in the text.

CONCLUSIONS

1. The proposed Force Gage can be designed to possess the desired natural frequency and damping characteristics.

2. The design formulas for the Rectangular, Trapezoidal and composite Types, are given by (2), (11) and (2), respectively.

3. Except for the composite type, the percentage difference between the theoretical and experimental values of f is less than 2%.

NOTATIONS

E	Young's modulus, psi, $E = 10 \times 10^7$ psi for Al
b	Width of plate, in
f	Natural frequency, cps
h	Thickness of plate, in
I	Moment of inertia, in^4
K	Spring constant, lbs/in
L	Length of equivalent cantilever beam, in
M	Bending moment, lbs/in
m	Mass, slug
P	Concentrated load acting at the free end, lbs
r	Width ratio
θ	Slope at ends
δ	Deflection at free end
ω_n	Natural circular frequency
ω_d	Damped circular frequency
ζ	Damping ratio

BIBLIOGRAPHY

1. Timoshenko, S., and MacCullough, G.H., Elements of Strength of Materials. Third Edition, 1949, Van Nostrand.

2. Thomson, W.T., Vibration Theory and Applications. 1965, Prentice-Hall.

3. Den Hartog, J.P., Mechanical Vibrations, Fourth Edition, 1965, McGraw-Hill.

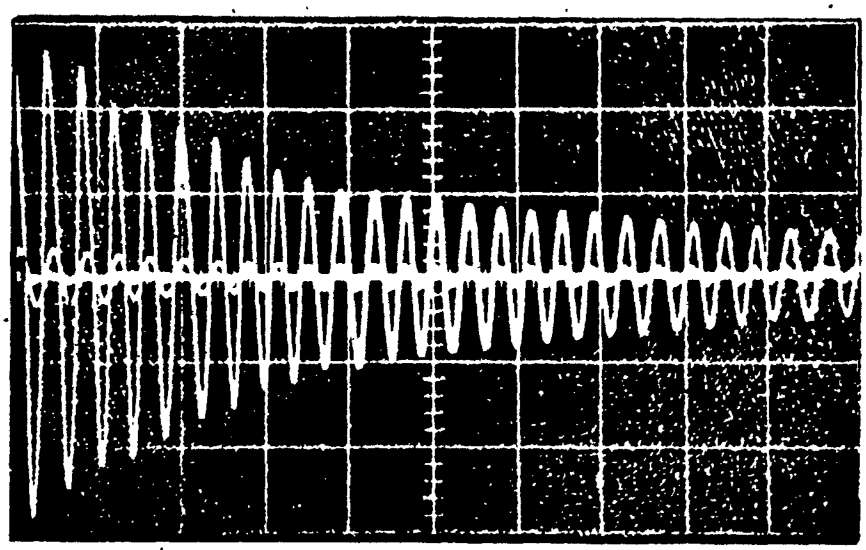

FIG. 1 LOGRÍTHMIC DECREMENT CURVE FOR THE TRAPEZOIDAL GAGE. SCALES:

Abscissa, 1 cm = 20 m sec,
Ordinate, 1 cm = .05 volts

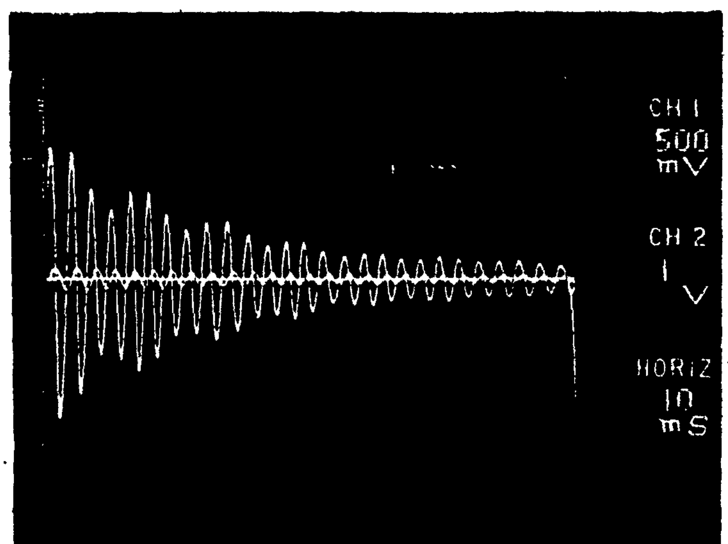

FIG. 2 LOGRITHMIC DECREMENT CURVE FOR THE COMPOSITE GAGE. SCALE:

Abscissa, 1 cm = 10 m sec.